Void Nucleation During Ductile Rupture of Metals: A Review

Philip J. Noell[a], Ryan B. Sills[b,c], Ahmed Amine Benzerga[d], Brad L. Boyce[a]

[a]*Sandia National Laboratories, Albuquerque, NM 87185, USA*
[b]*Sandia National Laboratories, Livermore, CA 94551, USA*
[c]*Department of Materials Science and Engineering, Rutgers University, Piscataway, NJ 08854, USA*
[d]*Department of Aerospace Engineering, Texas A&M University, College Station, TX 77843, USA*

Abstract

Ductile rupture in metals is a phenomenon that affects a wide range of applications from forming of automotive body panels to failure of pressure vessels. The incipient stage involves the formation of nanoscale internal voids, a critical transition state that is difficult to predict. Early experiments on ductile rupture led to several conflicting or competing models that describe the nucleation phase. The present review distinguishes the nucleation process based on the microstructural features that can trigger nucleation, e.g. vacancies, second-phase particles, grain boundaries, and dislocation cell boundaries; the conditions that drive nucleation, e.g. stress level, stress state, and temperature; and the materials properties that govern nucleation, e.g. modulus, yield strength, and work hardening. This review of observations and models leads to a critical assessment of the state of knowledge and provides guidance for future research directions, including a brief summary of the poten-

Email address: pnoell@sandia.gov (Philip J. Noell)

tial mechanistic changes to void nucleation processes in emerging material classes such as bulk metallic glasses, high entropy alloys, and nanostructured metals. This assessment also defines critical experiments and model developments that will enable improved prediction of ductile rupture processes and design of damage-tolerant materials. Such improvements in the understanding of the incipient phase of ductile rupture can lead to better materials, improved manufacturing and inspection protocols, more precise predictive models, more efficient engineering practices, and safer engineered structures.

Contents

1. Introduction: Early concepts and misconceptions

Rupture of materials has led to many of the most significant engineering disasters throughout history. The earliest records of concern regarding structural failure date back to the Code of Hammurabi in the 1700's BC, where punitive reparations were prescribed for failures associated with poorly built domiciles [1]. Over 100 years ago, the rupture of rivets led to two million gallons of molasses oozing into Boston's North End in 1919, resulting in 21 deaths [2]. During Typhoon Nina in August of 1975, 62 dams in the Henan Province of China experienced catastrophic structural failures, including the Banquio and Shimantan dams [3], leading to as many as 240,000 deaths. Overload failures in civil or aerospace structures, often occurring due to excessive loading and/or defected structural members, were responsible for the failure of several bridges and walkways [4, 5], explosive fuselage decompression, wing and empennage failures or engine separations [6, 7]. Naval vessels including Liberty Ships of World War II [8] and the Titanic [9] suffered notorious unexpected failures.

While this short list of catastrophic failures, often accompanied by the tragic loss of life, could be far longer, overload failure susceptibility is typically identified and addressed before a catastrophic event. Nevertheless, such failures lead to enormous consequences, in terms of lost revenue, delays in production, and unavailability of equipment. In 1983, the National Bureau of Standards released a report that estimated the annual cost of structural failures was $112B in the US alone, equating to 4% of the gross national product [10]. For this reason, conservative engineering practices provide a safety margin that mitigates uncertainty stemming from our limited under-

standing of failure. Not only can improvements in understanding guide better predictive models, but they can also motivate the development of improved materials and processes that ultimately enable safer and more efficient engineered structures.

Many of the aforementioned examples involved brittle fracture, where there are no signs of impending failure prior to a catastrophic event. For these problems, the advent of fracture mechanics in the 1950's [11], and the ensuing damage-tolerant design paradigm [12], provided a relatively robust solution for engineered prevention. However, there are a class of failure problems in more ductile materials that cannot be solved with fracture mechanics. Tearing during the forming processes for sheet metal is a classic example of ductile rupture in action. Ductile rupture is also used in the design of energy-absorbing safety structures for automobiles, often with the intent to delay fracture thereby enabling further plastic energy dissipation. These and other ductile rupture scenarios do not involve a well-defined pre-existing crack. As such, even elastoplastic fracture mechanics becomes dubious. Prior to the second half of the 1900's, the concepts behind ductile fracture were rudimentary, in part due to the limited ability to observe the microscale features of rupture, e.g. Figure 1. In the first half of the century, the understanding of the ductile failure process evolved in parallel with dislocation plasticity. For example, in 1923, Taylor and Elam suggested that rupture occurred by a process described as "slipping off" [13], and in 1949 Orowan described the process of internal cavity growth by dislocation slip on multiple independent lattice planes [14]. While these mechanisms for ductile rupture are still relevant to some ductile metals [15], they do not explain a vast majority of

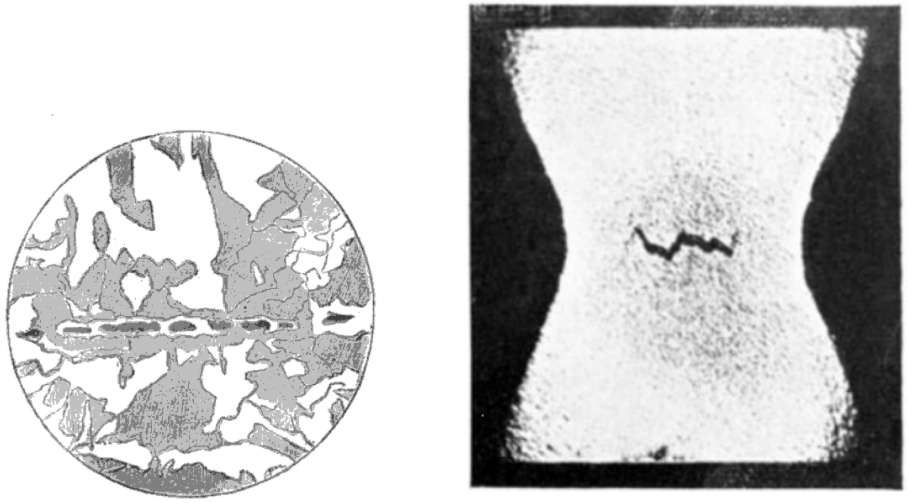

Figure 1: (a) A hand-drawn representation of voids in a "Siemens Steel Railway Axle" viewed through an optical microscope from an 1896 book titled "Microscopic internal flaws inducing fracture in steel". The field of view is approximately 200 μm. (b) A 1926 example of an internal crack in a tensile neck in aluminum revealed by serial sectioning and macrophotography, from reference [17].

failures in structural metals. In the second half of the 20th century, a growing realization emerged that most ductile rupture scenarios involved a combination of void nucleation, growth, and coalescence [15, 16]. Journal publication trends into the 21st century, shown in Figure 2, suggest that research related to void nucleation continues to expand substantially while the more general topic of fracture may be reaching a plateau.

Each of the three stages of void nucleation, growth, and coalescence involves different mechanisms, and therefore different dependencies on the driving forces (e.g local stress state, strain levels, and temperature), as well as different dependencies on material properties and microstructure. In cases of extreme ductility, materials can undergo void-free rupture by either necking to a point, or by Taylor's single-plane or Orowan's multi-plane catastrophic

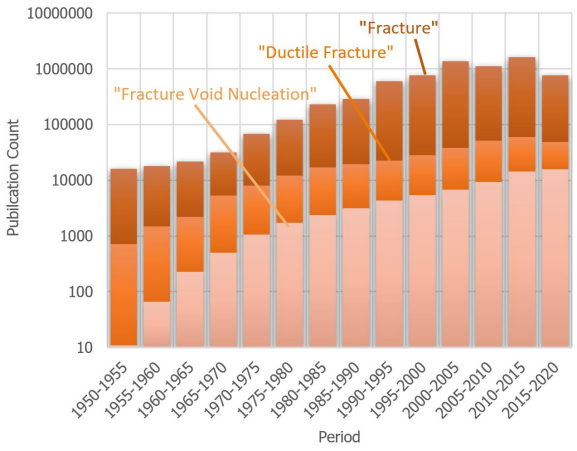

Figure 2: Publication trends related to the topic areas of "fracture void nucleation", "ductile fracture", and simple "fracture" based on Google Scholar data.

shear processes [15]. However, those failure processes are not considered here. Instead, we focus our attention on the nucleation phase of failure by void nucleation, growth, and coalescence. The void nucleation phase could be considered most important, as it represents the incipient process that triggers the transition state leading to eventual failure, yet the least is known about it. This is in part because the process occurs at the micro- or even nano-scale, often inside the material in regions of elevated stress triaxiality. Moreover, widely utilized models for ductile fracture, such as the Gurson-Tvergaard-Needleman formulation [18] (also see [19]), seem to work reasonably well but are purely phenomenological and thus overly parameterized. Indeed, a common model assumption is that the material contains pre-existing porosity. This is sometimes observed in practice, and it may be reasonable to assume that void nucleation in such materials is of secondary importance. Yet, in-situ studies using X-ray computed tomography (XCT) has shown that, in some cases, this porosity plays no significant role in determining final failure

[20].

While many engineering problems can be approached without understanding the void nucleation process, this is not always the case. In structural alloys such as magnesium, aluminum, and titanium alloys, the distribution and morphology of incipient voids profoundly influences many aspects of failure, including strain-localization and the failure mechanism [15, 16, 21–23]. Moreover, model benchmarking activities such as the Sandia Fracture Challenge [22, 23] have highlighted the shortcomings of existing continuum modeling approaches applied to common engineering materials, including a lack of consensus on the governing descriptions of incipient nucleation of damage in metals. Over the past decade, multiscale methods have shown increasing use for addressing open questions in fracture [24], but a microstructural-scale description for void nucleation is not well-established.

There are several possible mechanisms by which voids nucleate. These processes can act individually, competitively, or collaboratively, depending on the material and loading conditions. At the highest level, ductile fracture nucleation processes can be subdivided into two categories: particle-based nucleation, and particle-free nucleation, as shown in Figure 3. Within the particle-based methods, fracture either originates at the particle-matrix interface through decohesion or the particle itself cracks. Proposed particle-free processes for nucleation include vacancy condensation, defect accumulation at grain boundaries, and nucleation at dislocation cell boundaries.

The question of when and how a void forms depends on the length scale that is studied. To the human eye, the emergence of a void appears to happen very late in the deformation sequence, yet this is not because the

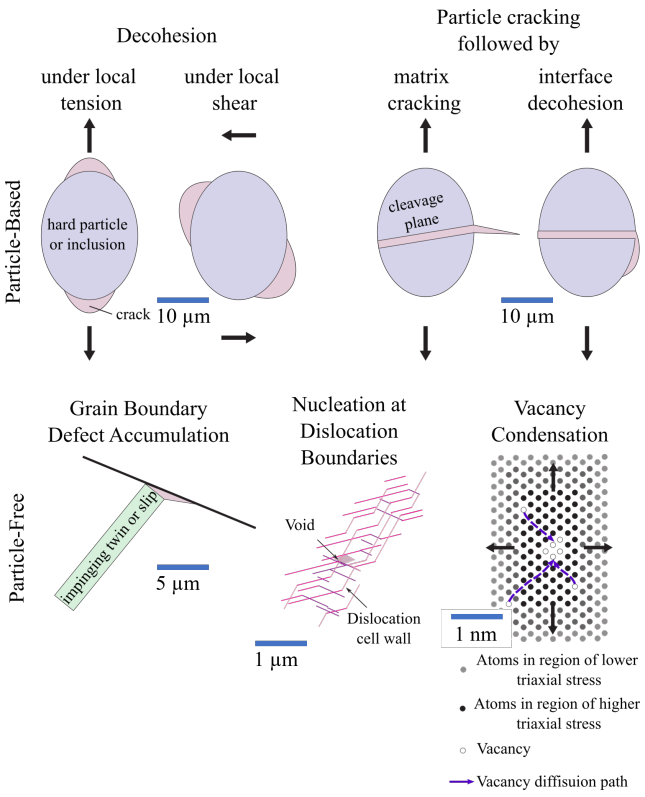

Figure 3: Schematic illustrations for mechanisms of void nucleation involving hard particles (top row) or at other microstructural features (bottom row). For reference, scale bars indicate the approximate length scales at which these mechanisms operate.

void has finally formed, but because the void is finally resolvable in the visible range. The same can be said of optical microscopy cross-sections, which were traditionally the most common tool utilized to infer nucleation processes. Numerous electron microscopy studies, using scanning electron microscopes (SEMs), and to a lesser extent, transmission electron microscopes (TEMs), have greatly altered our perception of nucleation. Yet even with these tools, it is not always clear that the process of nucleation was observed in its incipient state. Accordingly, many studies that portend to characterize nucleation may actually be observing some intermediate state of growth. This is likely the norm, not the exception.

The present review thus offers a multiscale perspective on void nucleation including experimental observations, theory, and simulations at the atomic-, nano-, microstructural, and continuum scales. While experimental observations at the atomic scale are largely non-existent, atomistic modeling of fracture has grown in utility over the past several decades as the scope of tractable computational domain sizes has increased. For example, molecular dynamics (MD) models have suggested that void nucleation could start with the stable condensation of just a few atomic vacancies within the material [25] at a length scale below the reach of nearly any experimental tool. However, such treatments still are typically constrained to sub-micrometer domain sizes and sub-microsecond timescales. Mesoscale modeling modalities, particularly discrete dislocation dynamics and polycrystalline plasticity, have gained increasing usage to represent the fracture process. These nanoscale and microstructural representations are complemented by parallel advances in experimental techniques including in-situ electron microscopy

and synchrotron high-energy diffraction microscopy [26–31] to better evaluate the role of precipitates/particles, dislocation substructures, etc. on the nucleation process. These new techniques are reshaping our perspective on the nucleation process below the continuum scale. Ultimately the goal is to integrate this mesoscale understanding into continuum-scale, macroscopic engineering descriptors of fracture which can relate how external driving forces, e.g. stress and stress-state, and material properties, e.g. yield strength and strain hardening, influence void nucleation.

Void nucleation can also play an important role in failure under extreme environments such as radiation, high strain rates, and elevated temperatures. These conditions are associated with blister/bubble formation, shock spallation, and creep rupture, respectively. To keep the scope of the present review constrained, we do not embark on detailed descriptions of those other rupture processes; the interested reader is directed to references [32–38] for more information on void nucleation during shock, references [39–43] for more information on void nucleation during creep, and references [44–49] on radiation-induced fracture processes.

Our goal here is to review the state of knowledge concerning void nucleation during ductile rupture of metals at quasi-static loading rates and near-ambient temperatures. Ductile fracture reviews have been published —some quite recently— by various authors in materials science [16, 50, 51] and solid mechanics [52–55]. None of these cover the topic of void nucleation in sufficient depth. Thus, this review of the subject may go as far back as 1979 [56].

The text below is divided into two major sections: one focused on the

role of microstructure in void nucleation (Section 2) and the other focused on insights gained from continuum-theory-based analyses of void nucleation (Section 3). In some sense, the primary thrust of void nucleation research is to marry the microstructural and continuum world views into a single comprehensive framework. As we show below, this is far from being achieved at present, but many recent experimental and modeling advances stand to change that in the coming years, as we enumerate in Section 4.

2. Microstructural aspects of void nucleation

Microstructural features can be described as a collection of 1D, 2D, and 3D defects, e.g. vacancies, dislocations, grain boundaries, and phase boundaries. There is a veritable multiscale zoo of these that influence ductile rupture, as illustrated in Figure 4. This microstructure and the corresponding arrangement of defects is not static, but evolves in response to deformation, temperature, and other stimuli. As it is clearly unrealistic to consider all possible defects in simulations of failure, we must determine the specific defect states in the microstructure that serve as dominant seed sites for void nucleation. Void nucleation is enabled by local plastic deformation at specific material heterogeneities [57]. Most studies have focused on the relationship between void nucleation and the properties of second-phase particles and inclusions (size, shape, etc.), as enumerated in Section 3. Little attention has been given to understanding the precise defect-defect interactions at these sites that enable void nucleation. In recent decades, the emergence of characterization tools such as electron backscatter diffraction (EBSD), combined with advances in computational tools, allowed these interactions to be studied in detail for the first time. This section first reviews deformation-induced

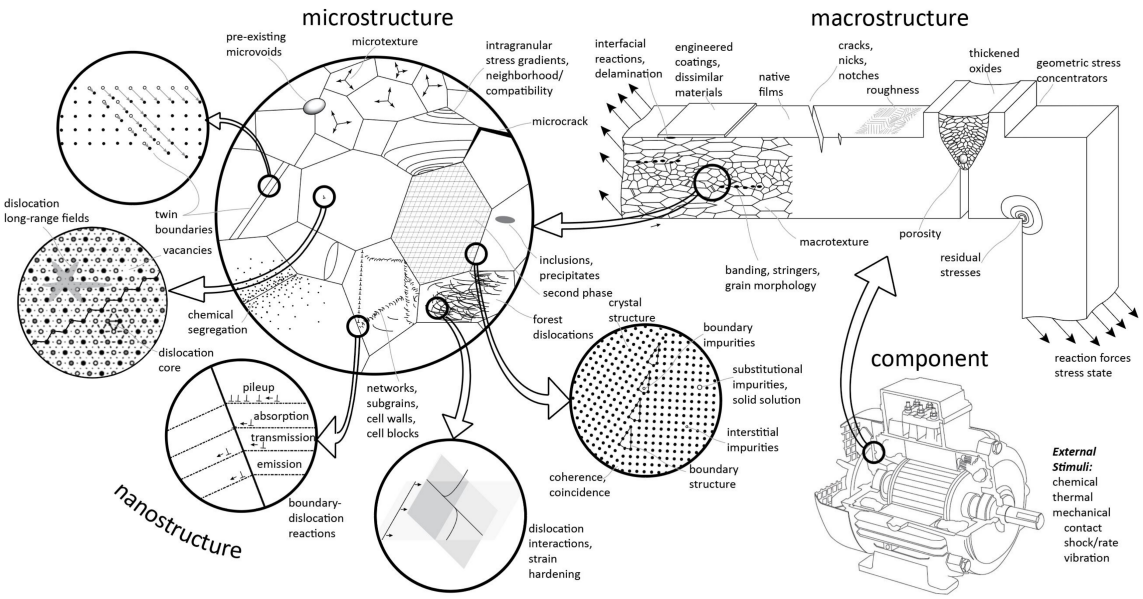

Figure 4: An overview of the diversity of "microstructure" in metals and alloys: a multiscale suite of features that can influence the ductile rupture process, and most other material phenomena. These features are established upon formation of the material and can evolve upon exposure to thermal, mechanical, chemical, radiation, or other stimuli. Adapted from [58].

defects and defect structures relevant to void formation. We then provide an overview of the microstructural features associated with void nucleation, both at deformation-induced defects and at the intersections between these and pre-existing defects.

2.1. Relevant deformation-induced defects and defect structures

Many defects and defect arrangements form and evolve during plastic deformation. This review considers four of these deformation-induced defects that are thought to be particularly relevant to void nucleation: vacancy clusters, dislocation pile-ups, dislocation boundaries, and deformation twins.

The process of formation for each defect type is briefly described. Particular attention is given to vacancies and vacancy clusters as these received relatively little attention in prior reviews.

2.1.1. Vacancies and vacancy clusters

Because vacancies (missing atoms) increase the entropy of a crystalline solid, leading to a reduction in its free energy, vacancies are always present in crystals above 0 K. Statistical mechanics shows that a crystalline solid has a temperature-dependent equilibrium vacancy concentration given by [57]

$$c_v^{eq} = c_{v0} \exp\left(\frac{-\Delta e_f}{k_B T}\right) \tag{1}$$

where k_B is Boltzmann's constant, T is the absolute temperature, Δe_f is the formation energy of a vacancy, and c_{v0} is a constant in the range of 2 to 10. Here we express the vacancy concentration as the fraction of lattice sites containing vacancies. For typical formation energies of common metals, equilibrium vacancy concentrations range from less than 10^{-20} at room temperature up to approximately 10^{-4} near the melting point [57].

These vacancy concentrations apply to a crystal at thermal equilibrium. There is strong experimental evidence that plastic deformation produces a vacancy supersaturation, with concentrations as large as 10^{-3} [59–61]. There are two general theories for how vacancies are produced during plastic deformation. Both theories rely on the fact that vacancies are either produced or consumed (depending on the glide direction) when non-screw dislocations move out of the glide plane containing their line and Burgers vector, i.e. climb motion.

The first mechanism, worked out in detail by Saada [62–64], is annihilation of non-screw dislocations of different glide planes. If the elastic inter-

action between the dislocations is attractive (typically the case if they can annihilate) and they are a short distance apart, the elastic interactions may be strong enough to induce climb motion. According to this model, the concentration of vacancies produced by cold-work to strain ϵ' is proportional to the work done as

$$c_v = \frac{A}{G} \int_0^{\epsilon'} \sigma d\epsilon \tag{2}$$

where G is the shear modulus, σ and ϵ are the applied stress and strain, and A is a constant on the order of 0.1 [65].

The second mechanism involves the formation of Burgers-vector-sized edge dislocation segments on screw dislocations after they intersect and cut through forest dislocations. If the line direction of the edge dislocation has a component out of the glide plane of the intersecting screw dislocation, the segment is termed a jog and can only move with the gliding screw dislocation by climbing. Cuitiño and Ortiz [66] proposed that the vacancy concentration will depend on the jog density, J, the slip strain rate $\dot{\gamma}$ and the dislocation density ρ as

$$c_v = \frac{b^2}{L} \int \frac{J\dot{\gamma}}{\rho} dt \tag{3}$$

where b is the Burgers vector and L is the mean-free path for the generation of a vacancy by a moving jog. Vacancy production by this mechanism is thought to occur homogeneously throughout the material. Several large scale atomistic studies have revealed this "jog dragging" mechanism for vacancy production [67, 68].

Measurements of vacancy concentration using electrical resistance, positron annihilation spectroscopy, and X-ray spectroscopy indicate that the vacancy supersaturation in a material increases with applied strain, as predicted by

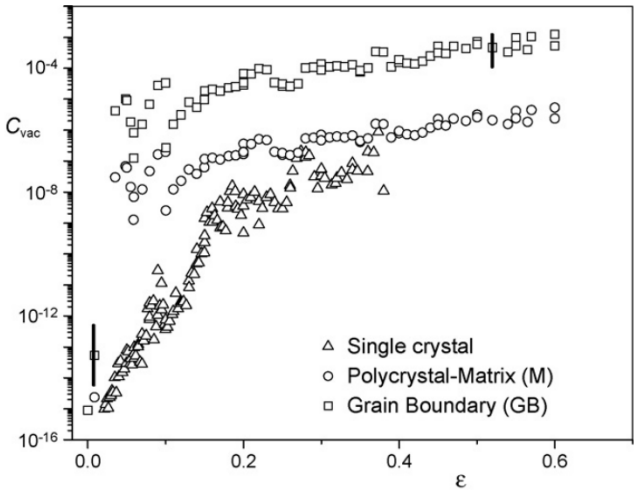

Figure 5: The vacancy concentration produced in copper samples during compression is shown as a function of strain. Vertical lines indicate uncertainty in the data. This figure is from reference [60]

both mechanisms [59, 61, 66, 69]. Example measurements of vacancy supersaturation in Cu as a function of applied strain are provided in Figure 5. Both positron annihilation spectroscopy and X-ray spectroscopy measurements of deformed samples indicate that there is an upper limit for the deformation-induced vacancy concentration of $\sim 10^{-4}$ at atmospheric pressure, which may be reached at strains of $\sim 100\%$ [65].

Studies of quenched and irradiated materials have shown that a supersaturation of vacancies will promote vacancy clustering [70–77]. There is a large body of literature on void nucleation in the context of classical nucleation theory, according to which the free energy change associated with formation of a n vacancy cluster is [48, 78, 79]

$$\Delta G = -nk_BT \ln\left(c_v/c_v^{eq}\right) - n\sigma^H\Omega + E_n \tag{4}$$

where σ^H is the hydrostatic stress, Ω is the atomic volume, and E_n is the

formation energy of the cluster. Often the cluster is approximated as a spherical cavity of radius r with isotropic surface energy γ, giving $E_n = 4\pi r^2\gamma$. Eq. 4 indicates that the primary driving forces for cluster growth are vacancy supersaturation (expressed as $c_v/c_v^e q$) and the work done by hydrostatic stress, which act to drive down the free energy.

However, unless vacancy clusters are stabilized by trapping at interstitial gases or the work performed by an applied hydrostatic stress, they collapse to form planar defects when they exceed a critical size on the order of 10 vacancies [70–77, 80, 81]. During ductile fracture, the primary stabilizing mechanism for vacancy clusters is thought to be the applied hydrostatic stress [65, 82]. The relationship between the size of the largest vacancy cluster that can form without collapsing and the applied stress is schematically illustrated in Figure 6. Very small vacancy clusters (< 10 vacancies) are intrinsically stable. With small to moderate cluster sizes ($\sim 10-50$ vacancies), the necessary amount of hydrostatic stress to stabilize the void increases with cluster size. However, since large voids are stable, the hydrostatic stress eventually begins reducing back to zero. The stress necessary for void formation can be produced either by macroscale loading or at the microscale from local stress fields due to other crystallographic defects or orientation mismatches between grains. For example, the atomistic simulations of Zarnas et al. [83] illustrated that the stress field of microcracks can serve to attract excess vacancies. However, below a threshold stress intensity, the effect is defeated by vacancy annihilation at the crack free surfaces.

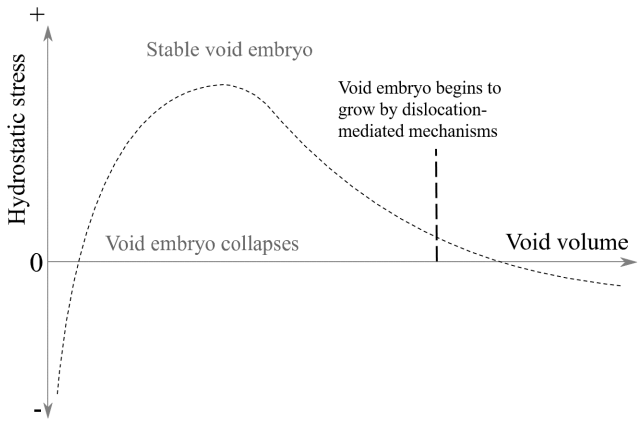

Figure 6: A qualitative plot of hydrostatic stress versus the volume of a stable vacancy cluster, i.e. one that will not collapse, is shown. This plot illustrates the concept that a vacancy cluster will collapse into a compact defect (such as a dislocation loop or a stacking fault tetrahedron) if the applied hydrostatic stress is too low.

2.1.2. Dislocation pile-ups

At stresses above the Peierls stress, glissile dislocations move through the lattice until encountering an obstacle such as a grain boundary. Dislocations moving on a shared slip system which are unable to climb or cross-slip out of the plane pile up at this obstacle as shown in the TEM image in Figure 7. The stress at the leading dislocation in a pile-up is a function of the number of dislocations involved (see Section 2.3) [84]. While pile-ups were believed to be important for void nucleation in a number of early theories, as discussed below, experimental evidence suggests that they are not common in deformed structural metals. Rather, dislocation networks tend to take on more intricate, patterned structures that preclude simple pile-up type structures from forming.

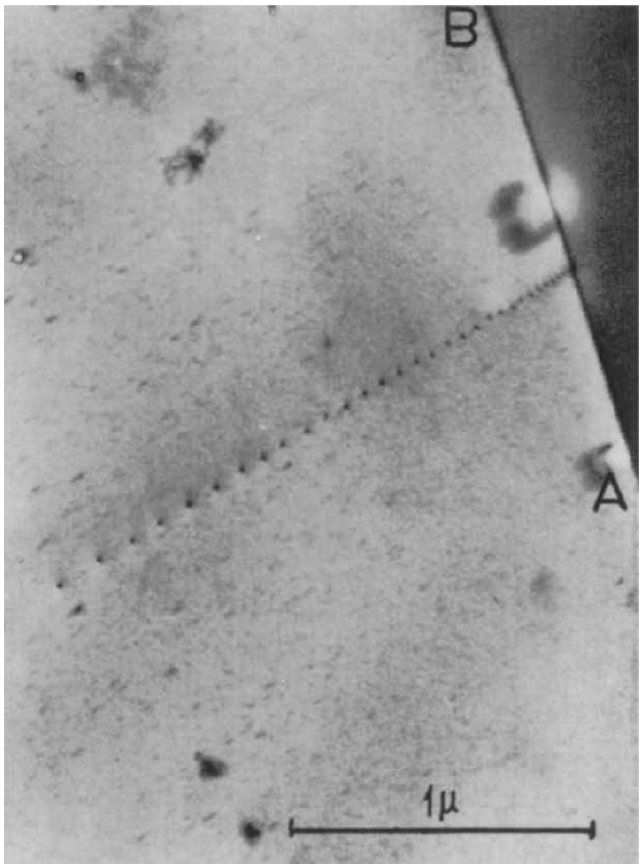

Figure 7: A TEM micrograph of edge dislocations in a pile-up configuration in BCC tungsten is shown. Such grain-boundary pile-ups were not observed to nucleate cracks in tungsten. This image is from reference [85].

2.1.3. Dislocation boundaries

With increasing plastic deformation, dislocation-dislocation interactions become more prevalent leading to an increasingly complex arrangement of sessile pinning segments. Ultimately this progression causes dislocations to cluster together into heterogeneous arrangements comprised of regions of high and low dislocation density. By $\approx 5\%$ applied strain, these heterogeneous dislocation structures are observed throughout metals that deform by slip [86–90]. These structures include dislocation cell walls and cell block boundaries and are also referred to as low energy dislocation structures (LEDS) [88]. The term dislocation boundaries will be used in this article.

Cell blocks and dislocation cell walls are illustrated in the TEM micrograph provided in Figure 8. Dislocation cell walls separate equiaxed, relatively dislocation-free volume elements (dislocation cells) and are almost always low-angle boundaries ($< 2^{\circ}$). Dislocation cells are usually organized into groups of extended, lamellar features known as cell blocks [87]. The differences in slip between neighboring cell blocks lead to the creation of so-called "geometrically necessary boundaries", which form to accommodate the deformation-induced rotations between cell blocks [91]. These block boundaries contain significantly higher dislocation densities and generally have larger misorientations across them than do cell walls [91]. More information on the dislocation structures produced by cold working can be found in references [87, 91–93].

2.1.4. Deformation twins

For some metals, particularly hexagonal close-packed (HCP) and low stacking fault energy face centered cubic (FCC) metals, plastic deformation

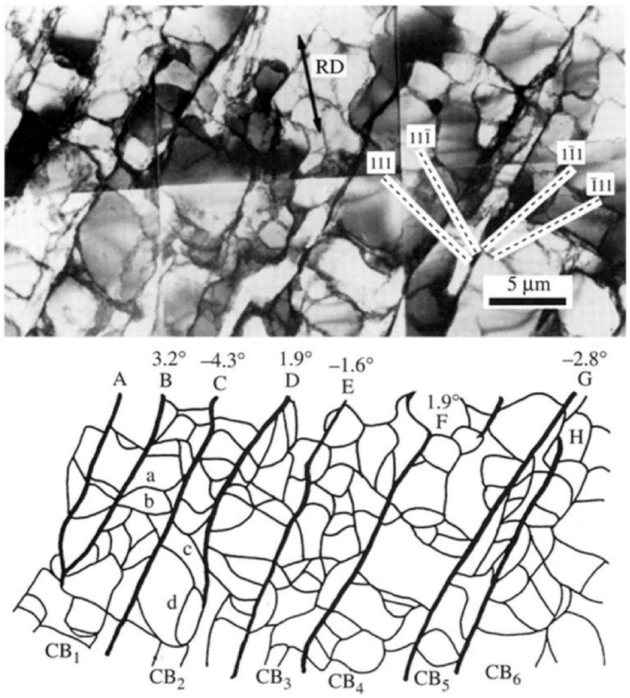

Figure 8: (a) A TEM micrograph and (b) a sketch of the microstructure in specimen of high-purity Al reduced 10% by cold-rolling are shown. Cell block boundaries (CB_x) are colored black in the sketch, while cell walls are colored light gray. The rolling direction (RD) is indicated in the micrograph. Similar microstructures are created by plastic deformation in other bulk metals that deform by slip. This image was taken from reference [94].

is accommodated by a mix of slip and deformation twinning. Deformation twinning is favored over dislocation slip by low temperatures [95] and high strain rates [96, 97] and occurs in HCP and BCC metals during shock [98] and cryogenic [99] testing. Deformation twins form heterogeneously throughout the material at locations typically associated with high stresses, e.g. grain boundaries and slip bands [100, 101]. The mechanisms governing the three stages of twin formation, i.e. nucleation, propagation, and thickening, depend on many factors and are areas of ongoing research. For more information on deformation twins the reader is directed to references [100, 101].

When a propagating twin is blocked by a grain boundary, particle, or other obstacles, this interface is generally thought to be associated with a significant stress concentration [100]. The distribution of stress around a deformation twin and its relationship to twin thickness, coherency, and the obstacle has been the subject of numerous experimental and theoretical studies [102–106]. A recent study of the stress distribution around twins in Zircaloy using high-resolution EBSD (HR-EBSD) showed that the maximum stress concentration occurred at the twin tip [102]. Example EBSD and HR-EBSD datasets from this study are provided in Figure 9. The magnitude of the stress concentration depended on the obstacle, with the greatest stress concentrations occurring at twin/twin intersections. However, this and other recent studies have not considered the stress concentration at the intersection between twins and second-phase particles or inclusions.

2.2. Void nucleation at deformation-induced defects

This section reviews observations of void nucleation at deformation-induced defects and several proposed theories for void nucleation at these features.

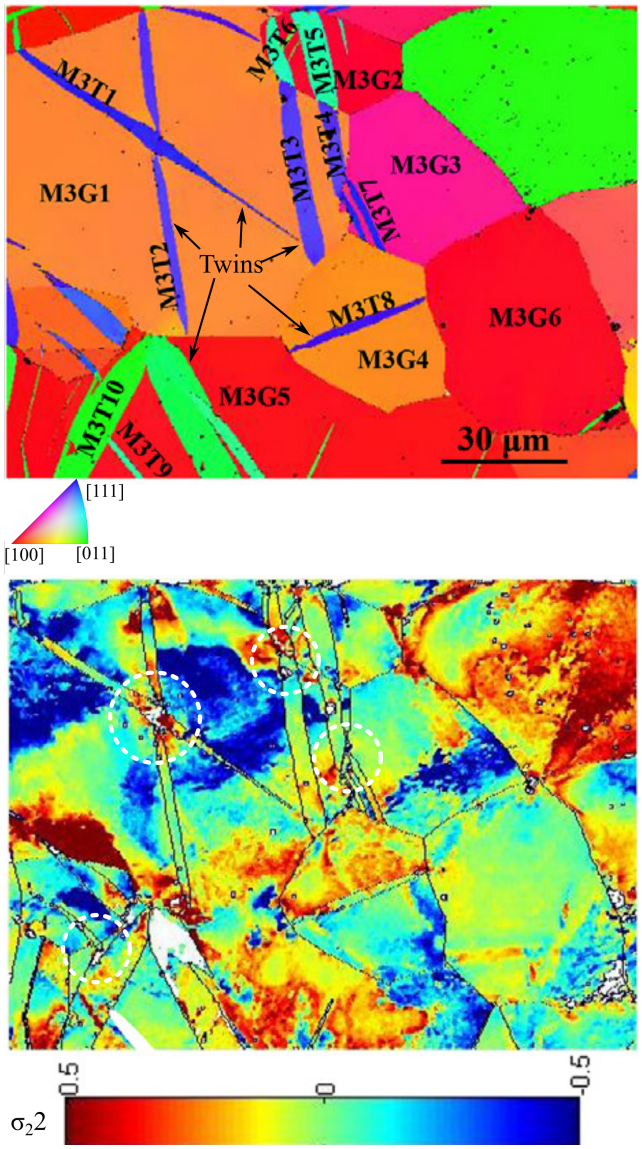

Figure 9: Example EBSD and HR-EBSD data from the microstructure around deformation twins in a Zircaloy-2 material deformed to 2.7% strain in tension are shown. EBSD data are shown as in inverse pole figure map in (a). Elastic stress σ_{22} are provided in (b). The scale of the log10 scale bar in (b) is GPa. Grains in (a) are labeled "M3GX", where X refers to a number. Twins in (a) are labeled "M3TX", where X refers to a number. A few twins are highlighted in (a). Four twin/twin intersections are circled in (b). Note that 2 are associated with areas of elevated stress while the other two are not. These images were adapted from reference [102]

.

Although the earliest theories of void nucleation proposed that dislocation arrays played a key role, intragranular void nucleation in the absence of particles remains the most poorly understood mechanism of void nucleation. Indeed, it was only recently determined that voids in ductile metals that deform by slip do not nucleate at grain boundaries [107], at least in some metals under quasistatic loading conditions. Instead, voids primarily form at the dislocation cell walls and cell block boundaries created by plastic deformation.

2.2.1. Dislocation combination

We begin with one of the earliest theories of void nucleation: dislocation combination. In 1958, Cottrell hypothesized that voids could form at slip-band intersections by dislocation combination [108]. The key concept is that certain dislocations can act as "cavity dislocations," meaning that voids can nucleate from the core of the dislocation. The prime example Cottrell considered was the reaction of two $\langle 111 \rangle$ dislocations in a BCC metal such that

$$\frac{a}{2}[\bar{1}\bar{1}1] + \frac{a}{2}[111] \rightarrow a[001] \tag{5}$$

The resulting dislocation is energetically favorable, and its Burgers vector is parallel to the $\{001\}$ cleavage plane in BCC metals; to quote Cottrell, it is a "cleavage knife." For these reasons, Cottrell proposed that this dislocation would form and nucleate a crack in the solid.

While this mechanism is elegant and simple, there is no direct experimental or theoretical evidence that voids can nucleate in this way. Since Cottrell proposed such a mechanism, our understanding of the dislocation core has significantly improved with the advent of modern atomistic simula-

tion tools [109, 110], and no study has revealed nucleation by this mechanism. For example, in recent large-scale MD simulations of plasticity in BCC Ta, many ⟨001⟩ junctions formed but no voids or cracks were observed to form over a variety of straining conditions [111].

2.2.2. Void nucleation at slip band intersections

Void nucleation at slip band intersections has been observed in MD simulations of low stacking fault energy (SFE) FCC metals [112]. Pang et al. found that when stacking faults intersected each other, they produced "vacancy chains" which subsequently grew via nucleation of dislocations. The sequence depicting this mechanisms is shown in Fig. 10. It is important to note that defect-free (perfect) crystals were used in these simulations and then loaded at a very high strain rate. It is unclear if this nucleation mechanism is relevant to lower strain rate loading of materials initially populated with dislocations.

Müllner [113] has analyzed the possibility of crack/void nucleation at intersections between deformation twins. He argued that the head of a secondary deformation twin could be treated as a dislocation wall (or, equivalently, a disclination dipole), and that the tensile stress/strain field below the wall would nucleate a crack in the primary twin. This nucleation would be suppressed if dislocations, which were either already present or nucleated by the local stresses, could relax the stress/strain field. From this viewpoint, thinner twins, which provide less volume for dislocations to nucleate within, and lower dislocation densities would promote void nucleation, because dislocation-mediated relaxation would be more difficult. Hence, Müllner argued his theory explained why austenitic steels become brittle

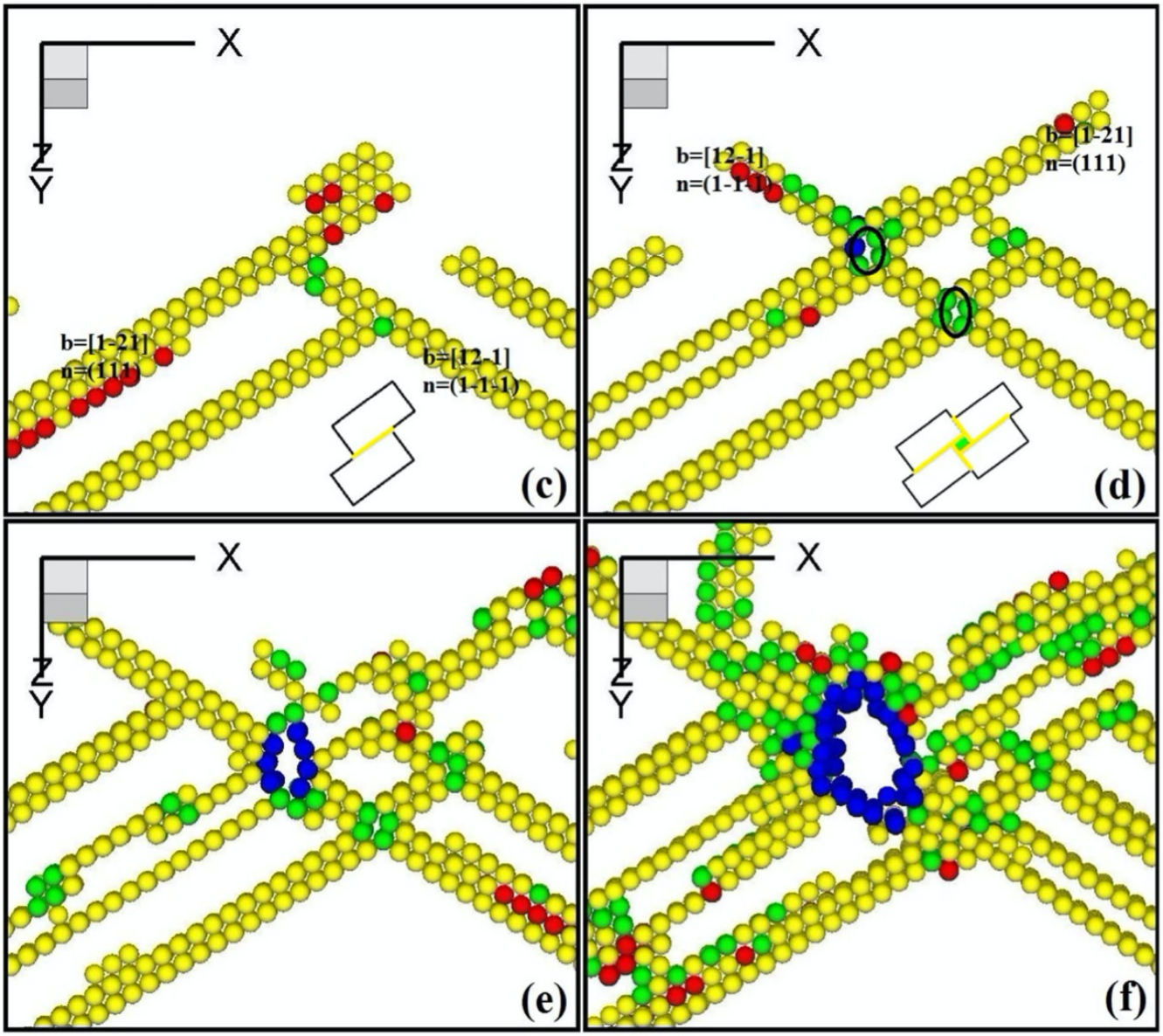

Figure 10: Nucleation of voids in low SFE FCC metals at stacking fault intersections via formation of vacancy chains. This figure taken from reference [112].

at low temperatures [113–115] where deformation twinning is the dominant deformation mechanism. This behavior is also observed in Ti alloys [50, 116]. Note that Müllner's theory predicts that thinner twins promote void nucleation.

2.2.3. Void nucleation by vacancy condensation and subsequent growth by dislocation adsorption

In contrast to any other void nucleation mechanism, voids formed by vacancy condensation are expected to be somewhat homogeneously distributed in regions of high stress. Such voids have been reported in studies of deformed Cu [117] and Au [118]. In Cu samples containing distributed CuO_2 particles, nanoscale ($\approx$ 10 to 100 nm) voids were observed to be homogeneously distributed throughout the necked gauge region of samples strained to 60%. Examples of these voids are shown in Figure 11. As many of these voids could not be associated with any microstructural features, the authors concluded that they nucleated at vacancy clusters. Similarly, Wilsdorf [118] observed distributed, $\approx$ 10 nm diameter voids near the crack flank of ruptured gold specimens. These can be seen in the TEM image provided in Figure 12.

Further evidence that vacancies can play a role in the formation of voids comes from the work of Dyson [119, 120]. It was observed that voids nucleated near grain boundaries in Nimonic 80A after room temperature deformation and subsequent annealing. No voids were observed before annealing, suggesting that voids nucleated by vacancy condensation when the vacancy diffusivity was increased.

From these studies, we conclude that vacancy condensation can create

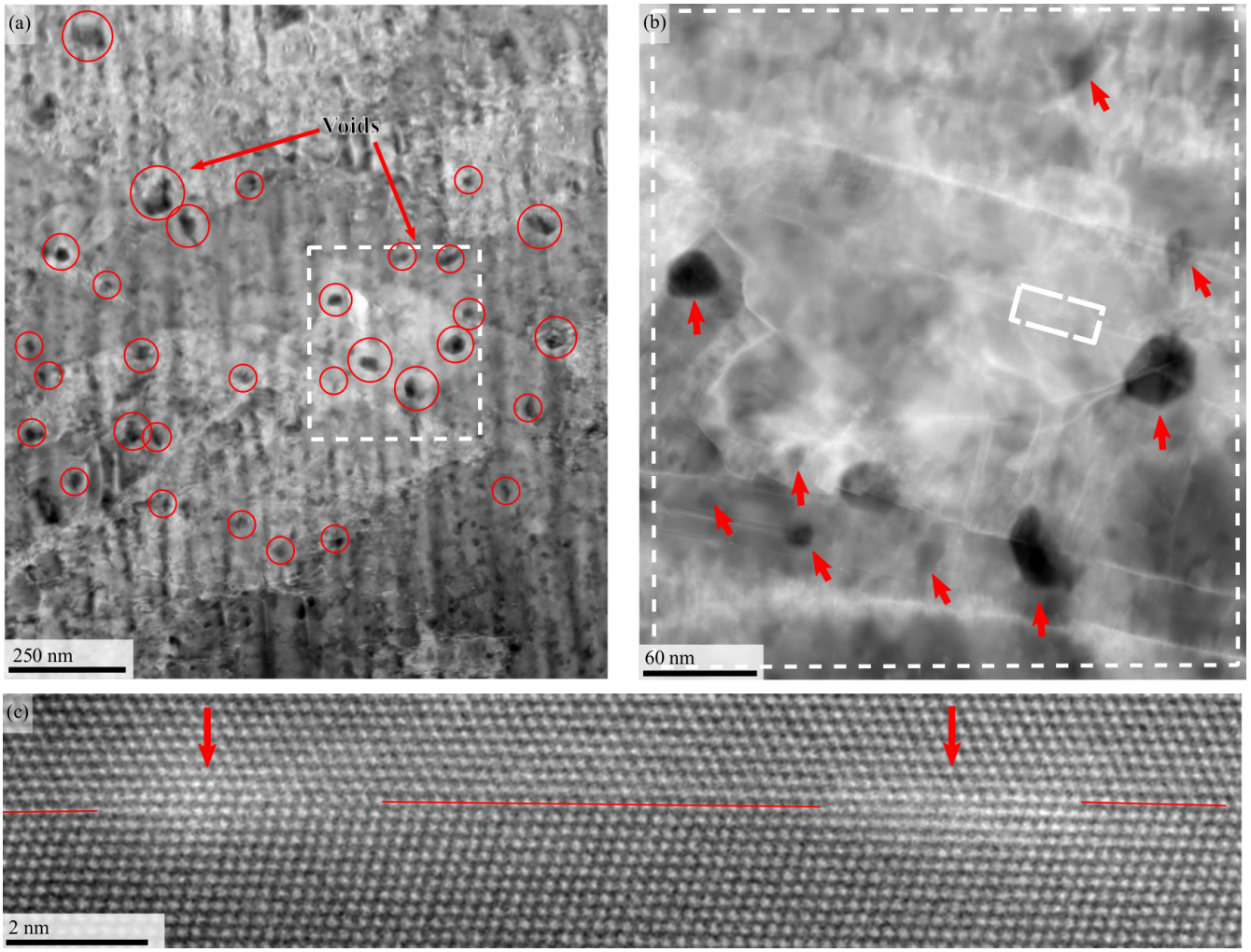

Figure 11: TEM images showing nanoscale voids thought to be created by vacancy condensation are provided. A high-magnification image of the boxed area in (a) is shown in (b). Several of the voids are highlighted with circles and arrows. These images were taken from a sample extracted from the center of the the necked gauge region of a Cu sample deformed to 60% strain. These images are from reference [117].

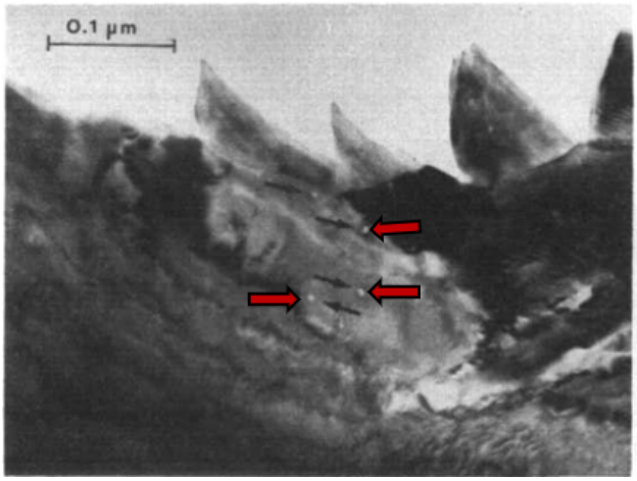

Figure 12: Nanoscale voids thought to be created by vacancy condensation can be seen near the crack flank of a ruptured gold specimens in this TEM image from reference [117].

voids during quasistatic, room-temperature deformation in at least some materials. However, vacancy diffusion is too slow to explain the growth of micron-scale voids during quasistatic deformation near room temperature. Indeed, it was observed that only a small fraction (≈ 1 in 10^4) of the nanoscale voids created by vacancy clustering in Cu grew to the microscale [117]. Voids created by vacancy clustering thus must grow by another mechanism to create failure-critical voids. This mechanism and its implications for void formation at deformation-induced defects is now considered.

It is generally agreed that void nuclei grow by dislocation-mediated mechanisms [66, 121]. There has been some controversy recently as to what the primary mode of dislocation-mediated growth is. While a number of authors have argued that voids grow by nucleating dislocations from their surface [122–124], Nguyen and Warner [125] showed that this process was too slow to explain experimentally observed growth rates relevant to quasi-static

loading. Recently, the authors [126] used molecular dynamics to show that voids are able to grow readily in the presence of a high density of dislocations by adsorbing the dislocations. From this viewpoint, a high dislocation density is necessary to enable voids to grow from the nanoscale to microscale, with the driving force for growth coming from the local hydrostatic stresses. Voids that grow in this manner would naturally be ellipsoidal in shape as they would be biased to grow along existing dislocation boundaries.

Consistent with the mechanism of void growth by dislocation adsorption, several studies reported that, in particle-free metals that deform by slip, voids primarily nucleate at dislocation boundaries. Early studies on void nucleation in particle-free metals, primarily conducted by Wilsdorf and coworkers, examined fracture of thin films of pure, single-crystal metals [127]. In-situ TEM investigations of void nucleation in single-crystal thin films of Be observed voids nucleating at dislocation boundaries [128, 129], as shown in Figure 13. Ex-situ TEM analysis of fractured thin-film α-Fe and Ag single crystals also observed voids nucleated at dislocation boundaries [118, 130, 131] suggesting that, in particle-free metals, deformation before fracture creates void nucleation sites, or facilitates early-stage growth in voids that were previously nucleated by vacancy condensation.

Dislocation boundaries are also the primary location where voids are observed in bulk, particle-free, polycrystalline metals. In high-purity Ta (a BCC metal), Noell et al. observed voids exclusively at dislocation boundaries, particularly cell block boundaries [107]. An example of this is provided in Figure 14. Consistent with a dislocation adsorption-mediated growth mechanism, voids were ellipsoidal [107]. No voids were observed at grain bound-

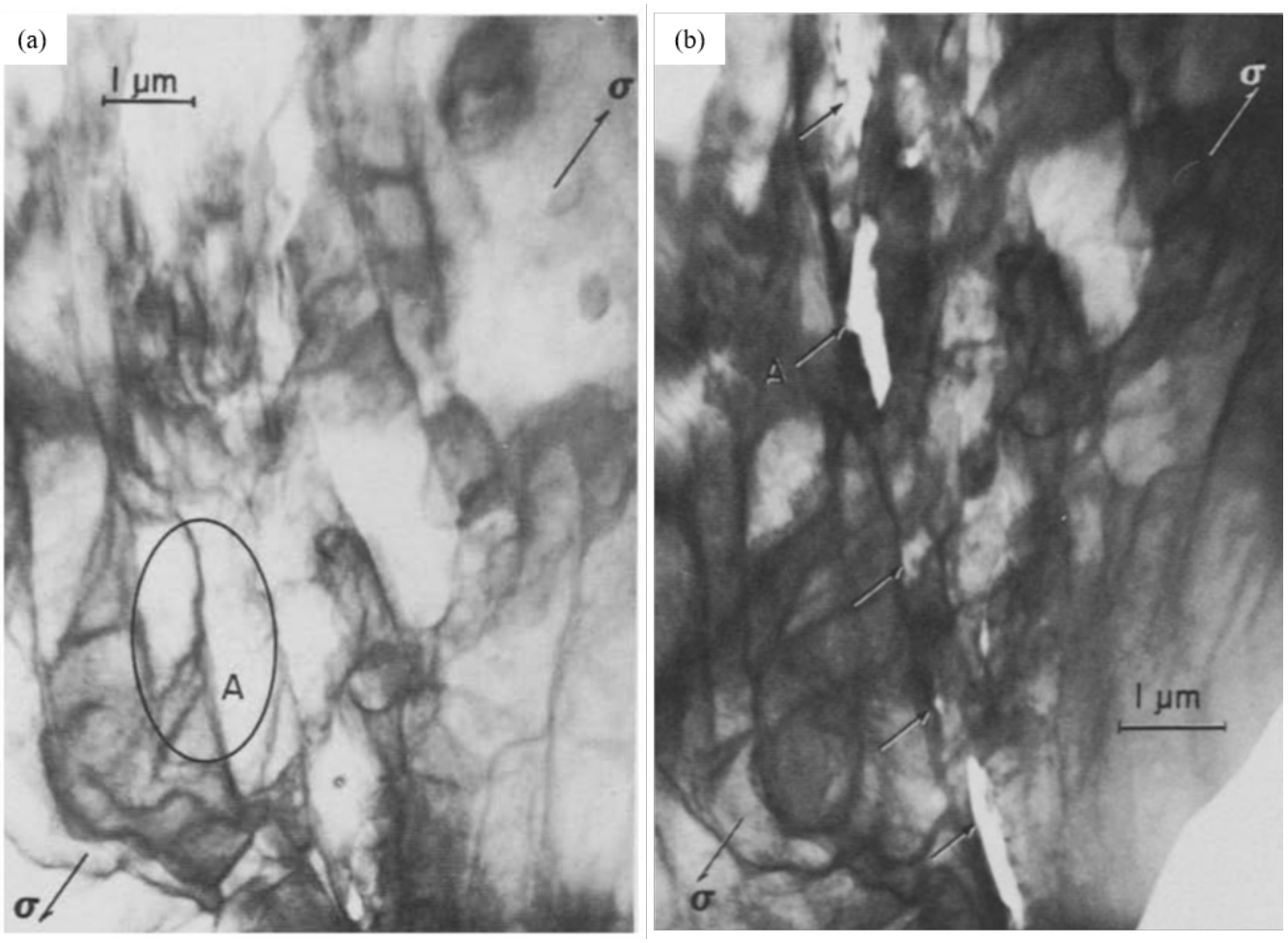

Figure 13: TEM micrographs of (a) a strained Be single crystal before and (b) after void nucleation. These images show micrometer-scale voids at deformation-induced dislocation boundaries, likely cell block boundaries. These images are from reference [129].

aries in this study. EBSD and transmission Kikuchi diffraction (TKD) data demonstrated that the misorientation angle across the dislocation boundaries associated with incipient voids was always greater than 5°. However, a large misorientation angle across a dislocation boundary was not always associated with voids. For example, the void shown in Figure 14 was located at a boundary with a misorientation of 15°, while the misorientation across a cell block boundary within ≈ 0.5 μm of this void was greater than 40° and no void was observed. A few voids were observed at dislocation cell walls rather than cell block boundaries. These results suggest that a simple metric such as misorientation angle across a dislocation boundary is not predictive of void nucleation, as suggested by early theoretical work [127].

A subsequent study of void nucleation in particle-free Al (an FCC metal) also observed voids at dislocation boundaries [82]. No voids were observed at grain boundaries. Unlike Ta, the incipient voids characterized in Al were associated with low-angle (≈ 2°) dislocation cell walls. These results indicate that dislocation boundaries are either important to void nucleation or the early-stage growth of otherwise nucleated nanoscale voids in particle-free metals that deform by slip, regardless of crystal structure. Voids may also emerge at dislocation boundaries in particle-containing materials, as observed by the authors in their study of void nucleation in a Cu material containing dispersed copper oxide particles. While a few voids were associated with second-phase particles, all were associated with one or more dislocation boundaries and most were particle-free [117].

Further evidence that dislocation boundaries are critical to the early stages of void formation came from several recent studies which showed that

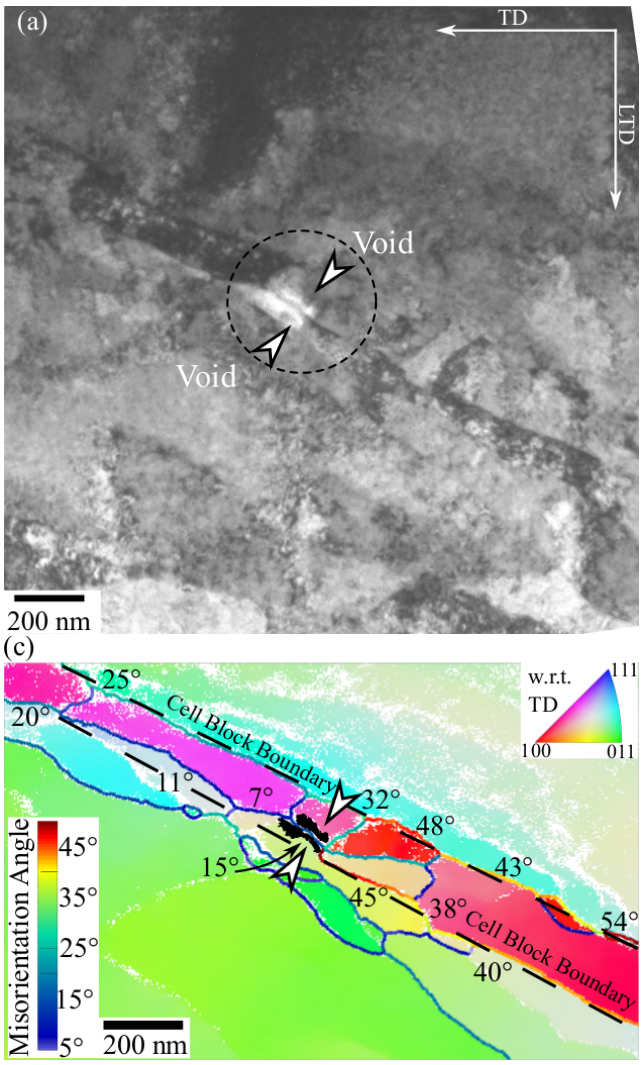

Figure 14: A TEM micrograph of incipient voids at a cell block boundary in a deformed, high-purity Ta material are shown in (a). Transmission kikuchi diffraction (TKD) data from the microstructure around the voids shown in (a) are presented in (b) as an IPF map colored with respect to the TD. The misorientation angle across each segment of the boundary is shown in (b). The misorientation across the portion of the cell block boundary at which voids emerged was significantly less than that across many nearby boundaries. These images are from reference [107]

voids do not nucleate in particle-free materials if the formation of dislocation boundaries is suppressed. In single-crystal Fe samples having different cross-sectional areas, the failure mode depended on whether or not dislocation boundaries formed [132]. EBSD data demonstrated that samples that failed by void nucleation, growth, and coalescence contained dislocation boundaries, see Figure 15. In contrast, failure by catastrophic shear [15] with no evidence of void nucleation occurred in specimens that were free of dislocation boundaries. Similarly, Lim et al. [133] observed that the failure of single-crystal Ta depended on whether dislocation boundaries formed. In this study, the formation of these boundaries depended on crystallographic orientation relative to the loading direction. Strain localization followed by the creation of a dense network of dislocation boundaries was observed in samples oriented with the [100] or [111] direction along the loading direction but not in samples oriented with the [110] parallel to the loading direction. Failure in the first two samples occurred by void nucleation, growth, and coalescence, while samples oriented with the [110] parallel to the loading direction failed by necking to a point. Incipient voids were observed at dislocation boundaries in samples oriented with the [100] or [111] direction along the loading direction.

When dislocation boundaries are annihilated by dynamic recrystallization, voiding is correspondingly suppressed. Such a case was observed in high-purity Al samples, where it was observed that void nucleation was suppressed in samples that underwent room-temperature dynamic recrystallization [82]. If these boundaries reformed after dynamic recrystallization, voids subsequently nucleated at them. These results indicate that dislocation sub-

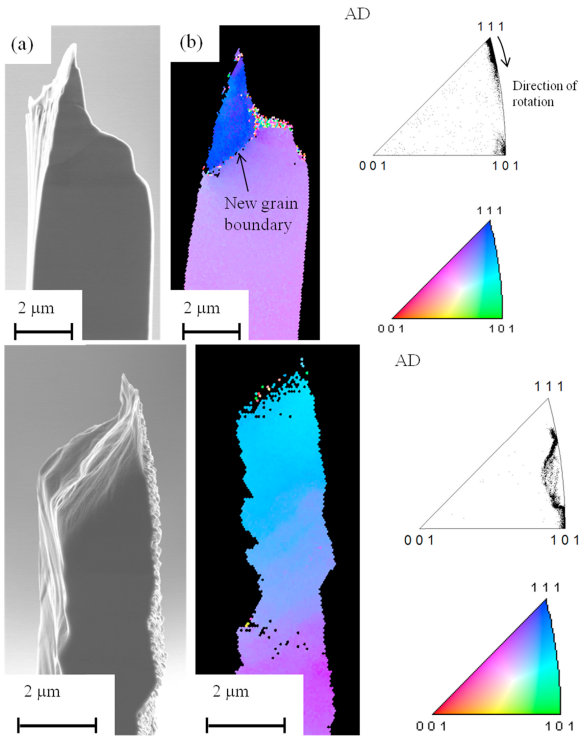

Figure 15: SEM images and inverse pole figure (IPF) maps of fractured Fe single crystals are shown. Images on the left show a specimen with a 28 μm^2 cross section while images on the right show a specimen with a 16 μm^2 cross section. Both samples had the same crystallographic orientation before deformation. The boundary labeled "New grain boundary" is a deformation-induced dislocation boundary. These images are from reference [132].

structure plays a critical role in void nucleation in particle-free materials.

These observations suggest that deformation-induced defects control the formation of microscale voids in ductile metals containing few or no particles. Voids appear to first nucleate homogeneously at the nanoscale by vacancy condensation. Nanoscale voids at dislocation boundaries then grow to the microscale via a dislocation adsorption mechanism. The location at which microscale voids form thus depends on the evolution of dislocation boundaries within the material.

2.3. Void nucleation at grain boundaries

Grain boundary decohesion is commonly observed during ductile rupture of materials with limited plasticity, e.g. in many HCP metals and BCC metals below their ductile-to-brittle transition temperature [114–116, 134–137]. This proposed mechanism is similar to particle/matrix decohesion, with one significant difference: while deformation of the particle is often fully elastic, the grains on either side of a boundary have (at least some) plasticity. As discussed in this section, grain boundary plasticity and the accumulation of dislocations on either side of the interface play a determinative role in grain boundary decohesion. These roles are often overlooked, though, and unrealistic mechanisms of grain boundary decohesion that only consider the local stress state [138, 139] or dislocation density at a grain boundary [108] are still invoked in many contexts [140–142].

This section presents experimental observations of grain boundary decohesion, discusses the deficiencies of early models of grain boundary decohesion, and presents recent theoretical work in this area. Because void nucleation by grain boundary cleavage does not fundamentally depend on the deformation mechanism (slip versus twinning), both of these cases are treated in this section. The case of brittle failure by grain boundary delamination, which may occur when hydrogen, solutes, or liquid metal segregates to the boundary [143], is outside the scope of the present review. The milder situation arising from grain boundaries weakened by intergranular precipitation leading to ductile intergranular fracture, which is often associated with particle-free zones in age-hardening alloys, is briefly treated at the end of this section

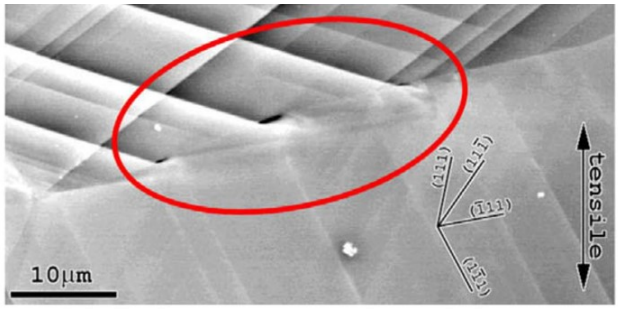

Figure 16: An electron channeling contrast image of three incipient voids at twin/grain-boundary intersections in TiAl is shown. This image is from reference [135].

In both pure and particle-containing metals that deform by twinning, voids are sometimes observed at grain boundary/twin intersections or twin/twin intersections. Ng et al. and Bieler et al. [135, 137] demonstrated that voids in TiAl (an intermetallic) primarily nucleate at grain-boundary/twin intersections. An example of this is provided in Figure 16. Bieler et al. [134] also observed that voids in high-purity α-Ti (HCP) nucleate at the intersection between T_1 (primary) and T_2 (secondary) twins, as shown in Figure 17.

At cryogenic temperatures, void nucleation in some materials occurs more readily at grain-boundary/twin intersections than at second-phase particles [113, 116]. This has been observed in the α-Ti alloy Ti-5Al-2.5Sn [116] and in nitrogen-alloyed austenitic stainless steels (FCC) [113, 115]. Recent studies of Mg alloys (HCP) indicate that void nucleation in these materials can also occur at lower stresses at grain-boundary/deformation twin intersections than at second-phase particles [144–148]. When deformation twinning was suppressed by decreasing the grain size of Mg alloy AZ31, void nucleation was suppressed and both the strength and ductility increased significantly [147, 148].

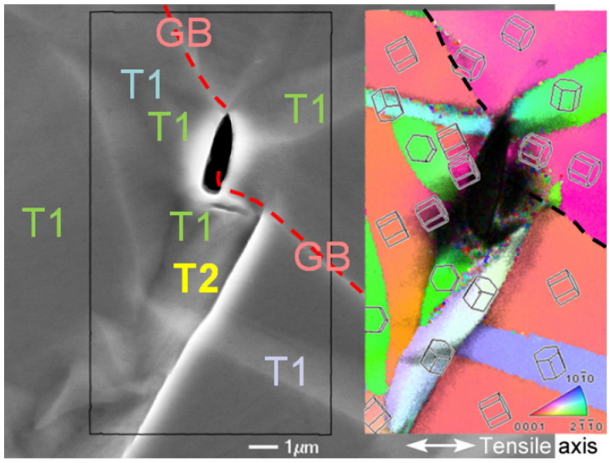

Figure 17: An image of an incipient void at the intersection of a T_1 twin, a T_2 twin, and a grain boundary in α-Ti is shown. This image is from reference [134].

The importance of grain boundaries to ductile fracture in BCC metals is apparent from testing single crystals, which often show tremendous ductility well below the ductile-to-brittle transition temperature of polycrystalline materials [142, 149–151]. Because of this, it has long been assumed that void nucleation in polycrystalline BCC metals begins at grain boundaries that act as barriers to dislocation transmission, such as that shown in Figure 7 [142, 152]. However, as discussed in the previous section, void nucleation in Ta and Fe is observed at dislocation boundaries.

For the case of relatively brittle BCC metals such as Mo and W, no direct observations of the microstructural features associated with void nucleation have been made for bulk materials. While it is unclear if TEM observations of void nucleation in thin-film tungsten samples translate to the bulk material, such a study observed that voids nucleated within arrays of edge dislocations formed on the {110} plane near grain boundaries [85]. Intriguingly, voids

were not associated with arrays of edge dislocations formed on {112} planes.

Void nucleation by boundary cleavage was also investigated in a recent atomistic study of a planar Σ9 grain boundary in tungsten [153]. It was observed that under some biaxial stress states, a void nucleated at grain boundary dislocations. In other cases, though, lattice dislocations nucleated at the grain boundary and subsequently acted as a nucleation site for voids. This result conflicts with a study by Fensin et al. [154] who performed MD simulations of shock spall at Al grain boundaries. They concluded that the presence of dislocation content at or near the grain boundary increased the stress that was necessary for void nucleation, since energy dissipation could also occur by dislocation slip. However, under these spall conditions Agarwal and Dongare [155] have showed that the shock direction can strongly influence the nucleation behavior. For example, void nucleation was associated with dislocation/twin activity during shock in the $\langle 0\,0\,1 \rangle$ and $\langle 1\,1\,1 \rangle$ directions, but not in the $\langle 0\,1\,1 \rangle$ direction. Hence, it is difficult to determine if the finding of Fensin et al. is universal since only three boundary orientations were considered. These studies suggest that the defect content and atomistic structure of the grain boundary interact in non-trivial ways to promote void nucleation.

MD simulations and experiments by Noell et al. also suggest that twin/grain-boundary intersections are important void nucleation sites [156]. During uniaxial loading at elevated temperature (300° C), it was observed experimentally that voids preferentially nucleated where annealing twins (which were present in the material prior to loading) intersected grain boundaries. MD simulations revealed the same preference for nucleation at annealing

twin/grain-boundary intersections. Further analysis of the MD results revealed that the driving force for void nucleation (in terms of the local atomic stress and energy) was no greater at these intersection sites. This led the authors to conclude that the activation barrier for void nucleation must be lower at these intersections sites, i.e. they are weak spots.

While there is strong evidence that the intersection between deformation-induced defects and grain boundaries promotes void nucleation, particularly grain boundary/deformation twin intersections, no theory has yet fully explained the mechanism by which these voids form. Several relevant theories, as well as the challenges with each, are now reviewed.

Early investigators hypothesized that, if a slip band is blocked by a grain boundary, the tensile stress at the head of the slip band could exceed the cohesive strength of the material and nucleate a void [139]. A schematic of this is shown in Figure 18. This mechanism of void nucleation is now known as the Zener-Stroh mechanism [141]. Zener predicted that the void would nucleate on a plane normal to the active slip plane within the grain in which the dislocation pile-up formed [139], while others predicted that it would happen in the adjacent grain or within a polygonized array of dislocations [14].

Both energy-based and strength-based failure criteria have been invoked with the Zener-Stroh mechanism. For example, Stroh [138, 157] computed the elastic strain energy in the tensile stress region below a pile-up and assumed fracture would occur when this energy exceeded the energy of the new free surfaces of the crack. Combining his result with analysis by Eshelby et al. [158] on the geometry of dislocation pile-ups, Low [159] determined that the critical number of dislocations in a pile-up for the energy-based theory

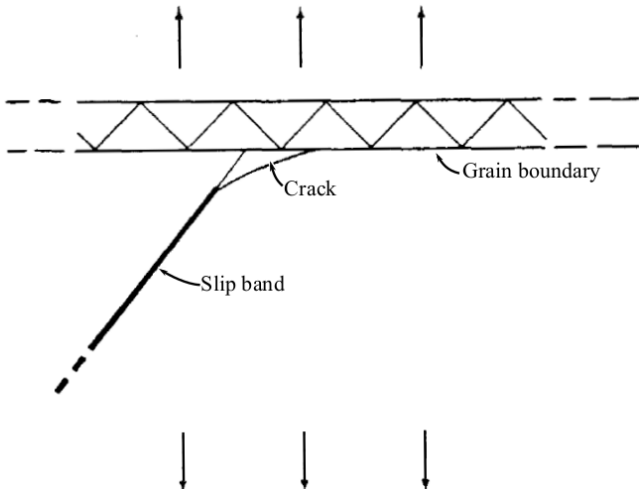

Figure 18: The Zener-Stroh mechanism of crack nucleation at a blocked slip band is illustrated. This image was modified from reference [139]. There is little experimental evidence that this mechanism occurs during quasistatic, room-temperature deformation.

was

$$n = \frac{3\pi^2\gamma}{8b\tau_a} \tag{6}$$

where γ is the surface energy, b is the magnitude of the Burgers vector, and τ_a is the applied shear stress. For common values of fracture stress and surface energy, this equation predicts that the pile-up must contain 10^2 to 10^3 dislocations for voids to nucleate in this manner [138, 157]. From the strength-based perspective, using Koehler's [160] expression for the maximum tensile stress ahead of a dislocation pile-up, the critical number of dislocations is

$$n = \frac{\sigma_{\text{tensile}}}{\alpha\tau_a} \tag{7}$$

where α is a constant on the order of unity. Assuming $\sigma_{\text{tensile}} \sim 10$ GPa and $\tau_a \sim 100$ MPa, we obtain $n \sim 10^2$ dislocations, similar to the energy-based theory. While the Zener-Stroh mechanism is appealing in many ways, it has been dismissed by many researchers over the years on the following grounds.

First, shear stresses on the order of the theoretical shear strength are necessary to form the pile-up [159]. Second, the large dislocation pile-ups invoked by these models do not generally form during plastic deformation [92]. Finally, large local stresses at the head of the pile-up are likely dispersed by secondary slip [161].

More recent studies have demonstrated that two interrelated factors determine if voids will nucleate by grain-boundary cleavage [115, 134]:

1. Does the geometric relationship between the active slip/twinning systems on either side of the boundary allow for easy slip transfer?

2. If not, can the local stress/strain at the boundary be relaxed either by existing dislocations or by the nucleation of new dislocations?

Depending on the orientation of the grains on either side of the boundary and the activated slip system(s), a range of slip transfer cases may occur. At the extremes, the boundary can either be impenetrable, with no shear transfer across it, or nearly transparent to dislocations, with near-complete transmission from one side to another. For most boundaries, though, slip in one grain is transferred imperfectly into the next and some residual grain boundary dislocations are left behind. In these cases, the shape change at the boundary must be accommodated by local slip in the neighboring grain.

Kumar et al. [136] determined that void nucleation at twin/grain-boundary intersections in TiAl is facilitated by residual dislocation content within the boundary. Based on their analysis, a fracture initiation parameter, F_1, was proposed as

$$F_1 = m_{\text{twin}} |\mathbf{b}_{\text{twin}} \cdot \mathbf{t}| \sum_{\text{other}} \mathbf{b}_{\text{twin}} \cdot \mathbf{b}_{\text{other}} \tag{8}$$

The geometric considerations associated with this parameter are illustrated in Figure 19 and the reasoning behind it is as follows. The Schmid factor of the operating slip (or twin) system, m_{twin}, drives a slip band (or twin) into the grain boundary, which then "opens up" the grain boundary by an amount that is proportional to $\mathbf{b}_{\text{twin}}$. The local tensile force $\mathbf{t}$ then acts to open the interface further by an amount proportional to $|\mathbf{b}_{\text{twin}} \cdot \mathbf{t}|$. However, this opening can be counteracted or relaxed by slip in the opposing grain, as long as the slip systems in that grain are aligned appropriately; the potential for such relaxation is proportional to $\sum_{\text{other}} \mathbf{b}_{\text{twin}} \cdot \mathbf{b}_{\text{other}}$, where $\mathbf{b}_{\text{other}}$ are the Burgers vectors in the opposing grain. As noted by Bieler et al. [134], this parameter is maximized when multiple slip systems in the neighboring grain accommodate the twin shear, leading to a higher residual dislocation content. This factor accounted for void nucleation events at twin/grain-boundary intersections in TiAl, though it has not yet been applied to other systems.

One interesting point is that the grain boundary normal, $\mathbf{n}_{\text{gb}}$, does not appear in Eq. (6) because including it did not improve the parameter's ability to predict failure [135]. This is in contrast to the failure parameter proposed by Zhang et al. [162], who studied void nucleation at twin/grain-boundary intersections in polycrystalline BCC Mo with MD simulations. Figure 20 shows an example from this study. The authors proposed that the propensity for void nucleation at the grain boundary is proportional to the grain boundary displacement induced by the twin/grain-boundary intersection,

$$\Delta = t(\mathbf{b}_{\text{twin}} \cdot \mathbf{n}_{\text{gb}}) \tag{9}$$

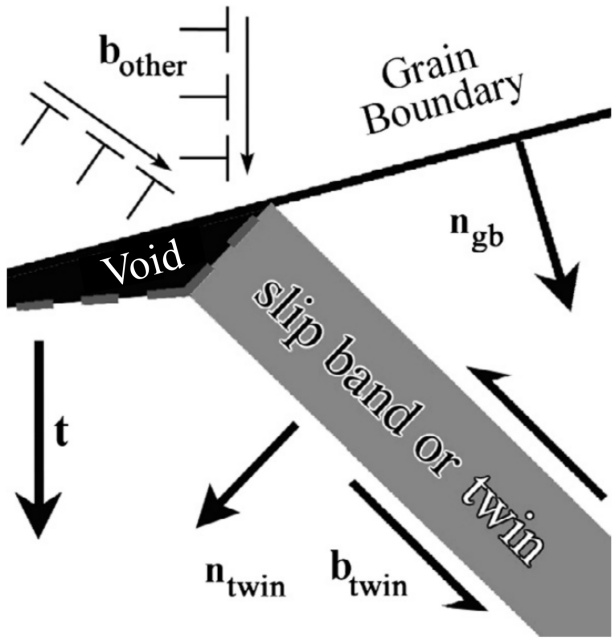

Figure 19: The relationship between stress state, geometry, and the slip and twinning systems across a grain boundary are illustrated. This schematic is from reference [134].

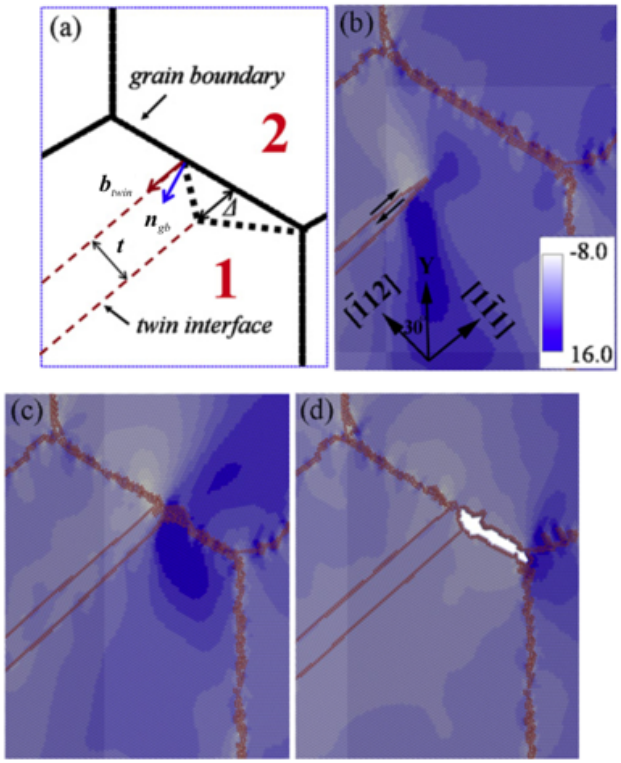

Figure 20: (a) A schematic of the void nucleation mechanism proposed by Zhang et al. [162] is shown. (b-d) The distribution of tensile stress in the Y direction at strains of (b) 3.3%, (c) 3.4%, and (d) 3.7% are shown. Twin growth is apparent in (b), the twin collides with the GB in (c) and the nucleated void is shown in (d). This figure is adapted from reference [162].

where the details of the geometry are shown in Figure 20(a). As this displacement increases, so too does the local tensile stress at the grain boundary, as shown in Figure 20(c-d). This implies that thicker twins promote void nucleation.

To conclude this section, the problem of intergranular ductile failure is considered as it is instructive for how microstructural changes near grain boundaries affect both the fracture mechanism and material properties. This situation is commonly observed in 7000-series aluminum alloys but can occur

in any alloy where precipitate-rich grain-boundaries surrounded by precipitate-free zones [163–167]. Precipitation of second-phases along the grain boundary creates a strong but brittle hard region along the grain boundary surrounded by a relatively soft precipitate-free zone (PFZ) with a lower yield stress but higher work-hardening rate than the grain boundary or grain interior.

Regarding material properties, it is generally observed that intergranular precipitation weakens the grain boundary and decreases material toughness and ductility [168]. Additionally, the likelihood of intergranular fracture increases with increasing stress triaxiality. Strain-localization within the relatively-soft PFZ either leads to void nucleation and coalescence within the PFZ or particle debonding and fracture along the grain boundary. Both cases lead to intergranular fracture. This mode of fracture has been examined using a variety of experiments, including in-situ tomography using Gallium-wetting along Al grain boundaries to highlight the crack path relative to the grain boundary [168, 169]. Models of the process, considering the PFZ and the grain boundary as separate phases have been proposed and reviewed in some detail by Pardoen et al [165]. More information on this phenomenon can be found in the reviews provided in references [165, 166, 170]

2.4. Void nucleation at second-phase particles and inclusions

Second-phase particles and inclusions are the most commonly observed sites for void nucleation during ductile rupture. These can play two distinct mechanistic roles in void nucleation, producing voids via particle cracking or via interfacial decohesion [171]. A trend in decreasing fracture toughness with increasing particle content and fracture toughness has been observed in some materials, though directly linking the two is non-trivial and this topic

will be discussed in some detail in Section 4.1. Additionally, the properties of the particles relative to the matrix, e.g. yield strength, have a profound effect on fracture toughness. A common example is the significant increase in fracture toughness observed in steels when sulfur is gettered as particles containing calcium, titanium and carbon, or lanthanum [172–174]. Thus, knowledge about the content, distribution, and nature of particles within an alloy, including recycled alloys [175], is critical to understanding its failure. The effects of particle properties on void nucleation are discussed in detail in Section 3. This section instead focuses on the mechanical drivers for particle-stimulated void nucleation within the matrix.

It has long been held that the mechanical drivers for particle-stimulated void nucleation are created by local plastic deformation at or near the particle/matrix interface. However, the specific deformation-induced defects associated with cracked and debonded particles are understudied, partially because characterizing these defect states, either experimentally or computationally, was a significant challenge until the last decade. Recent advances in experimental and modeling capabilities enabled several studies of the relationships between particle-stimulated void nucleation and deformation-induced defects. This section reviews these investigations, beginning with observations of void nucleation by particle fracture. The subsequent section examines void nucleation by particle debonding.

Many studies of particle-stimulated void nucleation have examined how particle size, shape, and volume density affect the critical stress and strain for void nucleation. This includes numerous investigations employing XCT to characterize void nucleation in-situ, including references [31, 176–187].

While these studies have provided significant insights into the mechanical conditions governing void nucleation, they provide little insight into the relationship between deformation-induced defects and particle-stimulated void nucleation because XCT cannot resolve microstructural features such as grain boundaries, twins, dislocations, or vacancies. Hence, these studies are not covered in the current review. More information on this topic can be found in the classic review articles in references [50, 51, 56] and the recent reviews of Pineau et al. [16, 188], the latter including data from in-situ XCT studies. Some of these works are revisited in Section 3, and relevant studies using tomography techniques to examine how deformation-induced defects affect void nucleation are presented here.

2.4.1. Void nucleation by particle fracture

Particle cracking depends on achieving a critical stress in the particle [56, 177] (see Section 3.2). The critical stress is produced by coherency stresses between the deforming matrix and the particle and by interactions with local crystal defects such as twins. For example, deformation twins were observed to cause cementite platelets to crack in ferritic steels tested at low temperatures [189]. In contrast, cracked platelets were not observed in specimens tested to the same stress level in the absence of twinning, which was obtained by testing specimens at room temperature. Studies of void nucleation in interstitial-free steel demonstrated twin/particle intersections were also preferential sites for particle fracture [190]. An example of this is shown in Figure 21. Beevers and coworkers demonstrated that specific twin types are associated with fracture of hydride platelets in zirconium [191]. Both $\{10\bar{1}2\}$ and $\{11\bar{2}1\}$ twinning was observed, but fractured platelets were only

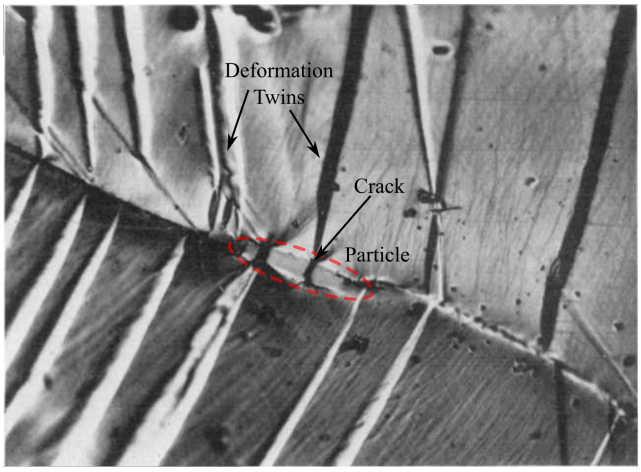

Figure 21: An optical image of a particle located in a grain boundary that is fractured at the intersection with a deformation twin is shown. Two cracks can be seen within the particle. This image was adapted from reference [190].

associated with $\{11\bar{2}1\}$ twins. The reason(s) for this were not determined.

For materials that deform by dislocation slip, it has historically been assumed that dislocation pile-ups enable particle fracture and decohesion, e.g. see the work of Ashby [192]. Both Gell and Worthington [190] and Barnby [193] reported observations of cracked particles associated with intense slip band markings. An SEM image of a cracked particle associated with slip bands in an austenitic stainless steel (316) is shown in Figure 22. In Al 6061-T6, Gross et al. observed that slip bands intersected many particles, but void nucleation by particle fracture was only observed at a handful of such particles [194]. Examples of fractured and unfractured particles are shown in Figure 24. In these studies, dislocation boundaries likely also formed during deformation. These are not visible using the secondary electron and optical imaging techniques employed in these studies.

Dislocation pile-ups may cause particle cracking by creating a stress con-

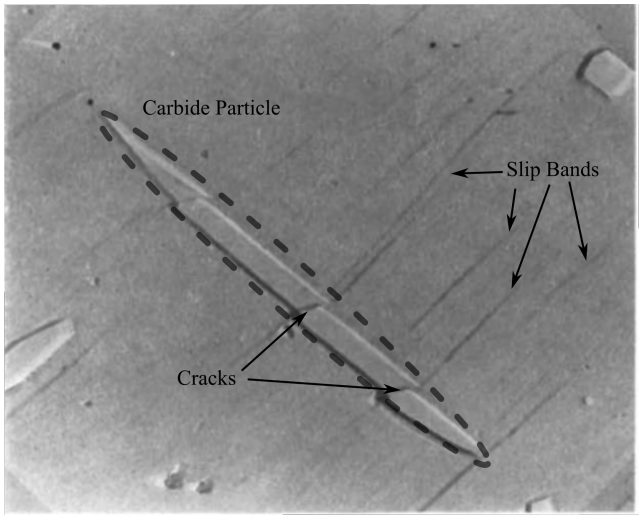

Figure 22: (An SEM image of a cracked carbide associated with slip bands in an austenitic stainless steel strained to 26% is shown. This image is from reference [193].

centration at the particle/matrix interface [138, 139]. However, there is still no direct evidence for this. Dislocation boundaries may play a similar role, as it was recently observed that fractured Fe-intermetallics in Al 6061-T6 are surrounded by high densities of dislocation boundaries [195].

The in-situ X-ray nanotomography study by Chawla and coworkers [196] indicates that dislocation/particle interactions are critical to understanding particle cracking. Size-dependent deformation modes were observed for θ' precipitates in an Al-Cu alloy, with small precipitates cracking and large precipitates deforming. It was further observed that cracked θ' precipitates were associated with dislocation pile-ups. Note that θ' precipitates are semi-coherent. For large θ' precipitates, it appeared that the stresses associated with dislocation pile-ups were insufficient for particle cleavage; instead, pile-ups caused localized lattice rotation that eventually created dislocation boundaries. It is unclear if these observations can be extended to

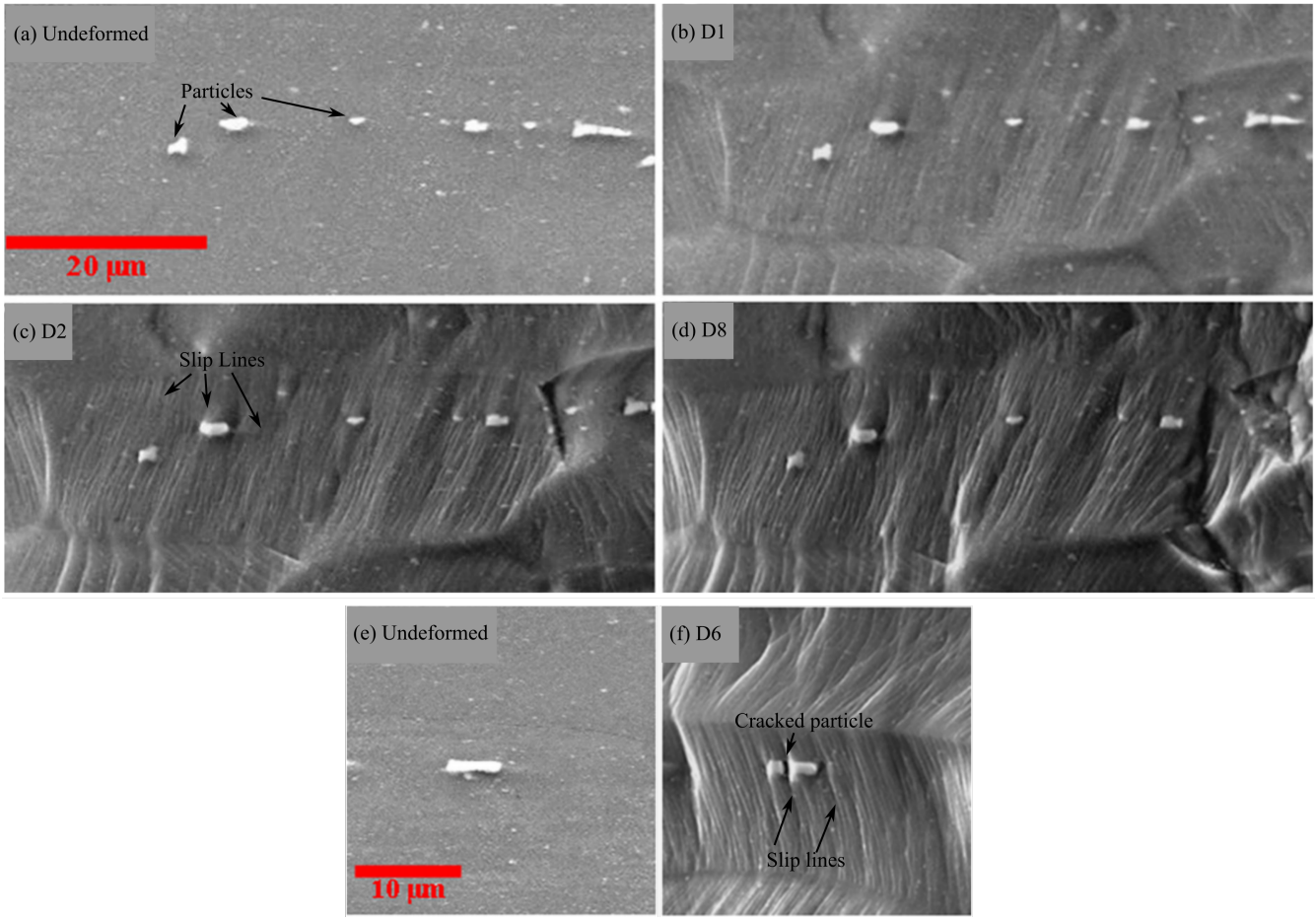

Figure 23: SEM images of Fe-intermetallics in an Al 6061 are shown. Images in (a) to (d) show a series of images of the same particles during deformation. Slip bands intersected these particles but none were observed to debond or fracture. Images in (e) and (f) show a particle before and after fracture, respectively. The location of fracture coincides with the intersection of a slip band. Due to the geometry of the test specimen, measurements of strain were not made at each loading step. The labels D0, D1, etc. refer to the initial state, the first step of deformation, and so forth. These images are from reference [194].

rigid, incoherent particles [176].

Failure at second phases, e.g. martensite, can be considered as a specialized case of failure at second-phase particles. Cracking and/or debonding associated with the relatively brittle martensite phase in ferritic-martensitic dual phase (DP) steels is one of the most studied examples of this. The primary damage mechanism in these steels depends on the volume fraction of martensite. At low volume fractions of martensite, the dominant mechanism is decohesion at ferrite/martensite interfaces, with cracks subsequently following ferrite grain boundaries [197, 198]. At high martensite volume fractions, the dominant mechanism is micro-cracking of martensite islands [198, 199]. In-situ digital image correlation (DIC) indicated that micro-cracking occurs at martensite islands intersected by highly strained regions within a ferrite grain, i.e. strain "hot spots" [200]. EBSD and secondary electron images suggest that both dislocation boundaries and slip bands formed in ferrite grains, though it is unclear if either of these were associated with martensite cracking [200]. Recently, combined in-situ microscopy and crystal plasticity modeling demonstrated that void nucleation in some dual-phase steels is due to substructure boundary sliding triggering damage at or near the ferrite/martensite interface [201].

2.4.2. Void nucleation by particle debonding

Dislocation boundaries appear to play an important role in void nucleation by particle debonding. Using TEM and EBSD, Noell et al. observed that debonded CuO_2 particles in a Cu material were consistently associated with the intersection between the particle and at least one dislocation boundary [117]. An example of this is shown in Figure 24. In interstitial-free

steels containing TiN precipitates, Kestens and coworkers [202] observed that particle delamination occurs at approximately the same macroscale strains (15-25%) as the transition from low-angle to high-angle cell block boundaries. EBSD data from this study suggests that particle delamination generally began at or near the intersection between particles and dislocation boundaries, though more detailed analysis is necessary to better establish this interpretation.]

Void sheeting is a specialized case of particle debonding whereby 'sheets' of voids nucleate in bands of intense shear between pre-existing voids [203]. This mechanism of void coalescence often sets the unstable end of catastrophic failure [15]. Void sheeting was covered thoroughly by Van Stone et al. [170] and Garrison et al. [204] in their reviews and will thus only be discussed briefly here. Key characteristics of void sheeting include the necessity presence of localized areas of elevated strain and a second population of closely-spaced microstructural features for void nucleation, e.g. submicron dispersoids [204]. For example, in Al 2000 and 7000 alloys nucleate by interfacial decohesion of the closely-spaced submicron dispersoids found in these materials [205, 206]. This occurs after voids form at large intermetallic constituent particles and only within shear bands between these voids. Similarly, Cox and Low observed sheets of secondary voids connecting debonded MnS inclusions in 4340 steels [171]. These secondary voids nucleated by decohesion of submicron cementite precipitates lying along martensitic platelet boundaries. The observation that these submicron dispersoids are not associated with voids except in the case of void sheeting indicates the critical role that localized slip plays in nucleating voids [171]. This mechanism re-

mains challenging to model, as the model must account for both deformation localization and void nucleation [207].

Several authors have studied void nucleation by particle debonding in defect-free crystals using MD. Two different behaviors have been observed based on crystallography. In FCC metals [208–211], void nucleation begins with crack formation at the particle interface followed by dislocation emission from the crack tip. In HCP and BCC metals [212], cracks appear to first nucleate in the matrix away from the particle interface, which then drive crack formation at the interface. It is important to note these simulations involved high loading rates and/or stresses exceeding 1 GPa; it is not clear if the same trends would be observed at lower strain rates/stresses.

One finding of note is the observation of two different debonding modes by Zhao et al. [25], as depicted in Figure 25. Under conditions of constant applied hydrostatic stress, the authors observed that an interfacial crack first nucleated as a small cluster of vacancies (atoms with excess volume) and subsequently grew via a so-called lattice trapped (brittle) fracture mechanism. The authors were able to fully characterize a rate law for thermally activated *lattice-trapped debonding* and demonstrate that it may be operable under typical quasi-static loading conditions. After reaching a critical size, dislocations emitted from the crack tip leading to *dislocation-mediated debonding*.

As a final note, we point out that ab initio techniques (e.g., density functional theory) have also been applied to the particle decohesion problem. In particular, interfacial strengths and works of separation [213, 214] have been computed for a variety of interface types. Often the interfacial strengths from

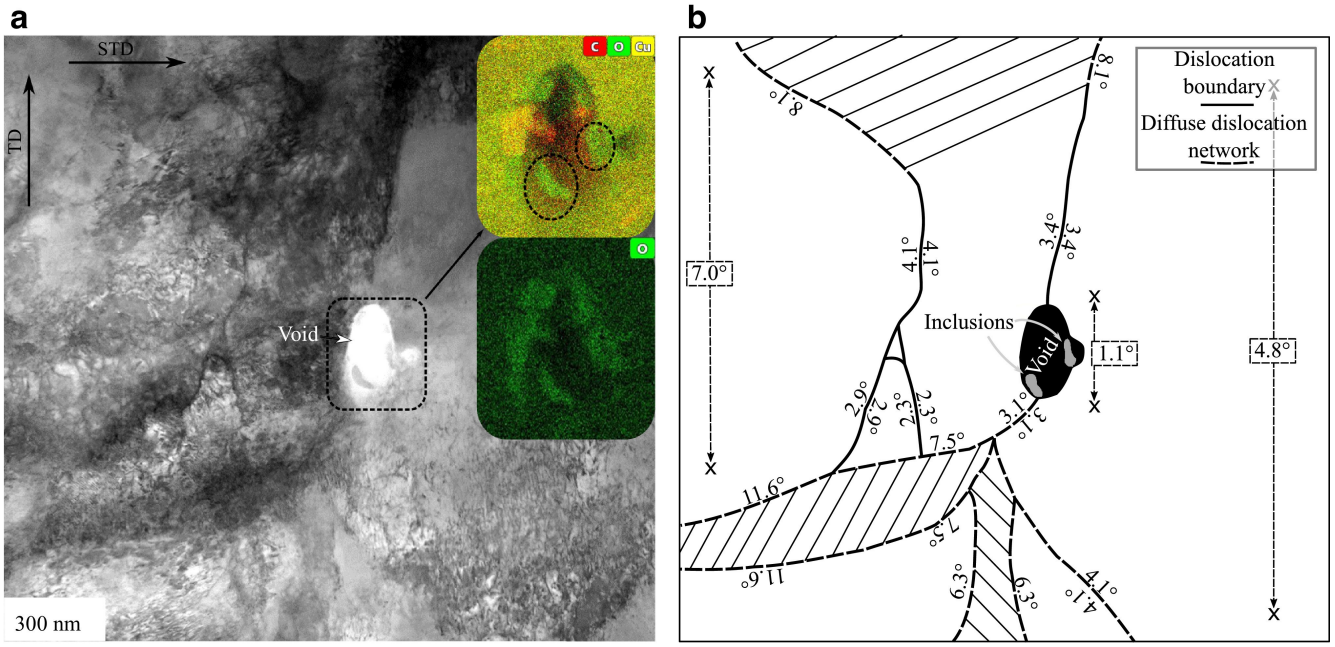

Figure 24: A TEM micrograph showing a debonded particle intersected by a dislocation boundary in a Cu material. This image is from reference [117].

these calculations exceed 10 GPa—far larger than the ultimate strength of structural metals. How to incorporate these fundamental atomistic properties into higher length scale models for particle decohesion is unclear.

2.5. Summary

In metals that deform by slip, second-phase particles and inclusions are the most common sites for void nucleation. In metals that deform by twinning, the intersections between twins and other microstructural features, including particles, grain boundaries, and other twins, are important sites for void nucleation. In particle-free metals that deform by slip and in some materials containing relatively few, small particles, vacancy condensation and subsequent growth by dislocation absorption along dislocation bound-

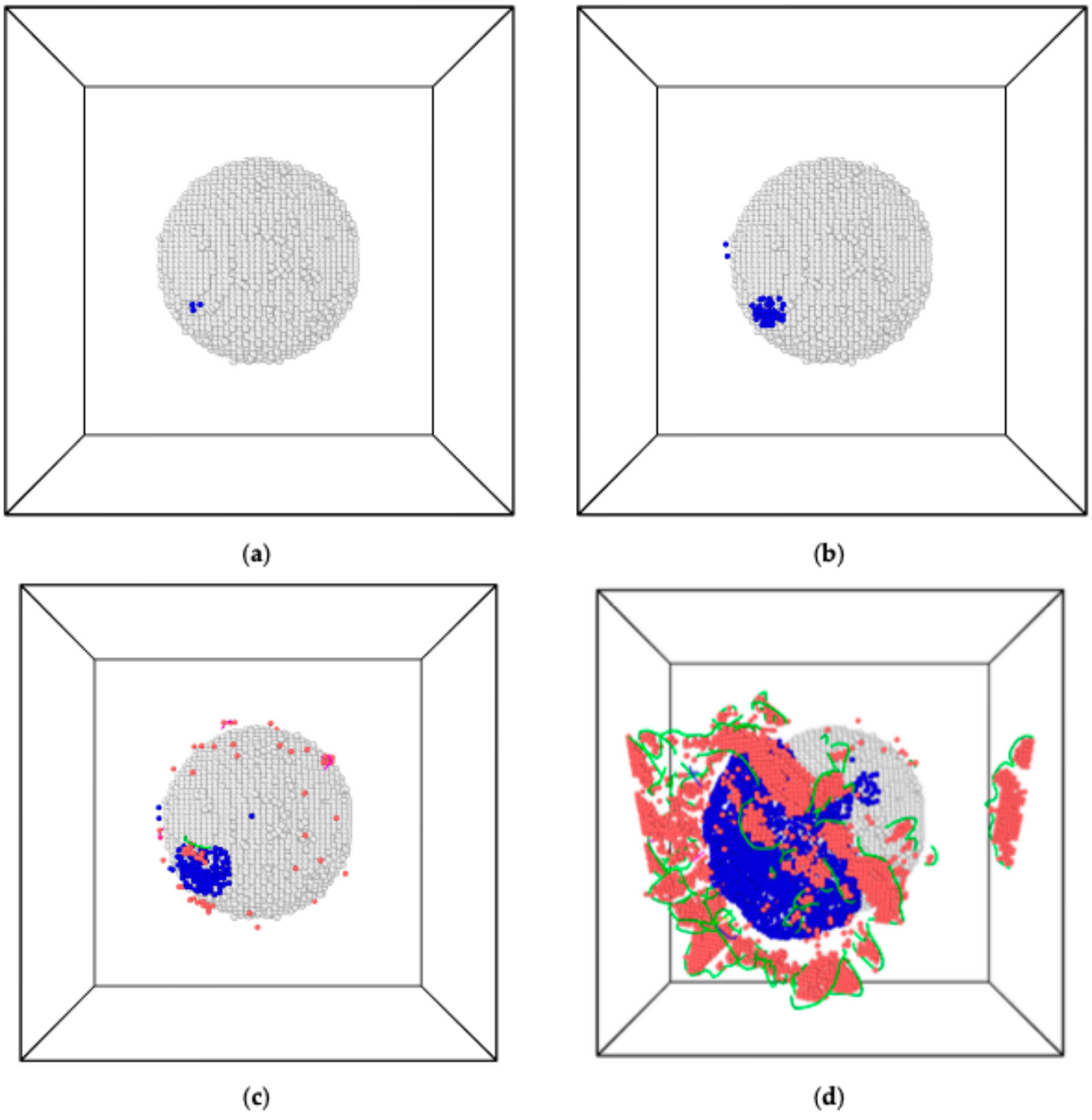

Figure 25: MD simulation snapshots of particle delamination. Blue atoms are associated with a crack. (a) Initial appearance of a small crack involving a few atoms. (b) Subsequent growth of the crack via lattice-trapped delamination. (c) Initial appearance of dislocations at the crack tips. (d) Rapid crack growth via dislocation-mediated delamination. Green lines are Shockley-Read partial dislocations. Red atoms are associated with stacking faults. This figure is taken from Reference [25].

aries appears to be the primary mechanism for forming voids. In all three cases, it is clear that deformation-induced defects, including vacancies and dislocation boundaries, contribute to void nucleation. For example, rather than grain boundaries, the dislocation boundaries created by deformation are the primary site for void nucleation in particle-free materials that deform by slip. In particle-free materials that deform by twinning, voids typically nucleate at deformation-twin/grain-boundary intersections. There is increasing evidence that particle fracture and debonding are also associated with dislocation boundaries and deformation twins. Without question, there is competition between the various void nucleation processes discussed in this section. The competition between particle fracture and debonding is well documented (see next Section) and is known to depend on the strength of the matrix or, in the case of dual-phase steels, the strength of the material. Competition between void nucleation at particles and particle-free nucleation has been observed, with particle-free nucleation occurring more readily than nucleation at second-phase particles in some materials. There is also likely collaboration between these mechanisms, e.g. nanovoids formed via vacancy accumulation may lead to particle debonding. The factors that govern this competition remain obscure. Lastly, we highlight that the vast majority of studies to date of void nucleation at the dislocation scale have focused on particle-free materials or relatively new materials, e.g. dual-phase steels. Significant opportunities exist to apply the techniques and theory described in this section to studies of void nucleation in "main-stream" engineering materials, e.g. Al alloys.

3. Continuum studies and frameworks for void nucleation

Although the first modeling attempts go back to the 1960s [215, 216], the modeling of void nucleation gained significant attention after the works of Tanaka *et al.* in Japan [217]. These investigations differed significantly in their approach. Some authors adopted the framework of physical metallurgy [56, 216, 218, 219] with early works being motivated by relating internal stresses in dispersoid-strengthened alloys to their plastic response. Such works considered dislocation–particle interactions within the classical theory of elasticity. Others approached the problem from the point of view of continuum mechanics [217, 220–223]. Results from the two types of approaches are often compared [51] whereas their respective domains of validity are sometimes quite distinct [224]. Furthermore, not all analyses have considered the same type of nucleation criterion. Some adopted an energy-based criterion [219, 220] while others a critical stress-based criterion [216, 221–223]. Yet others used a mixture of the two criterion [56, 217, 218].

With the development of computing power, modeling efforts evolved in the 1980s and 1990s toward numerical analysis. These used either the finite element method [225–227] or other methods [223, 228, 229] in the spirit of the pioneering works of Goodier [230] and Eshelby [231].

Here, we will not systematically discuss the assumptions underlying each approach or the formulas developed by the various authors. For this, the reader may refer to the early reviews in [50, 51, 224] or more recent ones [16]. In particular, Ref. [224] contains an interesting collection of void nucleation criteria developed prior to its publication. In what follows, we are rather concerned with identifying and compiling first-order effects of material

properties and loading conditions in void nucleation, irrespective of the basis (theoretical or experimental) of their establishment.

When void nucleation is mediated by second-phase particles, cavity formation may result from particle cracking or decohesion of the particle–matrix interface, Figure 3. Particle cracking is particularly favorable in elongated inclusions loaded parallel to their length. More generally, cracking occurs roughly perpendicular to the tensile principal stresses (one plane in simple tension; two in biaxial tension, etc.), or in the case of particles with strongly anisotropic toughness, along the cleavage plane with the highest resolved tensile stress. The so formed micro-cracks gradually open up, leading to particle fragmentation. This relaxes local stresses at the matrix–particle-fragment interface. The volume of a so-initiated cavity is thus often smaller than that of the particle, which remains attached to the matrix at other locations.

Decohesion (in tension) usually begins near the poles along the main loading direction, see Figure 3. The majority of experimental observations to date are available under uniaxial tension, but analysis shows that the location of first void nucleation remains the same under (biased) triaxial tension. The nascent cavity grows in volume by mere opening of the interface while propagating along the latter. Some authors have attempted to account for such details in modeling decohesion [232, 233]. The utility of such refinement is debatable depending on the particle–matrix system of interest. Here also, the volume of the formed cavity only exceeds that of the particle if decohesion is complete.

When void nucleation is not mediated by second-phase particles, it is thought to typically occur macroscopically in regions of high stress at other

weak interfaces that induce plastic discontinuities, e.g. at deformation-twin/grain-boundary intersections. While the details at the microscopic scale may involve complex vacancy clusters and dislocation/twin structures, see Section 2, at the macroscopic scale the notion of boundaries separating differently strained regions is akin to an Eshelby inhomogeneity problem. Accordingly, lessons learned from detailed analyses of particle–matrix systems can be employed. In this case, the particle is replaced with an inhomogeneity representing the eigenstrain that results from plastic strain incompatibility, say between two grains, the inhomogeneity being embedded in a homogeneous equivalent medium. As will be described where appropriate below, an approach of this type [234] can be used to analyze void nucleation in particle–matrix systems [222].

More generally, void nucleation may be characterized as heterogeneous versus homogeneous. The former is most common at particles and second phases. Homogeneous nucleation may occur due to cavitation instabilities [235, 236] or vacancy condensation [117, 118]. Many investigations of the latter are of theoretical nature, but cavitation instabilities are expected at extremely high stress triaxialities, as would prevail in some high-rate loading experiments leading to spall fracture [237] and evidence of vacancy condensation has been observed during ductile fracture [117, 118].

Several factors are known or expected to play a role in void nucleation in general and in particle-mediated cavitation in particular. They may be grouped in three categories: (i) rheological (elastic mismatch, relative hardness, relative plasticity, thermal expansion); (ii) morphological (particle shape, particle orientation, material texture); or (iii) thermo-mechanical

(stress state, strain state, temperature, strain rate, inertial forces). In order to bring a more quantitative perspective, some basic definitions are needed. Note that, throughout this section, we use lowercase superscripts (i, p) to denote critical values and uppercase superscripts (I, P) to denote driving forces. The following section focuses on the effects of these factors on void nucleation. Many of the studies discussed include both modeling and experimental work, with a focus on how continuum-scale factors influence void nucleation.

3.1. Definitions

It is convenient to characterize a matrix–particle system with its *relative hardness* [224]:

$$\vartheta = \sigma_y^{\mathrm{P}}/\sigma_y \tag{10}$$

with σ_y^{P} and σ_y denoting the yield strengths of the particle and matrix, respectively.

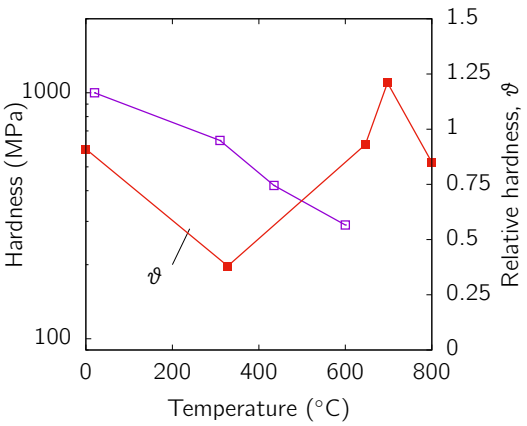

Figure 26: *Hardness of spheroidized manganese sulfide inclusions versus temperature in a 0.2% carbon steel. Adapted from [238].*

In practice, it is difficult to access the constitutive relation of a particle. Micro-hardness measurements are possible in principle [238] as are qualitative observations of deformation mechanisms in some inclusions [239]. However, not only are such studies scarce in the literature but they are also of limited scope, e.g. because of matrix confinement. Thus, the relative hardness at a given temperature (Fig. 26) is often taken to indicate the propensity for plastic flow in the particle relative to the matrix. The parameter ϑ is a strength index: $\vartheta < 1$ for soft particles and $\vartheta > 1$ for hard ones. By way of extension, if the particle is plastically non-deformable (rigid or elastic) then $\vartheta > 1$.

For non-particulate systems, such as multiphase materials, Eq. (10) may be used with the softest phase used as reference (matrix) at room tempera-

ture. Modern hardness characterization techniques, such as micropillar testing, have been used to measure the evolution with strain of ϑ, or its counterpart in terms of flow stresses, e.g. [240].

Next, one defines the *relative plasticity*[1] υ and *relative deformation* ϵ as

$$\upsilon = \dot{\bar{\varepsilon}}^{\mathrm{P}}/\dot{\bar{\varepsilon}}; \qquad \epsilon = \bar{\varepsilon}^{\mathrm{P}}/\bar{\varepsilon} \tag{11}$$

where $\dot{\bar{\varepsilon}}$ and $\bar{\varepsilon}$ denote mean effective strain rate and strain, respectively. Although similar quantities are used in metal forming, the notion of relative deformability for inclusions seems to have first been introduced by [241]. For an elastic matrix, the strain and strain rate are uniform in the inclusion [231]. This is not the case in general and only average values over the particle are meaningful in Equation (11). In the course of loading, both υ and ϵ evolve and are not necessarily equal. The use of one or the other, as a measure of relative plasticity, depends on the behavior of the matrix.

The relative plasticity of inclusions is indirectly measured based on machinability thus leading to various classes of inclusions with respect to their temperature-dependent relative plasticity [242]; also see [243] for a recent overview.

In addition to the notion of relative plasticity (ϑ, υ, ϵ), the contrast in stiffness between particle and matrix can have a large effect on load partitioning and stress distribution, especially at small strains. The relative stiffness E^{P}/E is used to quantify the modulus mismatch in particle–matrix systems. In comparison, a study by Wilner [228], restricted to spherical particles, has shown a negligibly small influence of the contrast in Poisson's ratios.

[1] also known in the literature as *relative deformability*.

The concepts evoked above permit a reduced number of rheological parameters to be highlighted, namely: relative hardness, ϑ; relative plasticity, υ; modulus mismatch, E^{P}/E. This list should be augmented with the hardening exponent of the matrix, n, (or a collection of hardening parameters in more elaborate characterizations of hardening). In general, the hardening properties of deformable inclusions are not well known and shall not be discussed further.

In addition to the rheological parameters introduced above, inclusion parameters, such as the particle volume fraction, mean particle dimensions and mean particle spacings, as well as thermomechanical parameters, such as stress state, strain rate and temperature, may all play a role in void formation. In conventional continuum analyses, no length scale enters the description and morphological parameters are reduced to particle volume fraction, f^{P}, and aspect ratios, w^{P}. For a remote stress state $\boldsymbol{\Sigma}$ with mean stress Σ_{m} and von Mises effective stress Σ_{eq}, the stress state is characterized by the dimensionless parameters $T \equiv \Sigma_{\mathrm{m}}/\Sigma_{\mathrm{eq}}$, known as the stress triaxiality ratio, and the Lode angle $\theta \equiv \frac{1}{3}\cos^{-1}(-L)$, with $\theta \in \left[0, \frac{\pi}{3}\right]$ and $L \equiv -\frac{27}{2}\det\left(\frac{\boldsymbol{s}}{\Sigma_{\mathrm{eq}}}\right)$ being the Lode parameter and $\boldsymbol{s}$ the stress deviator.

3.2. Nucleation criterion

In order to analyze the effect of the various parameters introduced above, it is useful to formulate a nucleation criterion. As in any problem involving fracture, two conditions are invoked:

1. the free energy must decrease as a result of nucleation, in the simplest case this means that the released (elastic) strain energy must exceed the surface energy (necessary condition);

2. the local stress (in the particle if rupture occurs; at the interface if decohesion prevails) must equal the stress required for either the particle to break or the interface to decohere, whichever mechanism is active (sufficient condition).

Some early studies [217, 244] had concluded that particles larger than ~ 250Å would satisfy the energy criterion when the stress criterion is met. Montheillet and Gilormini [224] observed that, if more realistic values of threshold stresses were employed, the formula established by Tanaka et al. would yield a critical size of order $\sim 1\mu$m. Thus, it is concluded that (i) a critical stress criterion is sufficient for particles larger than a micron; and (ii) developing such a criterion at such length scales is justifiable within the confines of continuum mechanics.

The following is therefore postulated:

1. There exists a critical stress for particle rupture, denoted σ_c^p, which characterizes the constituent material of the particle. Fundamentally, σ_c^p may represent a cleavage stress. More generally, it must be viewed as an effective stress of brittle fracture in the particle, for example

because of plastic deformation in it, as is the case for MnS inclusions [239] or other soft particles.

2. Likewise, there exists a critical stress for interfacial rupture, denoted σ_c^i, which characterizes the matrix–particle system. Fundamentally, σ_c^i may represent interfacial separation as would be inferred from universal binding curves by means of atomistic calculations. More generally, it must be viewed as an effective stress of brittle fracture at the interface, including such effects as those of impurities, mixed inclusions, interface waviness, etc.

Whether the critical stresses should be taken to depend on temperature is often debated. If, say the interfacial critical stress σ_c^i is viewed as the cohesive strength of atomic separation then it is reasonable to consider it as independent of temperature. In practice, both σ_c^i and σ_c^p are considered effective quantities and in that sense temperature dependence is plausible. Ultimately, this is a matter of scale and a continuum description alone cannot settle the issue. For this reason, σ_c^i for example may be viewed as dependent upon the cohesive energy of the matrix–particle interface, which can be altered by metallurgical modifications. The cohesive energy can be increased, for instance by addition of Cr in the MnS–ferrite system [245, 246], or decreased by segregation of impurities at the interface, e.g. of P in a carbide–ferrite system [247]. In high-strength steels, the gettering of sulfur in the form of sub-micron inclusions, such as Ti_2CS or CrS, clearly affects interfacial strength, e.g. [248]. For more recent developments in this regard, see [243] for steels and [249] for intermetallic particles in Al alloys.

The critical stresses σ_c^p and σ_c^i determine the material's resistance to void

nucleation. The driving forces that complete the formulation of concurrent nucleation criteria are essentially mechanical. They involve the maximum principal stress in the particle, σ_1^{P}, for fragmentation and the maximum normal stress at the interface, $\sigma_{\mathrm{n}}^{\mathrm{I}}$, for decohesion. Fragmentation occurs when

$$\sigma_1^{\mathrm{P}} \equiv \max_{\underline{x} \in V^{\mathrm{p}}} \sigma_1 = \sigma_{\mathrm{c}}^{\mathrm{p}}, \tag{12}$$

where it is understood that the maximum of the largest principal stress is taken over the entire volume V^{p} occupied by the particle. Concurrently, decohesion occurs when

$$\sigma_{\mathrm{n}}^{\mathrm{I}} \equiv \max_{\underline{x} \in S^{\mathrm{i}}} \sigma_{\mathrm{n}} = \sigma_{\mathrm{c}}^{\mathrm{i}}, \tag{13}$$

where the maximum of the normal traction is taken over the entire interface S^{i}.

Now, consider some arbitrary remote loading with ordered principal stresses $\Sigma_{\mathrm{I}} \geq \Sigma_{\mathrm{II}} \geq \Sigma_{\mathrm{III}}$. Stress concentration factors in the particle and at the interface are defined as

$$\kappa^{\mathrm{P}} = \frac{\sigma_1^{\mathrm{P}}}{\Sigma_{\mathrm{I}}}; \qquad \kappa^{\mathrm{I}} = \frac{\sigma_{\mathrm{n}}^{\mathrm{I}}}{\Sigma_{\mathrm{I}}} \tag{14}$$

where it should be noted that the principal stress directions in the particle may differ from those of the remote loading. With these definitions, nucleation criteria Equations (12) and (13) may be recast as:

$$\kappa^{\mathrm{P}} \Sigma_{\mathrm{I}} = \sigma_{\mathrm{c}}^{\mathrm{p}} \qquad \text{versus} \qquad \kappa^{\mathrm{I}} \Sigma_{\mathrm{I}} = \sigma_{\mathrm{c}}^{\mathrm{i}} \tag{15}$$

Alternatively, inhomogeneity induced stresses may be introduced such that: $\sigma_1^{\mathrm{P}} = (1 + \zeta^{\mathrm{P}})\Sigma_{\mathrm{I}}$ and $\sigma_{\mathrm{n}}^{\mathrm{I}} = (1 + \zeta^{\mathrm{I}})\Sigma_{\mathrm{I}}$ where ζ^{P} and ζ^{I} can be deduced from κ^{P} and κ^{I} and vice versa.

The problem of void nucleation thus reduces to determining the stress concentration factors κ^{P} and κ^{I} for fragmentation and debonding, respectively. Both dimensionless factors may depend on rheological parameters (ϑ, υ, ϵ, E^{P}/E), morphological parameters (w^{P}, f^{P}) and loading parameters (T, L). They also depend on the local configuration of microstructural defects, as discussed in Section 2. These latter dependencies are not discussed in this section. The extent to which each of the other parameters affect void nucleation, understood in the realm of concentration factors, is discussed below.

3.3. Effect of yield strength

There have been quite a few attempts to study the influence of matrix hardness, as measured by yield strength, on void nucleation. Much of this was pioneered by several works at Carnegie Mellon University. Reviews dating back to the late 1980s [50, 51] mention Psioda's work [250] on steels, but there were others concerned with Al alloys, e.g., [251]. Psioda employed adequate heat treatments to vary the yield strength of grade 300 maraging steels in the range $\sim$ 720–2070 MPa. The morphological parameters of the Ti_2S and Ti(C, N) inclusions were common to the series of steels and their interfacial strength presumably remained unaltered. In each heat, Psioda measured the fraction of inclusions with voids at various strain intervals to fracture. Van Stone et al. [50] as well as Garrison and Moody [51] infer from the data that void nucleation occurs at lower strains in higher strength materials[2]. The conclusion is reasonable but inferring it from Psioda's data seems far fetched because the notion of a nucleation strain is elusive. Psioda's experiments are quite original and may be used to infer the following:

1. When the fraction of Ti_2S inclusions with voids, f_{nuc}, is plotted against the effective plastic strain, as in Fig. 3 of [51], the data suggests that (i) at yield, between $\sim$19 and $\sim$35% of particles have already nucleated voids depending on the heat; and (ii) increasing material strength favors nucleation over a wider population of particles.

2. When the same volume fraction is plotted against the applied true

[2]In [51] this is explicitly stated p. 1038, yet rather curiously contradicted by their summary p. 1043.

tensile stress, as in Fig. 11 of [50], it becomes evident that as the strength of the steel increases "a higher applied stress is required for nucleation." Also, the increase in flow strength beyond initial yield further increases f_{nuc} (over 80% of particles have nucleated voids in the strongest heat, compare with $< 60\%$ in the solution treated steel).

3. Examining further the raw data in [250] reveals that: (i) Strain hardening remains unchanged with increasing strength, a factor that is not always independently controlled in experiments. (ii) The nucleation

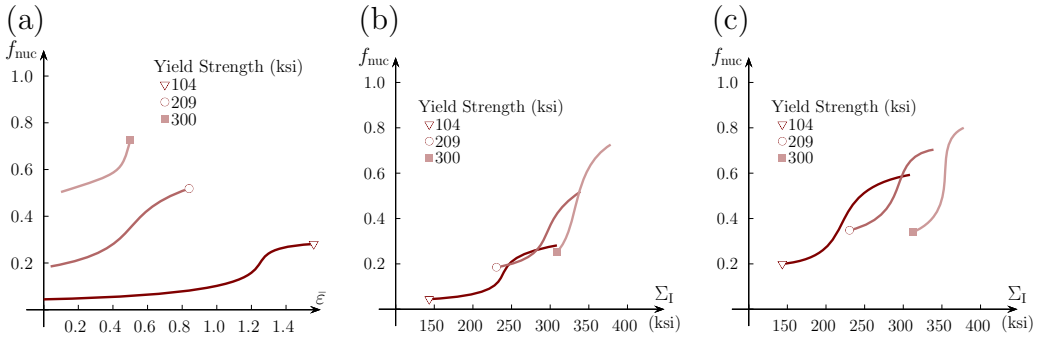

Figure 27: *Schematic void nucleation curves in maraging steels.* (a) Fraction of Ti(C, N) particles with voids, f_{nuc}, versus effective plastic strain. (b) f_{nuc} versus applied stress for Ti(C, N). (c) f_{nuc} versus applied stress for Ti_2S. *Adapted from [250].*

curves for the titanium carbo-nitrides are qualitatively similar to those of the titanium sulfides (Fig. 27c) with the major difference that the f_{nuc} versus stress data roughly follow a single master sigmoidal curve (Fig. 27b), unlike for Ti_2S (Fig. 27c). (iii) The fraction of Ti(C, N) particles with voids at zero strain is 5%; compare with 19% for Ti_2S. (iv) The Ti(C, N) particles are equiaxed whereas the Ti_2S are not. (v) There was a third population of inclusions: $\lesssim 0.1\mu$m TiC particles with

a volume fraction of $\sim 1\%$; compare with 0.24% for Ti_2S and 0.08% for Ti(C, N). (vi) The three highest strength steels had aging-induced $\sim 0.1\mu$m coarser precipitates, believed to nucleate voids late in the fracture process, just like the TiC particles.

Two additional complicating factors enter into play in interpreting Psioda's data, which were not addressed in [250] or previous reviews. The first is that significant nucleation appears to have occurred before macroscopic yield — unless that was due to processing— but no measurements were made in the elastic regime. On the potential effect of modulus mismatch on early nucleation see Section 3.7. Second, the Ti_2S particles are soft relative to the matrix. The effect of relative plasticity is addressed in Section 3.8.

Beyond Psioda's dated work, it would be fair to say that experiments investigating the effect of yield strength on void nucleation are still lacking. The main difficulty is that manipulations of strength usually affect strain hardening, which as will be shown below (Section 3.4), also has an effect on void nucleation. A notable example is that of Al alloys [249, 251]. For aerospace grade alloys (2000 and 7000 series) the decrease in toughness that accompanies the increase in yield strength is commonly interpreted by the loss of strain hardening capacity, which leads to an increased propensity for premature failure due to shear band formation in age-strengthened alloys, e.g. [251]. The effect of material strength has also been indirectly studied by varying the test temperature, e.g. [222], but that assumes that other effects do not come into play.

A more conclusive, albeit qualitative, effect of matrix hardness on void nucleation in Al alloys was demonstrated using model materials [252]. With

increasing matrix strength, the mode of nucleation changed from particle decohesion at low strength (Fig. 28a) to particle cracking at high strength (Fig. 28b). Whether this mechanism transition is consistent with observa-

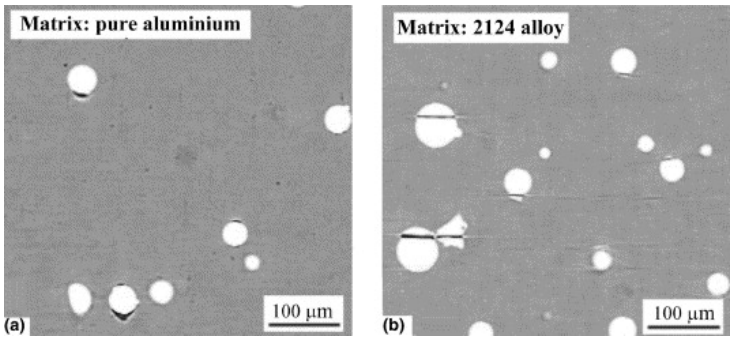

Figure 28: *Void initiation in tension of model metal matrix composites observed by high-resolution X-ray tomography. (a) Particle-matrix decohesion in a soft matrix (pure Al). (b) Particle cracking in a hard matrix (Al 2124). Printed with permission from Elsevier from [252].*

tions of void nucleation in Al alloys is difficult to ascertain given differences in inclusion rheology, size and shape between the model materials and commercial alloys. The mode of nucleation is rather more sensitive to particle elongation as well as temperature [249, 251]. On the other hand, the preponderance of particle cracking in high-strength steels is widely reported [51, 253].

3.4. Effect of strain hardening

Separating out the effects of strength and hardening on void nucleation is generally not possible in experiments. Maraging steels constitute a notable exception [250]. Some valuable results are also available from theory [222, 229].

Consider a particle–matrix system with, for the time being, hard particles ($\vartheta > 1$) and assume that nucleation does not occur in the elastic regime. As plastic deformation eventually takes place in the matrix, stress concentrations in the vicinity of the particle lead to spatially nonuniform strain hardening. A classical treatment of this effect amounts to an approximate extension of the so-called inclusion problem [217, 231] to the nonlinear case [222, 234]. The analysis is based on deformation theory and assumes uniform tangent moduli in the matrix. By way of consequence, the fields are approximated as uniform inside the inclusion such that $\kappa^{\mathrm{P}} = \kappa^{\mathrm{I}} \equiv \kappa$ and Equation (15) now simply writes:

$$\kappa\Sigma_{\mathrm{I}} = \min(\sigma_{\mathrm{c}}^{\mathrm{p}}, \sigma_{\mathrm{c}}^{\mathrm{i}}) \equiv \sigma_{\mathrm{c}} \tag{16}$$

Also, the inhomogeneity induced stress is estimated as:

$$\zeta\Sigma_{\mathrm{I}} = k\bar{E}\varepsilon_{\mathrm{eq}} \tag{17}$$

where $\zeta = \zeta^{\mathrm{P}} = \zeta^{\mathrm{I}}$ as above and k is a shape-dependent factor to be elucidated further below, $\bar{E}$ is an effective modulus and $\varepsilon_{\mathrm{eq}}$ is the effective plastic strain. Using a tangent-modulus based estimate for $\bar{E}$ leads to:

$$\zeta\Sigma_{\mathrm{I}} = \frac{k}{\beta}(\Sigma_{\mathrm{eq}} - \sigma_{\mathrm{y}}) \tag{18}$$

where Σ_{eq} is the von Mises effective stress, σ_{y} the initial yield stress of the matrix and $\beta \geq 1$ a heuristic factor introduced to capture nonuniform and path-

dependent strain-hardening around the inclusion, not explicitly accounted for in [234]. To obtain Equation (18), the authors also assumed that the tangent modulus is much smaller than the inclusion's elastic modulus. Recalling the identity $\kappa = 1 + \zeta$, the nucleation criterion Eq. (16) becomes, in view of Equation (18):

$$\Sigma_{\mathrm{I}} + \frac{k}{\beta}(\Sigma_{\mathrm{eq}} - \sigma_{\mathrm{y}}) = \sigma_{\mathrm{c}} \tag{19}$$

By construction, Equation (19) does not discriminate decohesion from fragmentation and is only valid in the plastic regime, but it embodies the effect of strain hardening in a simple way. For a nonhardening material, the inhomogeneous stress reduces to that due to elastic mismatch (not directly captured by Eq. (19)). The higher the hardening capacity of the matrix the larger the inhomogeneous stress and the more likely void nucleation.

The above criterion was tested by the Beremin group against experimental data for two pressure vessel low-alloy steels with elongated MnS inclusions as prime nucleation sites [222]. For one steel, data was available for two loading directions (rolling and through-thickness); for the other steel, data was available for three temperatures in the range 77K to ambient. The results were consistent with criterion (19) in that the slope and intercept of the fitting line were found to only depend upon the loading direction. For the slope, this reflects an inclusion shape effect through factor k. For the intercept, the orientation dependence reflects a change of mechanism from fragmentation when loading parallel to the MnS stringers to decohesion when loading perpendicular to them. In particular, a single critical stress (for fragmentation) was used to capture temperature dependence.

The nucleation criterion, Equation (19) can be rewritten so as to exhibit

dependence upon hydrostatic pressure. For axisymmetric loading, the criterion writes:

$$\Sigma_{\mathrm{m}} + k'\Sigma_{\mathrm{eq}} = \sigma_{\mathrm{c}}^{\mathrm{eff}} \tag{20}$$

with $k' = 2/3 + k/\beta$ and $\sigma_{\mathrm{c}}^{\mathrm{eff}} = \sigma_{\mathrm{c}} - k\sigma_{\mathrm{y}}/\beta$. A connection may then be drawn to an earlier model by Argon and co-workers [218], which has also served as a basis for a phenomenological model that is widely used in structural analysis [254]. Often, a criterion in the format (20) is used with adjustable parameters k' and $\sigma_{\mathrm{c}}^{\mathrm{eff}}$. The latter is then strongly temperature-dependent in materials with thermally activated plasticity, such as BCC metals (via the temperature dependence of σ_{y}). One disadvantage of using Eq. (20) is that the micromechanical basis underlying the criterion (through k in particular) is lost.

A pressure-dependent criterion in the format of Eq. (20) is also obtained, with a different parameterization, if one uses the secant modulus ($\Sigma_{\mathrm{eq}}/\varepsilon_{\mathrm{eq}}$) (as a crude estimate) for $\bar{E}$ in Eq. (17):

$$\Sigma_{\mathrm{m}} + k''\Sigma_{\mathrm{eq}} = \sigma_{\mathrm{c}} \tag{21}$$

with $k'' = k + 2/3$ and the same σ_{c} introduced in Eq. (16). However, such a criterion would lead to a strongly temperature-dependent σ_{c} and to inconsistent results given the physical meaning of k; see Fig. 10 and corresponding discussion in [222].

To date, criterion (19) does not seem to have been critically assessed. While valuable, the experimental validation offered in [222] has limitations in a number of respects: neglect of relative plasticity (see Section 3.8 for more details on this), uniform field approximation, constancy and significance of β, elastic modulus mismatch, to list but the most important factors.

The assumption of uniform tangent moduli is too strong: it is well known that mechanical fields are not uniform in the inclusion in the nonlinear case, e.g. [255]. Accounting for this non-uniformity would enable the propensity for decohesion versus fragmentation to be apportioned. In addition, in the Beremin criterion all heurism is included in the factor β which represents the hardening effect. Even considering that the format of Eq. (19) is appropriate, it is likely that history effects may not be quantitatively captured using a constant β. More work could be done to elucidate this effect.

Since accurate analytical estimates have remained elusive, various authors have resorted to computations with varying degrees of idealization [221, 225, 228, 229, 256]. Salient features of the computational estimates by Lee and Mear [229], were given in [257, 258] and are worth recalling here in context. These authors have employed a variational principle [259, 260] combined with a spectral representation of matrix deformation fields within the approximation of deformation theory. In spite of this limitation, the method is efficient in probing the parameter space and accurate for the problem at hand (no decohesion is modeled per se, hence no unloading).

Unlike Beremin-like models, the Lee–Mear analysis provides data relevant to both decohesion and fragmentation. Fig. 29 shows how the stress concentration factors κ^{P} and κ^{I} evolve with strain for two values of the strain hardening exponent (in a Ramberg-Osgood law) and two particle aspect ratios. From Fig. 29a and other results in [229], it appears that strain hardening has a negligibly small effect on stress concentration in the particle. A result of this sort would be difficult to ascertain on the sole basis of experiments. As for stress concentration at the interface, Fig. 29b, the effect is just as neg-

ligible for spherical particles ($w^{\mathrm{P}} = 1$) but becomes increasingly important for elongated particles, as illustrated here for $w^{\mathrm{P}} = 7$. However, the latter trend may not be as significant in practice because elongated particles loaded parallel to their axis typically undergo fragmentation, not decohesion. Under such circumstances, nucleation is governed by the hardening-insensitive κ^{P}, Fig. 29a.

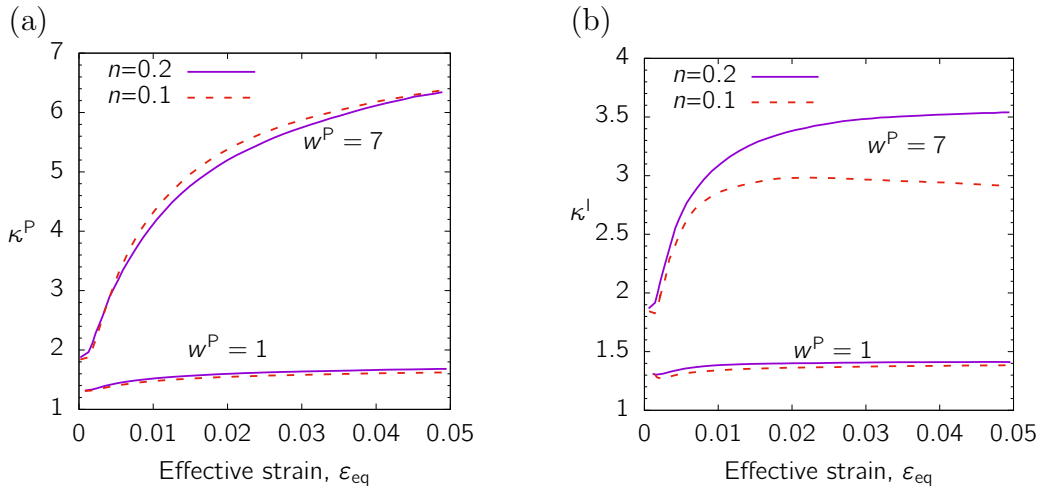

Figure 29: *Effect of the strain hardening exponent n on stress concentration (a) inside the particle; and (b) at the interface, for spherical ($w^{\mathrm{P}} = 1$) and elongated ($w^{\mathrm{P}} = 7$) elastic particles using $E^{\mathrm{P}}/E = 2$.* Case of uniaxial loading. *Adapted from [229].*

Analytical criteria that match the trends in Fig. 29 are still elusive. However, it is worth mentioning the attempt by Babout et al. [252] to distinguish between decohesion and fragmentation[3]. The formal basis is an earlier estimation of internal stresses in composites [261]. In their model, decohesion is taken to be strain-driven and, in their implementation, it is assumed to

[3]Unfortunately, the authors in [252] did not seem to be aware of the work of Lee and Mear [229].

begin at incipient plasticity. Because decohesion is immediate, they model stress relaxation in the particle using an effective stress concept so that the competition between the two mechanisms reduces to continuing decohesion until complete relaxation versus a switch to fragmentation upon attainment of a critical stress. An attractive feature of their model is a void nucleation mechanism map. However, the model is not general enough to be used and suffers from several weaknesses. Perhaps the most important one is that it deals with the average stress in the particle. This implies that the only way to discriminate among nucleation mechanisms is through the "effective" threshold conditions (recall that a critical stress for fragmentation is used but no critical interfacial stress per se). In actuality, stress concentration inside the particle may far exceed that at the interface (Fig. 29); this alone may be mechanism-discriminant, even if the critical stresses at the interface and inside the particle were the same.

3.5. Effect of stress state

A maximum principal stress criterion, Eq. (12), or a maximum normal interfacial traction criterion, Eq. (13), imply some dependence of void nucleation upon the state of remote stress. For example, the effect of hydrostatic stress (or negative pressure) is apparent in the format of Eq. (20). More generally, to the extent that the nucleation process can be viewed as isotropic, Equation (15) may be rewritten as:

$$\kappa \left(T + \frac{2}{3} \cos\theta \right) \Sigma_{\mathrm{eq}} = \sigma_{\mathrm{c}} \tag{22}$$

where superscripts are dropped for simplicity so that σ_{c} refers here to either decohesion or fragmentation and κ the corresponding concentration factor. The stress state is fully described by the dimensionless parameters T (stress triaxiality) and L (Lode parameter). Notable stress states include: axisymmetric loading with a major axial stress (arbitrary T and $\theta = 0$ or $L = -1$); axisymmetric loading with a major radial stress (arbitrary T and $\theta = \pi/3$ or $L = 1$); plane strain loading (arbitrary T and $\theta = \pi/6$ or $L = 0$), including simple or pure shear for which $T = 0$.

Only under the first type of loadings have estimates for κ been systematically obtained [229]. Clearly, for non-spherical particles the process cannot be isotropic and criteria (22) must be viewed as approximate in that regard. Fig. 30 shows typical evolution with strain of the interfacial and particle stress concentration factors over a range of triaxialities.

Clearly, the stress concentration is more intense under uniaxial loading ($T = 1/3$) and gradually decreases with increasing triaxiality. This trend holds irrespective of the particle aspect ratio w^{P}, the modulus mismatch

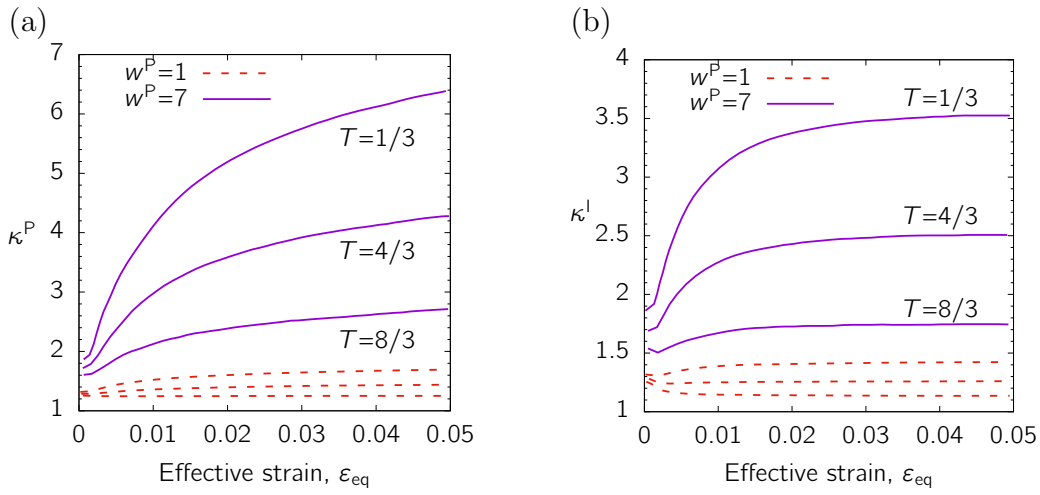

Figure 30: *Effect of the stress triaxiality ratio T under axisymmetric loading on stress concentration (a) inside the particle; and (b) at the interface, for spherical ($w^P = 1$) and elongated ($w^P = 7$) elastic particles using $n = 0.2$ and $E^P/E = 2$.* For both sets of results T increases from top to bottom curves. *Adapted from [229].*

E^P/E or the strain hardening exponent n. Note in passing the effect of particle elongation; also see Section 3.6 below.

The fact that high stress triaxiality leads to less stress *concentration* does not imply that void nucleation is favored at low triaxiality. What is of particular importance here is that the *driving stress* increases with increasing triaxiality. This is not immediate from Equations (12) and (13) or the basic form (15) of the nucleation criteria. However, this becomes clear having expressed the latter in Eq. (22). For the results shown in Fig. 30, the Lode angle $\theta = 0$ and, at any stage of deformation, the von Mises effective stress Σ_{eq} entering Eq. (22) is basically equal to the flow stress of the matrix (dilute limit of isolated particles). As the triaxiality T increases, κ clearly decreases (Fig. 30) but the driving stress is set by the product $\kappa(T+2/3)$ and increases within the range considered.

There are practical implications to Fig. 30 and like results. If plots of $\Sigma_{\rm eq}$ versus effective strain $\varepsilon_{\rm eq}$ were available it would be apparent that the critical stress $\sigma_{\rm c}$ would be attained at significantly lower strains as the triaxiality increases. In general, however, such plots are not readily available from experiments and the question of whether void nucleation truly depends on the hydrostatic stress (or negative pressure) has long been debated in the literature. Unfortunately, the issue has often been summed up in a rather confusing way in some influential work [221, 253], probably pervading to the present day. Typically, experimental data has been presented in one of two ways when investigating void nucleation criteria. In the first, e.g. [250, 253], the fraction of particles with voids is plotted versus the remote strain or remote applied stress; see Fig. 27 for instance. A variant of this method directly reports the void volume fraction [262, 263] or the number fraction of voids [264, 265] versus strain. In the second, threshold curves are plotted in stress space using appropriate measures, aided by finite element computations of local fields [221, 222, 266].

In general, a void nucleation theory rooted in the framework outlined in Section 3.2, as specialized in Eq. (22), leads to a nucleation strain that is a strongly decreasing function of triaxiality. Let us now examine whether the body of experimental data accumulated since the 1970s allows to verify or falsify such predictions. The early experiments of Cox and Low [253] support the thesis of a strong effect; see for example [51]. Their data for a commercial purity 18 Ni maraging steel are replotted in Fig. 31. Comparison is made between data collected using smooth specimens (low triaxiality: 1/3 prior to necking then gradually increasing post-necking) and notched specimens

(significantly higher triaxiality). In smooth specimens it takes up to a strain

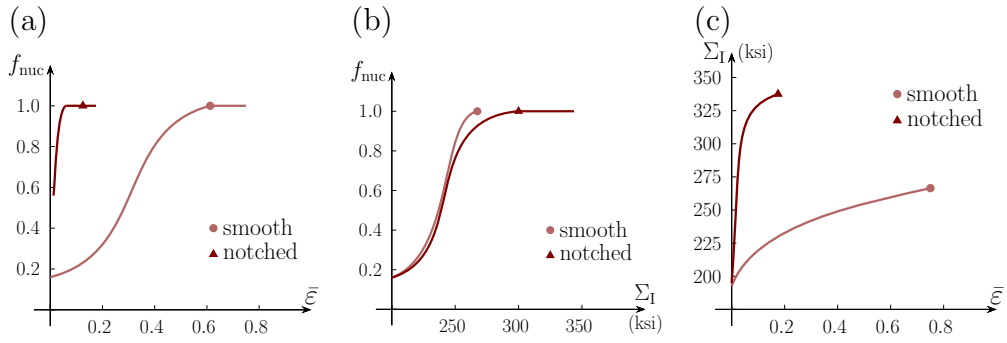

Figure 31: *Void nucleation curves in a maraging steel using (a) the true strain and (b) the average applied stress, as the independent variable. (c) Tensile curves for the steel. Adapted from [253].*

of ∼0.6 before all inclusions in the zone of interest have nucleated voids, Fig. 31a. By way of contrast, the strain hardly exceeds 0.1 in the notched bars before the same stage is attained.

Interestingly, Cox and Low [253] state: "[Their] Fig. 8 [i.e. Fig. 31b here] demonstrates that the level of tensile stress triaxiality has no measurable effect on void nucleation in these maraging alloys." This view, which has pervaded in segments of the literature, is founded in their replotting the data in terms of the average applied stress F/A with F the applied load and A the current area at the neck or the notch root, Fig. 31b. In doing so, the data for smooth and notched bars collapse into a single curve and Cox and Low seem to infer the absence of a triaxiality effect from this. This reasoning is obviously faulty[4]. As stated in opening this section, an effect of the major principal stress, with F/A as a surrogate in the experiments, im-

[4]The authors may have revisited their interpretation of their own experiments in [50].

plies pressure-sensitivity. In essence, the results of Fig. 31b and the like only give credence to the fundamental character of a maximum principal stress or interfacial traction criterion. Then, combining the theoretical results about stress concentration, Fig. 30, with the actual tensile stress levels, Fig. 31c, demonstrates that the driving stress is much higher in notched specimens than in smooth ones, thus resulting in the outcome of Fig. 31a.

Curiously, Argon has entertained a similar confusion in his final work on the topic [221] synthesizing earlier research by his group [218, 267, 268]. Adopting the general form of Equation (13), his criterion for interfacial debonding reads (using our notation):

$$\sigma_{\mathrm{n}}^{\mathrm{I}} = \sigma_{\mathrm{c}}^{\mathrm{i}}, \qquad \text{with} \quad \sigma_{\mathrm{n}}^{\mathrm{I}} \approx \Sigma_{\mathrm{eq}} + \Sigma_{\mathrm{m}} \tag{23}$$

The interfacial stress $\sigma_{\mathrm{n}}^{\mathrm{I}}$ was estimated using the threshold method, which relies on hybrid experimental and computational input. The experimental basis consists of round tensile bars with artificially machined necks [218] deformed to fracture. The spatial threshold corresponds to a distance from the fracture surface at which the density of separated particles has vanished. At such locations, deemed critical, the hydrostatic stress Σ_{m} and the effective plastic strain, $\varepsilon_{\mathrm{eq}}$, were evaluated from finite element calculations [268] so that the local flow stress $\Sigma_{\mathrm{eq}}(\varepsilon_{\mathrm{eq}})$ could be evaluated. Then, according to the nucleation criterion in [267], reproduced in Equation (23), the critical interfacial stress $\sigma_{\mathrm{c}}^{\mathrm{i}}$ was determined as the sum of the so-computed Σ_{m} and Σ_{eq}. In Fig. 11 of [221], Argon summarized all data for the first time by plotting $\sigma_{\mathrm{c}}^{\mathrm{i}}$ for up to eight levels of superposed hydrostatic tension Σ_{m} and three materials (two steels and a Cu alloy). The data unequivocally gives credence to a critical interfacial normal stress criterion. However, Argon

notes: "The data which do not fit the straight-line form suggested by equation (11)[5] [...] suggest that for the range of mean normal stress applied in these experiments the effect is not as large as was expected." The effect is just as large as expected, but the lines in his Fig. 11 were ill-conceived.

Argon's criterion in Eq. (23) delivers a precise (and accurate) prediction of the triaxiality effect. Recasting it in the format of Eq. (22) with $\theta = 0$ one gets:

$$\kappa = 1 + \frac{\frac{1}{3}}{T + \frac{2}{3}} \tag{24}$$

which gives values slightly smaller than the steady-state values of Lee and Mear [229]. Limited to spherical particles, the above analytical estimate has practical value.

In a paper that is mostly known for the cohesive zone methodology, Needleman [226] introduced putative notions of void nucleation strain and effective void nucleation stress. He obtained results that clearly show a decreasing nucleation strain with increasing triaxiality. His results are, however, limited to $T > 2/3$ and nucleation by decohesion. As discussed by Benzerga and Leblond [269], a triaxiality of 2/3 is the limit below which complete decohesion would be impossible and Needleman's nucleation strain would be infinite. Needleman also hypothesized that the effective nucleation stress be significantly smaller than the critical stress σ_c^i, which is the counterpart of the peak cohesive strength in his model. To date, this proposal does not seem to have received the attention it deserves.

Figure 32 illustrates the phenomenon of void locking by the particle,

[5]The reader will note that Eq. (11) in [221] is erroneous. The correct form is that of Equation (23), which is the same as Eq. (6) in [267] or Eq. (1) in [218].

which typically occurs for $T < 2/3$. The situation corresponds to an oxide in the neck of a high-strength low alloy steel tensile bar loaded *in situ* [270]. Strain incompatibility between matrix and particle induces transverse compression such that decohesion cannot be complete. A sophisticated analysis of void locking may be found in [271, 272]. For a triaxiality above 2/3, interfacial tractions are all tensile, but it may take even higher triaxiality to reach the interfacial strength around the particle for complete decohesion.

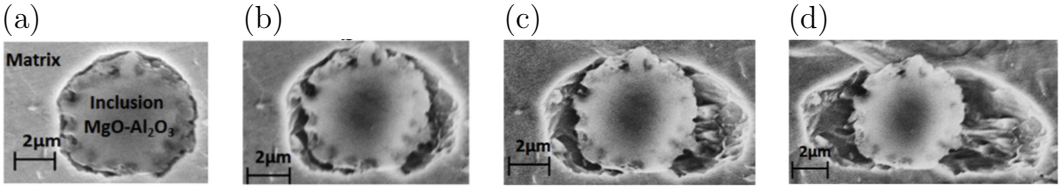

Figure 32: *Void nucleation by decohesion in tension. Adapted from [270].*

Investigations of the third stress invariant (or the Lode parameter L) on void nucleation remain scarce. Horstemeyer and Gokhale [273] posited a model motivated by fracture mechanics applied to an incipient crack (in the particle or at the interface). Their criterion includes dependence upon both T and L, but that only enters because of an assumed dependence of the flow stress upon T and L. Other (micromechanical) studies did not set out to explore the effect of L; yet some trends may be inferred by comparing various results. Most analyses considered axisymmetric stress states (arbitrary $T \geq 1/3$; $L = -1$) [226, 229]. However, the first detailed finite element study by Argon et al. [267] focused on plane strain states (arbitrary $T \geq 0$; $L = 0$). The fact that their estimate of stress concentration (see Eq. (23)) is close to that of Lee and Mear suggests a weak effect of the Lode parameter. In addition, if their basic estimate obtained for pure shear holds irrespective of

L then the stress concentration factor in shear is at least 1.5. This result complements the findings in [229], which did not consider shear dominated loadings. Systematic analyses are needed to ascertain this.

Figure 33 illustrates the process of particle debonding under shear-dominated loading. A state of pure shear being equivalent to tension and compression along diagonals, the debonding process is similar to that in tension at an angle. Here too, locking by the inclusion occurs since the triaxiality (nil in shear) is lower than 2/3. One quantitative difference with tension is that it takes much more straining under shear to cause visible decohesion. One reason for this may be the lack of a driving force for growing the nascent void cap, given the low triaxiality that prevails in shear.

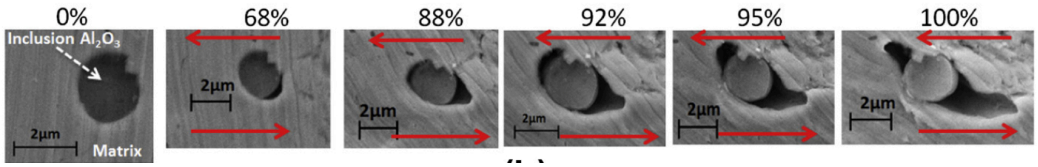

Figure 33: *Void nucleation by decohesion in shear. Adapted from [270].*

Given a mechanism of nucleation (decohesion versus cracking), the effect of stress state may be understood based on what precedes. Whether the stress state affects changes in the nucleation mechanism itself is very much plausible. For example, sufficiently brittle particles may break under uniaxial loading and decohere under sufficient triaxiality. More generally, the influence of stress state on the *mode* of nucleation is established, regardless of the mechanism [224]. If particles were to break in tension perpendicular to the tensile axis, then in compression they would break due do (local) tensile stresses induced perpendicular to the remote compression. This constitutes

a mode of particle cracking which is quite different from tension. It may explain that larger strains may be needed in compression before the same fraction of particles with voids are observed; compare Figs. 14 and 15 in [273].

3.6. Effect of particle shape

Particle shape effects have essentially been confined to particles that can be regarded as ellipsoidal and the possible effects of sharp corners in crystallographically faceted, cuboidal, plate, or needle-like particles are not here considered. Further, in this continuum-scale interpretation, the anisotropic properties of the matrix and particle, as well as the possible interfacial anisotropies, are also not considered. Nevertheless, even in this first approximation, particle shape plays a key role in void nucleation. Critical stress criteria based on continuum mechanics are well suited to incorporate this effect. Indeed, solutions to the inclusion problem lead to explicit, albeit complex, expressions for the inhomogeneity induced stress in terms of descriptors of particle shape. The solution is exact in the elastic case [231] or approximate in the elastoplastic case [234]. The two solutions were employed by Tanaka *et al.* [217] and Beremin [222], respectively. Thus, the Beremin criterion, Eq. (19), involves the shape dependent factor $k(w^{\mathrm{P}})$ where w^{P} refers to the aspect ratio of the particle modeled as spheroidal, Fig. 34.

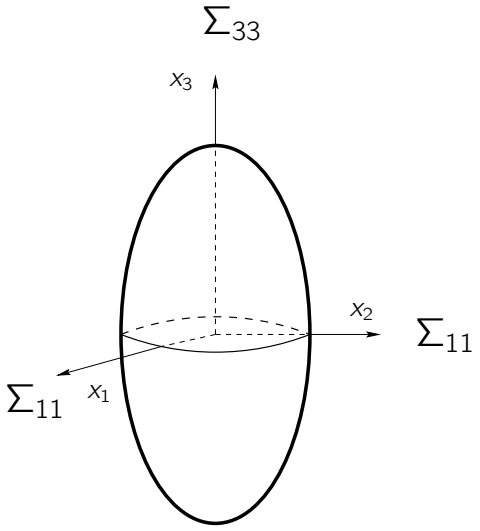

Figure 34: *Spheroidal particle under remote axisymmetric loading. The aspect ratio w^{P} is defined as the major semi-axis (along x_3) divided by the minor semi-axis, such that $w^{\mathrm{P}} > 1$ for prolate particles and $w^{\mathrm{P}} < 1$ for oblate ones.*

In fact, the expression for k depends on the relative orientation of the particle with respect to the loading; see Fig. 35. To illustrate the effect of w^{P}, consider the case of uniaxial loading. The Beremin stress

concentration factor then reads:

$$\kappa = 1 + \frac{k}{\beta}\left(1 - \frac{\sigma_y}{\Sigma_{eq}}\right) \qquad (25)$$

For simplicity, take $\beta = 1$ and consider a power law hardening matrix with $n = 0.1$ and a strain of 0.05, which according to Lee and Mear's results would correspond to steady state. Then, for an elongated particle, say $w^P = 10$, the shape factor k is about 8.5 resulting in $\kappa \sim 3.4$ for longitudinal loading (Fig. 35a) and 2.8 giving $\kappa \sim 1.8$ for transverse loading (Fig. 35b). For a flat particle, say $w^P = 0.1$, one finds $k = 2.2$ and $\kappa \sim 1.6$ for longitudinal loading (Fig. 35d) and $k = 6.4$ and $\kappa \sim 2.8$ for transverse loading (Fig. 35e). For reference, $k = 1$ and $\kappa \sim 1.3$ for a spherical particle. None of these values is exact but the relative change shows how effective stress concentration becomes when a particle is loaded along its largest dimension. For off-axes loadings, Beremin does not provide explicit formulas. Marteleur et al. [274] have recently proposed a tensorial reformulation of the Beremin criterion that would enable, in principle, predictions of void nucleation when the principal axes of loading are not aligned with those of the particle. They provided, however, no data for such loading situations.

For a linear elastic matrix, the stress and strain fields are uniform inside the inclusion [231]. However, for an elastoplastic matrix the fields are not uniform. Yet, the inclusion problem solution [234] upon which the Beremin criterion is based as-

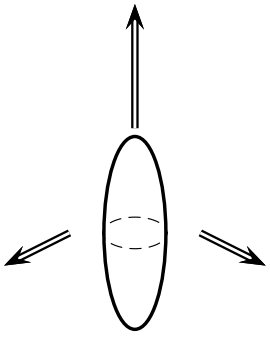

(a) $k(w) = \frac{2}{3}\left(-1 + \frac{1}{3}\frac{1+2w^2}{2\ln(2w-1)-1}\right)$

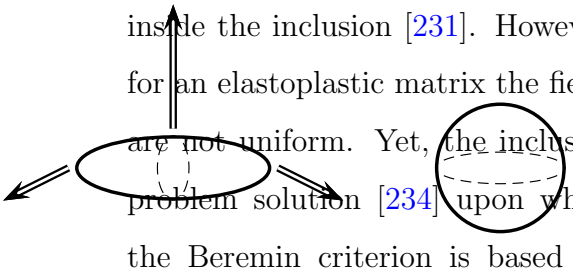

(b) $k(w) = \frac{1}{2}\left(1 + \frac{1}{9}\frac{1+2w^2}{2\ln(2w-1)-1}\right)$ (c) $k = 1$

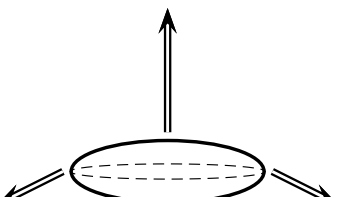

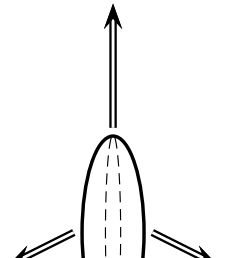

sumes uniform fields inside the inclusion. For this reason, the criterion predicts the same stress concentration inside and at the interface and hence cannot discriminate decohesion from particle cracking. Here again, recourse to the numerical results of Lee and Mear [229], which extend those of Wilner [228], is useful. An example is shown in Fig. 36 depicting the distribution of the interfacial normal traction along the interface. The results are shown for two values of the particle aspect ratio and two triaxiality levels. Under uniaxial loading (Fig. 36a), if local debonding initiates it is much more likely to propagate for spherical particles than for elongated ones. For high triaxiality (Fig. 36b), the interfacial normal traction is everywhere tensile and more uniformly distributed, irrespective of the particle aspect ratio. Therefore, once debonding initiates it will likely continue to complete separation.

These results have significant implications. For nucleation by particle fracture, the normal stress is roughly uniform in the meridian plane [229]. However, interfacial debonding is a process with an initiation and a propagation stage, as evidenced by cell model analyses [226]. Depending on triaxiality, void locking by the particle may prevent complete debonding, typically

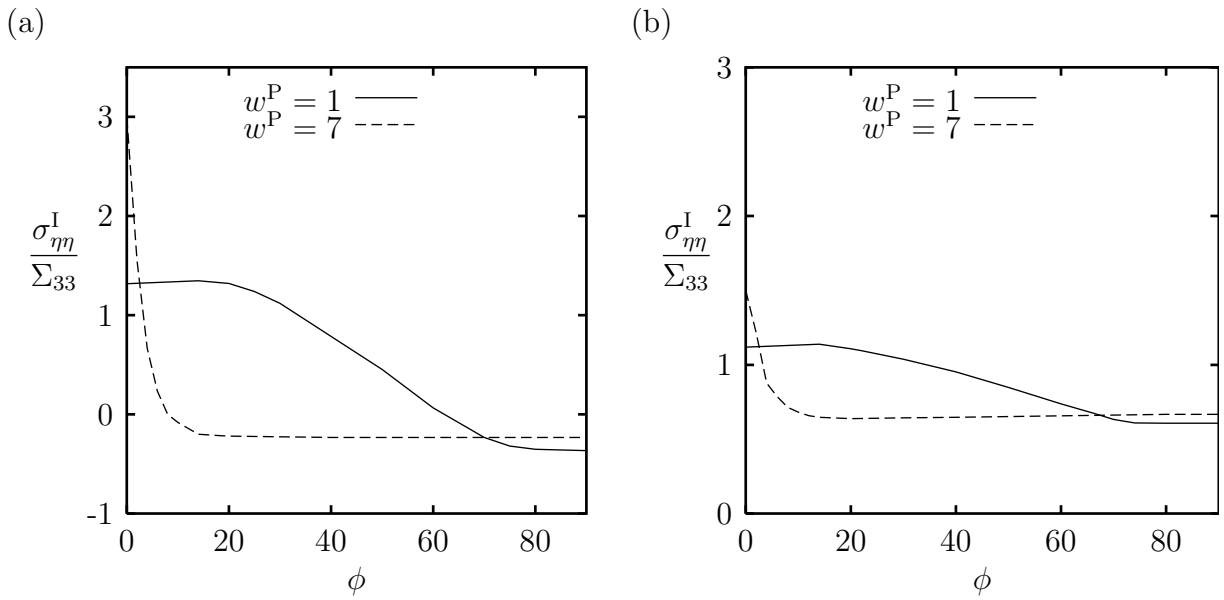

Figure 36: Interfacial normal traction, normalized by remote axial stress Σ_{33}, versus the angle ϕ measured from the x_3-axis. Results are shown for two particle aspect ratios, $n = 0.1$, $E^{\mathrm{P}}/E = 2$ at an effective strain of $E_e = 0.03$. (a) Uniaxial loading ($T = 1/3$); and (b) $T = 8/3$. Adapted from [229].

for $T < 2/3$ [272]. Even at higher triaxiality, the strain range over which debonding takes place can be significant [226]. Under such circumstances, the basic format of criterion (13) is adequate for initiation but not for complete void formation.

With this in mind, and referring back to Fig. 29 the effect of particle shape on stress concentration is perhaps the strongest among all relevant factors (rheological, morphological or loading related). The higher the aspect ratio the stronger the stress concentration. While this was shown for particular values of n and E^{P}/E, it holds for any other values. Interestingly, the stress intensification is even larger inside the particle. To quantify this, Fig. 37 shows the ratio $\kappa^{\mathrm{P}}/\kappa^{\mathrm{I}}$ versus strain for uniaxial loading. As soon as plastic

flow sets in, stress concentration inside the particle is greater than at the interface. The difference between κ^{P} and κ^{I} is enhanced by a large particle aspect ratio. For a material with a large strain hardening capacity (high n) stress concentration is enhanced at the interface but not much inside the $w^{\mathrm{P}} = 7$ particle; see Fig. 29. Hence, a large hardening capacity tends to decrease the difference between the two types of stress concentration. A practical implication of these predictions is that if the particle and interfacial strengths are equal ($\sigma_{\mathrm{c}}^{\mathrm{p}} \sim \sigma_{\mathrm{c}}^{\mathrm{i}}$), then particle fracture would be favored over decohesion for large aspect ratios. This prediction is largely consistent with experimental observations.

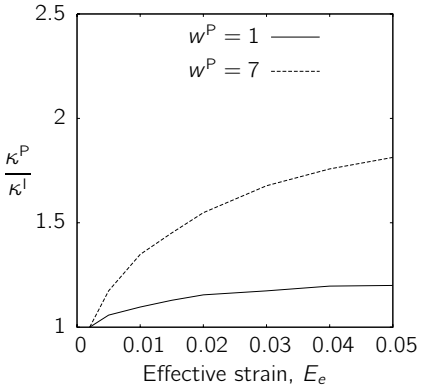

Figure 37: *Particle stress concentration factor, κ^{P}, relative to the interfacial stress concentration factor, κ^{I}, versus effective strain E_e for uniaxial loading ($T = 1/3$), $n = 0.1$, $E^{\mathrm{P}}/E = 2$ and two particle aspect ratios. Adapted from [229].*

3.7. Effect of modulus mismatch

To our knowledge, there are no systematic experimental studies of the effect of modulus mismatch between particle and matrix. Therefore, much of what is known about this effect is based on analysis. Typically, the particle has been modeled as rigid [226, 267] or elastic [217, 222, 229, 231]. When modeled as elastic, the particle is generally taken as more stiff than the matrix. We are not aware of analyses taking into account yielding in the particle; see Section 3.8 for a summary of what is known about relative plasticity effects. In what follows, the particle is assumed to be elastic.

If there is no modulus mismatch then any stress concentration would require the onset of plastic flow in the matrix. If the particle has a higher modulus compared to the matrix, some stress concentration is expected before yielding in the matrix. One issue is whether the elastic stress concentration has any incidence on subsequent stress concentration, that is after matrix yielding. Fig. 38 reports some results due to Lee and Mear [229] showing the effect of E^{P}/E on the interfacial stress concentration factor. The influence of modulus mismatch is significant at small strains, but essentially disappears after sufficient straining.

In general, both κ^{I} and κ^{P} increase with E^{P}/E, all things being equal. Thus, if the critical thresholds are low enough for nucleation to occur at small strains, then stiff particles would favor nucleation. This trend is consistent with findings by Tanaka *et al.* [217]. However, if the critical stress is high enough for nucleation not to occur before a few percent of plastic strain then the influence of modulus mismatch would be of second order. Here again, it is worth noting the convoluted effect of particle shape, Fig. 38b. The

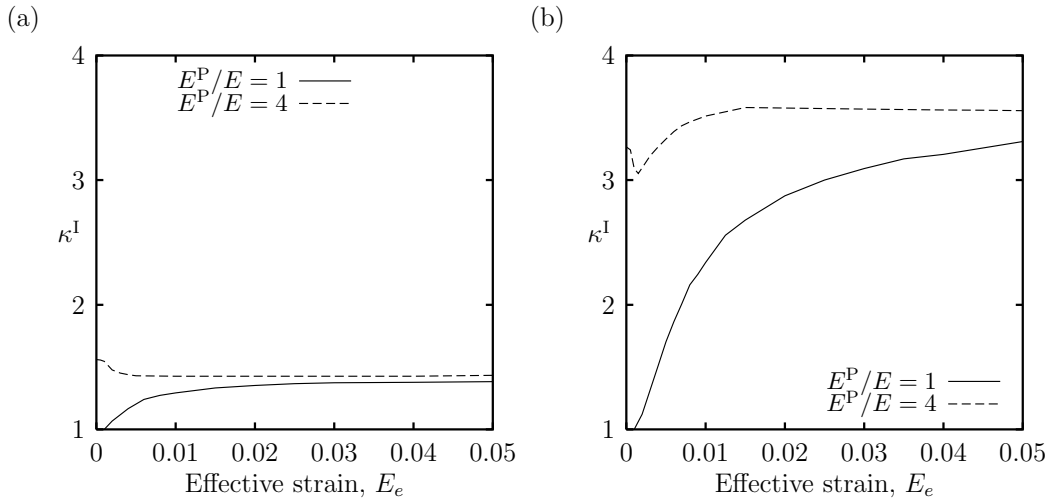

Figure 38: Interface stress concentration factor, κ^{I}, versus effective strain E_e for $n = 0.2$, uniaxial loading ($T = 1/3$) and two values of the modulus mismatch E^{P}/E (a) Spherical particle, $w^{\mathrm{P}} = 1$; and (b) Elongated particle with $w^{\mathrm{P}} = 7$. Adapted from [229].

sensitivity to modulus mismatch is more significant for elongated particles loaded parallel to their main dimension.

3.8. Effect of relative plasticity

In steels, commonly encountered particles are oxides, carbides, nitrides and sulfides. Oxides and carbides are both harder and stiffer than the Fe matrix. However, sulfides are typically softer. For example, the qualitative difference between the nucleation curves of carbo-nitrides and sulfides in Psioda's data (compare Fig. 27b and c) may be discussed on the basis of relative plasticity effects. Indeed, the Ti_2S particles are soft relative to the matrix so that $\vartheta \leq 1$ for all heats considered in [250]. Thus, increasing the strength of the steel amounts to decreasing ϑ; cf. Equation (10).

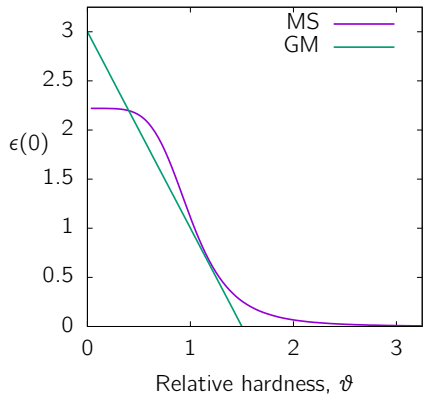

Figure 39: *Initial relative applied strain, $\epsilon(0)$, versus relative hardness, ϑ, as predicted by two models.* Model MS: matrix and inclusion are hardenable; Model GM: matrix and inclusion are perfectly plastic. *Adapted from [275].*

Fig. 39 shows the theoretical evolution of relative deformation with ϑ. The plotted value $\epsilon(0)$ refers to the initial state. The model labeled 'MS' is an approximate formula derived by interpolating McClintock's results [276] for a linearly viscous (Newtonian) behavior and ideal plasticity (extreme nonlinearity) [277]. The model labeled 'GM' is based on the work of Gilormini and co-workers [223] assuming perfectly plastic phases. Both models compare very well against experimental results, e.g. [278]. These results show that as ϑ decreases, the relative deformation of the inclusion increases, thus decreasing the interfacial normal

stress as well as the maximum principal stress in the inclusion (relaxation effect). The remotely applied stress Σ_{I} must therefore increase before either nucleation criterion is met, Equations (12) and (13). This may explain the trend noted by Van Stone *et al.* [50]. Further discussion of this point will be provided in Section 4.

Another example where the relative plasticity of sulfides is expected to play a role is in estimating nucleation thresholds in C-Mn ferritic steels. The particles of interest are here manganese sulfides (MnS) having either fiber or disk morphology depending on whether processing is by rolling or forging, respectively. Based on experimental measurements combined with analysis, Beremin [222] determined the thresholds for decohesion and particle cracking to be about $\sigma_{\mathrm{c}}^{\mathrm{i}} \sim 820$ MPa and $\sigma_{\mathrm{c}}^{\mathrm{p}} \sim 1120$ MPa, respectively. These values were determined based on observations of decohesion when loading perpendicular to the main axis of the inclusions and cracking when loading parallel to the inclusions. One issue is why decohesion does not occur under longitudinal loading since its threshold is lower. Part of the answer lies in the particle aspect ratio, which induces a stronger intensification of stress concentration inside the particle when compared with the interface; see Fig. 29. However, the results in Fig. 29 are contingent upon the particle remaining elastic throughout the deformation process. This is questionable for MnS inclusions on account of their basic properties. Indeed, MnS inclusions are half as stiff as the ferritic matrix [279] while being just as hard at the ambient and much softer at elevated temperatures (see Fig. 26). The modes of plastic deformation of MnS particles have been studied by Van Vlack *et al.* [239].

Therefore, when the steel–MnS system is deformed (parallel to the parti-

cles) it is likely that MnS inclusions yield first, thereby leading to significant stress relaxation, especially inside the inclusions. One implication is that the threshold stresses σ_c^i and σ_c^p are much closer together, and in fact closer to the lowest of the two values determined by Beremin since MnS yielding is unlikely under transverse loading. This fact has been taken advantage of in analyzing the damage and fracture anisotropy of this class of steels [280, 281] by assuming early nucleation. This issue deserves more attention for more general sulfides or other soft particles.

3.9. Size Effects

Void nucleation and early-stage growth span length scales from the atomic to the micron scale. It is thus expected that size effects manifest in various ways. What is of particular importance is whether there is a particle size below which particle-based nucleation is, in practice, unlikely. An equally important question is whether a large particle size favors or rather inhibits nucleation. This probably depends on the mechanism of nucleation, decohesion versus brittle cracking. Also, whether a size effect, if any, is affected or caused by local variations in particle volume fractions has been investigated. We shall see that on most, if not all of the above listed issues, there is no consensus in the literature.

Several length scales naturally emerge. The first type is microstructural, importantly the particle size and to a lesser extent the particle spacing. The second length scale is deformation driven and is well represented by the spacing of dislocations in the vicinity of the particle. The third length scale pertains to the nucleation mechanism itself: a cohesive length if the process is driven by an interfacial stress or a critical flaw dimension if particle crack-

ing prevails. Finally, in the case of a steep strain gradient, the geometric constraints on dislocation plasticity may represent a fourth length scale, not discussed at length here but reviewed in [282].

We are not aware of any analysis that accounts for all types of length scales. The problem has been approached in three ways. The basic ideas and conclusions of each approach are outlined below with an aim to pave the way for further research on the matter. We note at the outset of this section that none of these approaches account for the deformation-induced defects discussed in Section 2 and their influence on particle size effects.

3.9.1. Continuum micromechanics

In the first approach, the only length scale considered is the particle size. An energy criterion is necessary in that the energy stored in the particle, and released upon nucleation, must equal or exceed the energy required to form new surfaces. Since the former scales with the volume of the particle, the latter with its surface area, the inequality results in a particle size dependent strain to nucleation. This critical strain is a lower bound. On the other hand, a stress criterion is often sufficient for nucleation of a void. Within the confines of continuum mechanics, the driving stress is size-independent thus resulting in a particle size independent critical strain. Satisfying both criteria concurrently results in a critical particle size, d_c. The energy criterion governs nucleation for sufficiently small particles whereas the stress criterion governs nucleation of particles larger than the critical size. The process is shown schematically in Fig. 40a.

A classical treatment of this sort is by Tanaka et al. [217]. It is limited to decohesion under remote uniaxial tension and for a spherical inclusion. Yet,

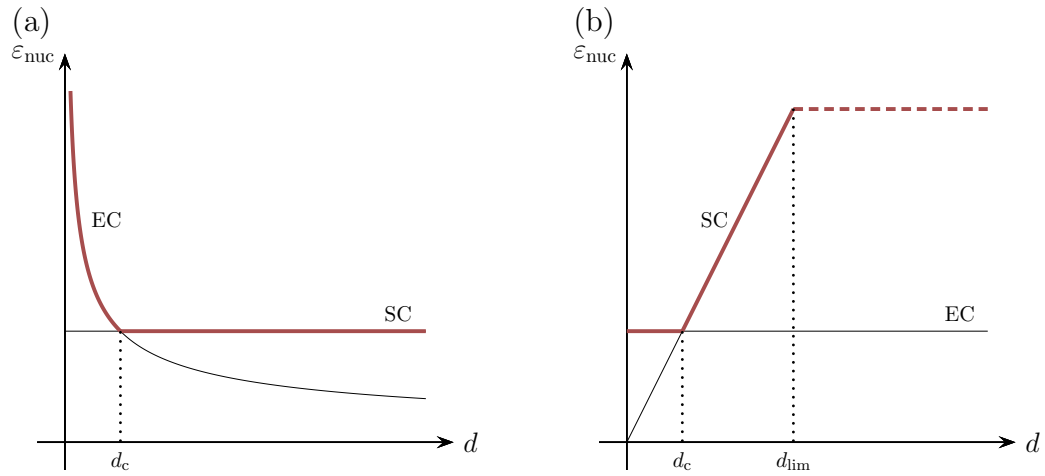

Figure 40: Strain to nucleation versus particle diameter, as predicted by typical methods of (a) continuum micromechanics and (b) dislocation plasticity. EC and SC refer to the energy criterion and stress criterion, respectively.

it illustrates the key trends in terms of size effects, as predicted by this type of approach. Determination of the critical diameter d_{c} hinges on estimating the maximum interfacial stress, the critical stress $\sigma_{\text{c}}^{\text{i}}$, the surface energies of both the particle and the matrix as well as the assumed fraction of the free surface formed in calculating the change in strain energy (e.g., the size of the crack). The total stress was taken as the sum of an inhomogeneity induced stress (modulus mismatch effect) and an internal stress in the particle (due to plastic deformation being restricted to the matrix). Both components were estimated using the transformation strain theory of Eshelby [231, 283]. The critical stress was estimated as the ideal strength of the weaker side (particle or matrix). Also, the total surface area was considered, although it should be noted that a putative inclusion was assumed in the cavitated state to account for partial contact with the matrix.

Using this method, the critical diameter was found to lie in the range

10–20 nm. This estimate is robust in that it was found to hold for wide ranges of applied stress (0 to $E/100$) and particle stiffness (same as matrix to infinite—rigid). There are reasons to question a continuum analysis at such a scale. But before doing so in the next section, it is important to note the uncertainties underlying the above treatment and study their effect on a better estimate of d_c.

There is uncertainty in various aspects of the treatment of Tanaka et al. The stress field based on Eshelby's solution [231, 283] is likely an overestimation of the actual stress in the nonlinear case. This can be, in principle, revisited using the results in [222, 234] which better account for plastic relaxation. The critical stress taken as either $E/10$ or $E^P/10$ is clearly an overestimation, as pointed out in [224]. Surface energies can be better estimated with today's computational chemistry methods. Finally, Tanaka et al. took the total surface area of the particle, but as pointed out in [56], only a void cap opens up at the poles under uniaxial loading and slowly propagates. On account of all four factors, it is likely that both the stress criterion estimate and energy criterion estimate would go down, with the former being affected more by the use of ideal strength as a critical stress for decohesion. Details aside, some of these factors could lead to an order of magnitude change in d_c. Thus, a more accurate continuum micromechanics estimate (yet to be fully developed) for d_c would lie in the range 100–500 nm, if not above it.

3.9.2. Dislocation-based approach

Interestingly, the same cut-off $d_c \sim 10$ nm was invoked by Argon et al. [267] to justify a continuum analysis above it. This could hardly be justified

based on what we know today about micron-scale metal plasticity [257, 284]. Regardless of the order of magnitude of d_c, there is consensus that below d_c the continuum approach cannot be relied upon to determine nucleation thresholds and dislocation plasticity should be used.

Two length scales are included, at least implicitly, in dislocation-based approaches: the particle size and the dislocation spacing (via the dislocation density). A well-known theory of this sort is due to Goods and Brown [56]. Their theory predicts a *size-independent* estimate of the nucleation strain below a critical size d_c and a *size-dependent* nucleation strain above it. This trend contrasts with continuum micromechanics, Fig. 40.

In its simplest form, the theory proceeds from the same energy criterion as Tanaka et al.'s:

$$V^{\mathrm{p}}\Delta e_{\mathrm{el}} + S^{\mathrm{p}}\Delta\gamma \leq 0 \tag{26}$$

where e_{el} is the elastic strain energy per unit volume stored in the particle, γ is the surface energy and Δ refers to a change from before to after cavitation. Also, V^{p} and S^{p} denote the particle's volume and surface area, respectively, assuming complete decohesion. Their estimate of Δe_{el} is based on an analysis by Brown and Stobbs [219] which gives:

$$\Delta e_{\mathrm{el}} = -\mu^{\mathrm{p}}\epsilon_{\mathrm{p}}^{*2} \quad \text{with} \quad \epsilon_{\mathrm{p}}^{*} = a\sqrt{\frac{b}{d}\varepsilon_{\mathrm{eq}}} \tag{27}$$

where μ^{p} is the shear modulus of the particle and $\epsilon_{\mathrm{p}}^{*}$ is a measure of strain incompatibility, which is a convenient dimensionless measure of internal stress [219]. In Equation (27), b denotes the Burgers vector, d the particle diameter, $\varepsilon_{\mathrm{eq}}$ an effective plastic strain and a a constant close to unity[6]. Substituting

[6]The constant $a/\sqrt{2}$ was taken as unity in [56] (using the radius $d/2$ and with $\varepsilon_{\mathrm{eq}}$

Eq. (27) into Eq. (26) delivers the critical strain for nucleation:

$$\varepsilon_{\mathrm{nuc}} = \frac{6}{a^2}\frac{\Delta\gamma}{\mu^{\mathrm{p}} b}, \tag{28}$$

which is independent of particle size d. Clearly, this result is rooted in equation (27). Although phenomenological in nature, this relation has a rather sophisticated micromechanical basis (in the sense of dislocation plasticity) since $\epsilon_{\mathrm{p}}^{*}$ is related to the number of Orowan loops around the particle. To account for partial debonding, Goods and Brown also propose a heuristic modification that lowers equation (28) without changing the qualitative picture.

Following Ashby [216] and Tanaka et al. [217], Goods and Brown formulate a concurrent stress criterion for interfacial failure, formally just like Eq. (13). There is no self-contained exposition of their void nucleation theory, since the chief concern of Brown and co-workers had earlier been to develop a physical metallurgy theory of work hardening in particle-strengthened systems; see [219] and references therein. For this reason, their derivations contain uncertainties[7]. Since we are concerned with qualitative trends, we have

interpreted as the engineering shear strain), but that is clearly an approximation. In [219] $a/\sqrt{2} = 0.7$.

[7]Brown and Stobbs [219] first estimate the interfacial stress under remote shear using limit analysis but the yield criterion was unspecified; it is likely a maximum shear stress criterion. If the matrix shear yield strength is used then $c \approx 4.2$ in Eq. (29). Hence, if σ_{eq} is taken as the matrix yield stress in tension $c = 2.1$. If a Taylor correction is assumed, as Brown and co-workers often do, then $c = 1.4$. If finally the hydrostatic component of uniaxial tension is included then $c \approx 1$, which is close to other estimates. For reference, Argon's finite element calculations and the Lee–Mear estimate would give $c \approx 1$. However, there is no indication that any such assumptions should be incorporated in their analysis [56]. It is likely that the discrepancy is due, for the most part, to the fact that the velocity fields used by Brown and Stobbs are *not* kinematically admissible in that they are inconsistent with the remote boundary conditions. The discrepancy is due, at least in part,

introduced some constants where appropriate. Their criterion is formally similar to Argon et al.'s [267], and writes Eq. (23):

$$\sigma_{\mathrm{n}}^{\mathrm{I}} = c\sigma_{\mathrm{eq}} + \Sigma_{\mathrm{m}} = \sigma_{\mathrm{c}}^{\mathrm{i}}, \tag{29}$$

where the notation σ_{eq} is used instead of Σ_{eq} to emphasize that it is the *local* flow stress in the vicinity of the particle that dominates in their criterion[8]. It is given by:

$$\sigma_{\mathrm{eq}} = \alpha\mu b\sqrt{\rho_{\mathrm{loc}}} \tag{30}$$

where ρ_{loc} denotes the local dislocation density, μ is the shear modulus of the matrix and α a material-dependent constant calibrated on experiments[9]. The local dislocation density was estimated after complete relaxation using a plastic zone size used in their upper bound estimate, and takes the form:

$$\rho_{\mathrm{loc}} = g\frac{\varepsilon_{\mathrm{eq}}}{db} \tag{31}$$

with g a geometric factor[10]. On account of both Eqs. (30) and (31), the stress criterion (29) delivers a critical strain to nucleation given by:

$$\varepsilon_{\mathrm{nuc}} = \frac{1}{\alpha^2 c^2 g}\left(\frac{\langle\sigma_{\mathrm{c}}^{\mathrm{i}} - \Sigma_{\mathrm{m}}\rangle}{\mu}\right)^2 \frac{d}{b} \tag{32}$$

---

to the different particle geometry (square in [219] versus spheres in [229, 267]). A relatively large value of c, hence of stress concentration, is used in the Goods–Brown estimates of the nucleation strain. Interestingly, Ashby and co-workers have used $c = 1$ in conjunction with the Goods–Brown nucleation criterion when constructing fracture mechanism maps [285].

[8] We have omitted the flow stress of the 'background medium' whose contribution is small because it scales with the volume fraction of particles. This has no incidence on the size effect.

[9] The value of α can be obtained by calibration on: (i) flow stress data giving $\alpha \approx 0.19$; or (ii) internal stress data underlying $(27)_2$ giving $\alpha \approx 0.13$; see [219]. The fact that the two values are close is good for model consistency.

[10] For a plane square particle of side length d, Brown and Stobbs find $g = 8/3$, which they then convert to $g = 3.3$ for a spherical particle of equal volume.

which, unlike the energy based estimate of Eq. (28), is particle size dependent. In Eq. (32), $\langle . \rangle$ denotes Macaulay brackets ($\langle x \rangle = x$ for $x > 0$, zero otherwise).

Model consistency imposes that constant a entering $(27)_2$ be related to the other three by: $a = c\alpha\sqrt{g}$ such that the prefactor in Eq. (32) is in fact $1/a^2$, which evaluates to 1.0[11].

In this approach, the interfacial stress is nothing but the uniform internal stress inside the particle, which results from strain incompatibility between particle and matrix ($\sigma_{\mathrm{n}}^{\mathrm{I}} = \mu\epsilon_{\mathrm{p}}^{*}$). That the latter evolves parabolically with the overall plastic strain seems to be supported by experiments and gives credence to the linear relation between local dislocation density and strain, as per Eq. (31). Thus, it takes more straining to nucleate at large particles since stress enhancement increases with the number of dislocations. Everything in this model hinges on Eq. (31), from which $(27)_2$ is obtained, so that both the size-independence of the energy criterion and the size dependence of the stress criterion follow. Interestingly, the derivation of Eq. (31) bears little connection, if any, to dislocation plasticity; it relies upon an (inaccurate) limit analysis in [219].

Two characteristic cutoffs for the particle diameter emerge when the constitutive description resolves the dislocation spacing. The lower cutoff d_{c} is when the energy criterion and stress criterion are met concurrently. Equating the nucleation strains in Eqs. (28) and (32) gives, taking into account the

[11] Using the Brown–Stobbs estimates of the constants: $\alpha \sim 1/7$, $c \sim 4.2$ and $g \sim 3.3$, the prefactor in Eq. (32) evaluates to 0.85 (half of 1.7 since we use the diameter d instead of the radius; see Eq. (15) in [56]).

identity $a = c\alpha\sqrt{g}$[12]:

$$d_c = \frac{6\Delta\gamma}{\mu^p}\left(\frac{\mu}{\langle\sigma_c^i - \Sigma_m\rangle}\right)^2 \tag{33}$$

For illustration, consider a particle as stiff as the matrix ($\mu^p \approx \mu$), say 70 GPa then with $\Delta\gamma = 1$ J/m^2, $\sigma_c^i = 1.5$ GPa and for negligible hydrostatic tension one finds $d_c \sim 200$ nm. Below this value, the stress criterion is easily met (Fig. 40) but the stored energy is not enough to form new surfaces and nucleation is governed by the energy criterion at a specific strain evaluated from Eq. (28) to 0.34, irrespective of particle size. This lower cutoff was not discussed by Goods and Brown [56]. It falls well within the putative range predicted by continuum micromechanics, corrected as above.

The higher cutoff, d_{lim}, is determined by the domain of validity of the dislocation approach advocated in [56] and like treatments. For sufficiently large particles, the local flow stress is not so different from the background flow stress. One may thus expect that for $d > d_{lim}$ continuum plasticity is better suited to provide the nucleation condition. This regime is indicated in Fig. 40 with a dashed line representing a size-independent critical stress criterion. To estimate d_{lim}, Goods and Brown study the rate of hardening around the particle, which from Eq. (30) may be written as:

$$\sigma_{eq}\frac{\partial\sigma_{eq}}{\partial\varepsilon_{eq}} = \frac{1}{2}g\alpha^2\mu^2\frac{b}{d}$$

where use has been made of Eq. (31). At the critical size $d = d_{lim}$ the hardening rate is indistinguishable from the overall hardening rate and σ_{eq}

[12]Note the advantage of having carefully dealt with the various constants introduced in [56, 219]: none of them appears in Eq. (33), which only depends on fundamental quantities.

is identified with the yield stress σ_y so that:

$$d_{\lim} = \frac{1}{2} g \alpha^2 \frac{\mu^2}{\sigma_y} \left(\frac{\partial \sigma}{\partial \epsilon} \right)^{-1} b \tag{34}$$

Using $\sigma_y \sim \mu/750$, $\frac{\partial \sigma}{\partial \epsilon} \sim \mu/300$ and the previously given constant values, Goods and Brown find a critical radius of 1–2μm. Another illuminating illustration would be for the maraging steels studied by Psioda [250] for which the yield stress in the strongest heat was $\sigma_y \sim 2$ GPa and the hardening rate is as above. This leads to an order of magnitude smaller estimate for $d_{\lim}$. This is significant and suggests that in high-strength steels, a continuum analysis could be valid for particle sizes as small as, say 0.1μm.

3.9.3. Cohesive zone modeling

Quite a few cell model analyses have been carried out for matrix–particle systems. The principle of such analyses and their salient findings was reviewed in [53]. Most of these assume perfect bonding between matrix and particle. As such, they are limited to examining local stress and plastic strain distributions more accurately than could be obtained analytically. However, the parameter space explored in such studies is much more restricted than, say the analyses by Lee and Mear [229], which we have used as basis for continuum analyses in previous sections. Most relevant to the present section is that both the work reviewed in [53] and that of Lee and Mear [229] are not positioned to infer anything about size effects. A cohesive zone formulation unifies energy and strength criteria. When a cohesive description of the particle–matrix interface is incorporated, the analysis provides insight into the size effect.

Two length scales enter any cohesive zone modeling of void nucleation:

the particle size and the cohesive length. For example, in the well-known work of Needleman [226], the process of debonding of a spherical particle from the surrounding plastically flowing matrix was analyzed using a traction–separation law to describe the gradual loss of cohesion at the interface. The key parameters of the cohesive law are the peak strength, $\sigma_{\max}$, and the cohesive length, δ, which represents the displacement jump at complete separation, Fig. 41. For the axisymmetric loadings considered, the stress triaxiality ratio T was varied between 2/3 and 2.

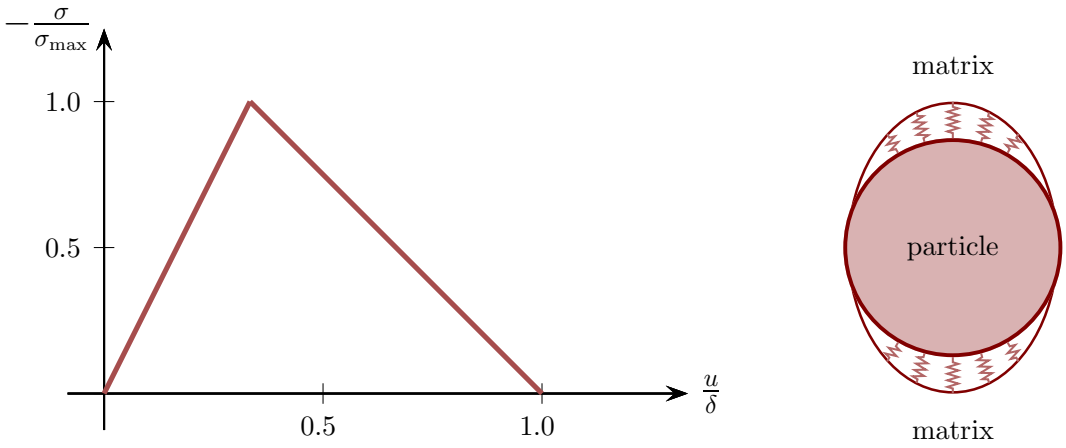

Figure 41: Schematics of a cohesive zone formulation and its parameters.

Fig. 42a shows how the volumetric strain, which is related to the void volume fraction, typically evolves with the overall axial strain (solid line). In this type of analysis, the nucleation strain may be identified with the cohesive strain at initial debonding (~ 0.068 in the example of Fig. 42a) or the strain at complete separation (~ 0.34). The two measures are quite different from each other. For this reason, Needleman defined the nucleation strain ε_{nuc} as that for which the curve giving the volumetric strain versus E_{33} coincides, at

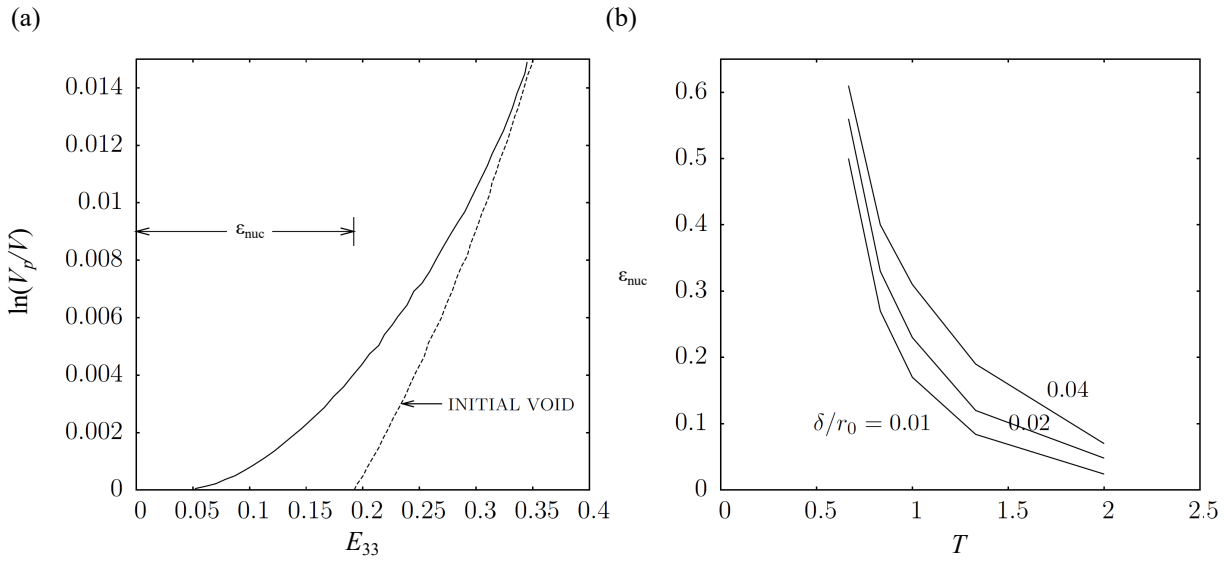

Figure 42: (a) Plastic volume change, $\ln(V^p/V)$, versus overall axial strain, E_{33}, for a particle volume fraction $f_{\rm p} = 0.0104$, a triaxiality $T = 1.33$ and interface parameters $\sigma_{\max} = 3\sigma_{\rm y}$ and $\delta/d = 0.02$. The $\ln(V^p/V)$ versus E_{33} curve for a 1.04 percent volume fraction of initial void is shown shifted by an amount $\varepsilon_{\rm nuc}$ along the strain axis. (b) Nucleation strain, $\varepsilon_{\rm nuc}$, versus stress triaxiality for three values of δ/d ($r_0 = d/2$). Adapted from [226].

large strains, with the curve corresponding to an initial void having the same size as the particle, and shifted by $\varepsilon_{\rm nuc}$. If the solution exists, it is unique. The procedure is illustrated in Fig. 42a for which the value $\varepsilon_{\rm nuc} = 0.19$ is intermediate between strains at initial and complete debonding.

With d denoting the particle diameter, as above, varying the ratio δ/d, at fixed work of separation, amounts to varying the particle size. For a sufficiently small particle ($\delta/d = 0.02$), initial debonding occurs at an angle $\approx 30^\circ$ off the axis of symmetry due to strain concentration there. The void volume fraction then begins to increase, Fig. 42a, the crack rapidly propagates toward the symmetry axis and a spherical void cap opens. In a second

stage, decohesion proceeds toward the mid-section. Thus, a sufficiently large value of δ/d gives rise to "ductile" interface behavior, while smaller values lead to a more brittle mode of separation.

Fig. 42b shows the predicted dependence of the nucleation strain upon the stress triaxiality T for three particle diameters and $\sigma_{\max}/\sigma_{\mathrm{y}} = 3$. A size effect on void nucleation is predicted, as expected since the interface model involves a characteristic length, δ. However, the dependence upon interfacial strength $\sigma_{\max}$ was found to be stronger. Although not analyzed by Needleman, the size effect is expected to vanish for particles greater than a few microns. For illustration, consider parameter values representative of iron carbides in spheroidized carbon steels. For $\sigma_{\max} = 1$ GPa and a work of separation about 10 J/m^2, one finds $\delta \approx 10$ nm so that the particle diameters in Fig. 42b are 1, 2 and 4 μm.

The results in Fig. 42 are only indicative. In some cases, they tend to underestimate the nucleation strain since the actual values are expected to strongly depend on the interfacial properties used in the simulations. Carbides in steels, for instance, are known to be much more resistant to void nucleation than would be predicted on the basis of Fig. 42. Yet, the above definition of $\varepsilon_{\mathrm{nuc}}$ also leads to an overestimation of the nucleation strain at low triaxialities.

A detailed analysis such as Needleman's [226] shows that void nucleation is a process with a beginning and, eventually, an end. In fact, the definition of $\varepsilon_{\mathrm{nuc}}$ entails that it is unbounded for $T < 2/3$, as void nucleation is never complete in that case. Other cell model studies [272, 286, 287] investigated the range of triaxialities below 2/3, which was the cutoff in the analyses of

[226]. Most such analyses assume, however, no bonding between particle and matrix and thus focus on the contact interaction. For $T < 2/3$ void nucleation is incomplete because the normal tractions are compressive near the mid-section (see e.g. Fig. 36). This is in keeping with the experimental observations in Fig. 32. The above analyses did not explore the size effect, e.g. [288].

The same cohesive zone formulation was used by Shabrov and Needleman [289] to investigate particle clustering effects. Three length scales are now involved: two of the microstructural type (particle size and spacing) and a mechanism related length scale (the cohesive length δ). Even by today's computational power, such analyses are quite demanding. The analyses were thus two-dimensional, within a plane strain framework. In addition, a relatively large volume fraction of particles (0.16) was used. While such values may be representative of precipitates, say carbides in steel, the size of precipitates would warrant an adequate plasticity formulation in the matrix that resolves the dislocation spacing. Also, Needleman's definition of nucleation strain in [226] could not be followed when dealing with many particles and ε_{nuc} was defined as the overall strain when a drop in the effective stress was observed, corresponding to first decohesion.

With this in mind, important trends emerged in [289], which are likely to persist within limits for three-dimensional particle distributions and lower particle volume fractions. At fixed, and sufficiently large particle size, regular distributions were found to have higher values of the nucleation strain ε_{nuc} than clustered ones. However, for small particles, the size effect and the clustering effect have opposite trends. Clustering tends to decrease ε_{nuc} but

a reduction in particle size tends to increase it. These results are mostly relevant for metal matrix composites and they are worth revisiting for situations closer to structural materials.

3.9.4. Statistical treatments of particle size effects

Particle size is known to influence the stress (or strain) at which the particle cracks. Because impurities and particles are often ceramics, particle fracture can be considered to be stress controlled and follow a Weibull distribution [290, 291]. We note that this is not always the case: plastic strain in the matrix and particle-particle interactions can alter the local stress field leading to a significant deviation from stress-controlled Weibull statistics, particularly in the case of a relatively soft matrix compared to the particle [183]. In many cases, however, the stress for cracking of ceramic particles is governed by the fracture toughness of the particle and the distribution of defects within it. For example, void nucleation is impeded when MnS particles are replaced with Ti_2CS particles, which have a significantly higher fracture toughness [172]. Defect distribution depends on particle size, with the probability of large internal defects, including pre-existing nano or microcracks, increasing with increasing particle size. Indeed, it is generally observed that large particles are more likely to crack than small particles [292, 293]. Weibull statistics have been used successfully to predict the likelihood of particle cracking as a function of particle size for several Al alloys [183, 273, 294] and provide some experimental validation of the Beremin model [295].

A key challenge with using such statistical approaches for predicting particle cracking is the difficulty of measuring the fracture toughness of ceramic particles [296]. Indirect ways to determine it by relating the fraction of broken

particles to an average particle stress have been implemented [177, 293, 297]. This approach depends strongly on multiple factors, including how particle size and aspect ratio are measured and accounted for and the model used to assess particle stress [298]. Particle damage has also been monitored via the evolution in Young's modulus, as implemented by Mortensen and coworkers, and used to determine particle fracture toughness [294]. Although this approach is promising for metal-matrix composites with high volume fractions of second-phase particles, it is challenging to implement in many engineering alloys, which have second-phase particle volume fractions on the order of 1 % or below. Indeed, given the relative length scales and confinement by the matrix, the fracture toughness of particles remains ill-defined.

3.10. Void nucleation in continuum damage modeling

Homogenization is needed to develop a continuum formulation of void nucleation suitable for structural computations. In doing so, particles are smeared out, whether homogenization proceeds from first principles or by empirical relations. A fundamental internal state variable is the void volume fraction f, which is comprised of a contribution from void nucleation, f_n, and a contribution from void growth, f_g. In general, the rate of change of f must account for the growth of pre-existing voids in the elementary volume and for the formation of new ones:

$$\dot{f} = \dot{f}_{\mathrm{g}} + \dot{f}_{\mathrm{n}} \tag{35}$$

This simple relation, initially introduced by Gurson [299] and further developed by Needleman and co-workers [18, 254, 300] has a fundamental character. Indeed, if ω and Ω respectively denote the void volume and total volume

then the rate of change of void volume must come in part from the growth of pre-existing voids, $\dot{\omega}_{\mathrm{g}}$, and in part from the nucleation of new ones, $\dot{\omega}_{\mathrm{n}}$. On the other hand, the matrix being incompressible, the rate of change of total volume, $\dot{\Omega}$, is only related to void growth; one may write $\dot{\Omega} = \dot{\omega}_{\mathrm{g}}$ but not $\dot{\Omega} = \dot{\omega}_{\mathrm{g}} + \dot{\omega}_{\mathrm{n}}$. Consequently, since $f = \omega/\Omega$ one has

$$\dot{f} = \frac{\dot{\omega}}{\Omega} - \frac{\omega}{\Omega^2}\dot{\Omega} = \frac{\dot{\omega}_{\mathrm{g}} + \dot{\omega}_{\mathrm{n}}}{\Omega} - \frac{\omega}{\Omega^2}\dot{\Omega} = \left(1 - \frac{\omega}{\Omega}\right)\frac{\dot{\Omega}}{\Omega} + \frac{\dot{\omega}_{\mathrm{n}}}{\Omega} \tag{36}$$

By posing $\dot{f}_{\mathrm{n}} \equiv \dot{\omega}_{\mathrm{n}}/\Omega$, Eq. (35) follows with

$$\dot{f}_{\mathrm{g}} = (1 - f)\ \mathrm{tr}\,\dot{\boldsymbol{\varepsilon}} \tag{37}$$

using a standard kinematical relation for the dilational part of the rate of deformation $\dot{\boldsymbol{\varepsilon}}$. The growth part in Eq. (35) is thus given by a fundamental relation, Eq. (37), which together with a plastic flow rule can be associated with yield criteria for either growth [301] or coalescence [269]. On the other hand, the nucleation part, $\dot{f}_{\mathrm{n}}$, is usually supplied through empirical relations, guided by micromechanical analyses. It is useful to analyze the linkage between empirical laws for $\dot{f}_{\mathrm{n}}$ and past micromechanical analyses in order to eventually incorporate recent advances, if and where needed.

The basic format proposed by Gurson [299] and eventually settled in [254] identifies a "driving variable" v to express the nucleation rule as:

$$\dot{f}_{\mathrm{n}} = \mathcal{G}(v)\dot{v} \tag{38}$$

where $\mathcal{G}(v)$ is a memory function, typically parameterized as a Gaussian:

$$\mathcal{G}(v) = \frac{f_{\mathrm{N}}}{s_{\mathrm{N}}\sqrt{2\pi}} \exp\left[-\frac{1}{2}\left(\frac{v - v_{\mathrm{N}}}{s_{\mathrm{N}}}\right)^2\right] \tag{39}$$

Note that $\int_{-\infty}^{+\infty} \mathcal{G}(v)\, \mathrm{d}v = f_{\mathrm{N}}$ so that $f_{\mathrm{N}} \leq f^{\mathrm{P}}$ is the volume fraction of particles with voids, equal to f^{P} if all particles nucleate voids (by decohesion). Also, v_{N} is the mean threshold value of v, and s_{N} is a standard deviation.

Conventional nucleation rules adopt one of two driving variables, or sometimes a combination: the effective plastic strain $\bar{\varepsilon}$ and the hydrostatic stress Σ_{m}. If both are used then up to six parameters are needed, including two separate fractions of particles, one per mechanism (strain-controlled versus stress-controlled) with the constraint $f_{\mathrm{N}}^{(1)} + f_{\mathrm{N}}^{(2)} \leq f^{\mathrm{P}}$. That stress nucleation thresholds are distributed according to a normal law, Eq. (39), is supported by sigmoidal nucleation curves of the type shown in Fig. 27b or Fig. 27c.

Whether void nucleation occurs primarily by interfacial decohesion or by particle cracking has implications on continuum formulations. Only when decohesion prevails does the additive format of Eq. (35) hold. Indeed, when decohesion occurs the volume of the nascent void is identified with that of the particle (the interfacial void volume is typically neglected.) But this identification does not hold if the particle breaks. Two elements are needed to model this. First, an empirical nucleation rule, Eq. (38), may still be used but under the constraint $f_{\mathrm{N}} \ll f^{\mathrm{P}}$. This is often overlooked in the literature. Unlike for decohesion, the volume of the nascent micro-cracks cannot be neglected, because if it were Eq. (35) would reduce to $\dot{f} = \dot{f}_{\mathrm{g}}$, which would lead to no damage growth with no initial void content. Second, some idealization of the nascent micro-cracks is needed since their evolution should be tracked. Using a projected area argument, the micro-cracks may be replaced with spherical voids such that a conventional Gurson model is used to predict the growth term $\dot{f}_{\mathrm{g}}$. This is a crude approximation. A better way would con-

sist of employing extensions of the Gurson model to account for void shape effects, especially for penny-shape cracks e.g. [302, 303]. Recent examples of such usage may be found in [304, 305]. However, these works assume an initial micro-crack content thereby neglecting nucleation altogether. More work is needed in this area, particularly for a class of less ductile metals; see [305] for a discussion.

4. Discussion of challenges and future opportunities

In previous sections, the state of the art in terms of a local condition for nucleation has critically been synthesized. On that basis, points that merit discussion include the following: (i) How void nucleation impacts strength–toughness tradeoffs; (ii) How to utilize the local nucleation condition in a continuum damage formulation where particles and voids are not explicitly represented; (iii) What input(s) from modeling at length scales below the continuum is expected to play a key role in void nucleation; (iv) What role experiments play in advancing the field.

4.1. Nucleation-controlled versus coalescence-controlled toughness

Is delaying nucleation beneficial to ductility and toughness? Goods and Brown [306] open their famous review by the assertion: "If cavity nucleation could be delayed or suppressed altogether, large increases in ductility could be achieved." But the matter may not be as trivial as it sounds. For some materials, it is commonly reported that voids are not observed until incipient failure of the test piece, but dimples are present on fracture surfaces. Typically, "late nucleation" is invoked to interpret such observations. Yet, in all such instances the ductility is much less than in materials with profuse and

early nucleation. Consider for instance the case of some functional materials (ductile SMAs [307, 308], Fe-Co-2V [309]); or most importantly, compare Al or Mg alloys [194, 310] with steels having similar strength levels [222].

Clearly, delaying nucleation is beneficial if ductility is nucleation-controlled [311]. In particle-mediated ductile fracture, two cases are worth distinguishing to avoid complicating factors having to do with strong interaction among scales. If the particles acting as void initiation sites affect strength (e.g. carbides in steels or precipitates in dispersion-strengthened alloys as in the early studies by Ashby, Brown and co-workers) then it is questionable to adopt a modeling framework that assumes separation of scales. By way of extension, this difficulty applies to situations where void initiation is deformation-induced, as in multiphase steels [312] or materials deforming by twinning [313, 314].

A practical situation is when the void-nucleating particles do not affect strength. This is the case for oxides, sulfides, nitrides and mixed inclusions thereof in steels, intermetallic particles in Al alloys, etc. Taking the limit of a vanishingly small volume fraction of such particles amounts to infinitely delaying void nucleation (by one of two particle-mediated mechanisms of Fig. 3). The above question reduces then to whether a material with no inclusions at all is more ductile and tough than a material with inclusions. Again, all things kept the same, the answer is not as trivial as claimed by Goods and Brown [306]. This is so because of a potential change in failure mechanism when particles are not present [15]. Whether the new mechanism is mediated, say by grain boundaries or shear bands, the transition between particle-mediated fracture and shear failure for example is not continuous

and it is both conceivable and reported for Al alloys that the ductility set by shear failures may be significantly lower than when it is particle mediated. Indeed, if the particles are widely spaced (this is usually the case) such that ductility is coalescence-controlled, then stable void growth occurs until ligament microscale instabilities occur [303].

The role of void nucleation in coalescence-controlled fracture is not adequately taken into account by current modeling frameworks. The intervoid spacing plays a key role in setting the coalescence condition [269] but in an evolution problem, void nucleation sets the initial conditions. In a given material volume, what needs to be determined is the fraction of particles that nucleate voids. That requires a statistical framework that uses the single-particle analyses of previous sections as a basis. But single-particle analyses are clearly not sufficient, unless all particles are assumed to nucleate voids, as may be the case at very high stress triaxiality. There is a direct connection between the initial void spacing, which affects void coalescence to first order, and the fraction of particles that actually nucleate voids. Models of this sort are lacking.

Garrison and co-workers have investigated, over a period of time, factors that affect the scaling of fracture toughness with inclusion characteristics, particularly for high-strength steels [51, 248, 262, 263, 315, 316]. Key factors include the inclusion volume fraction, the inclusion spacing and the resistance to void nucleation. For example, it was found that gettering sulfur as CrS instead of MnS led to significant increase in fracture toughness and that was attributed to delaying void nucleation. However, the latter was ascertained from nucleation curves obtained on tensile specimens (as in Fig. 31) for which

the tensile ductilities remained unaltered (see e.g. Table II in [263]). Factors other than resistance to void nucleation must have played a role. Further research is needed along these lines to clarify the trends, especially in high-strength alloys.

Application of the Rice–Johnson model [317] (whereby failure occurs at a critical distance from the crack tip) leads to a fracture toughness that scales as $f^{-1/3}$ with f the particle volume fraction [315]. More recent and elaborate computations by Srivastava et al. [318] have shown that the scaling goes as f^{-n} with $n \sim 2/3$. Even more recent computations show that the scaling exponent n depends on parameters of the fracture process, such as mean nucleation strain and critical void volume fraction for coalescence [319] but all values are such that $|n| > 2/3$. Various factors may explain the difference between predictions based on the Rice–Johnson model and more sophisticated computations. First, the scaling developed in [315] is for a single population of primary particles. In the calculations of [318] there are two populations with distinct nucleation criteria (stress based for large particles, strain based for small ones). The values of volume fractions in [315] are within the usual range for structural materials (getting cleaner every decade) whereas Srivastava et al. used relatively large values of f. This is important because if a scaling is available from experiments for a given material system and that scaling turns out to be closer to -1/3 than say to -2/3 (or above in absolute value) then that in itself may be suggestive of a dominant nucleation mechanism that is different from how the process has been so far idealized. More research is needed in this area, particularly on the implications of void nucleation in setting the scaling of fracture toughness with various factors,

some of which may be controlled by means of metallurgical manipulations.

4.2. From discrete to continuum modeling - theoretical considerations

Perhaps the most significant remaining gap in the theory of void nucleation is establishing sound connections between macroscale concepts of void nucleation enumerated in Section 3 (critical stress, critical strain, relative mechanical properties of matrix and particle) and the influence of microscale defects and deformation phenomena detailed in Section 2 (dislocation structures, vacancies, twins). At present, such connections are minimal if existent at all. Ultimately, the influence of void nucleation on ductile fracture manifests as a connection between the macro- and microscales: global stresses are the primary drivers of nucleation while each nucleation event is subject to the details of its microstructural locality. The fact that studies at the two scales do not "speak" to each other, therefore, severely hinders our ability to accurately predict void nucleation (and its consequences) and our ability to develop new, high-performance materials needed by future engineering applications.

To start remedying this disconnection of scales, we must begin by questioning some of the basic tenets of continuum modeling of void nucleation. Perhaps the most basic aspect of continuum models is the assumption that void nucleation occurs at some *critical stress* (or strain) which is a property of the particle-matrix system. The existing atomistic literature on void nucleation indicates that if such a critical stress does exist, it cannot be an intrinsic property of the particle-matrix interface itself. This is because of the simple fact that observed nucleation stresses are far too large to be consistent with experimental observations of void nucleation. For example,

Zhao et al. obtained a critical nucleation stress (at 0 K) of 10 GPa for a θ-particle in Al [25]. Similar orders of magnitude have been obtained for other material systems [213, 214]. Given a typical yield strength of $\sim$ 200 MPa for Al alloys, a local stress concentration of 50$\times$ would be necessary for this critical stress to be reached. This must mean that the critical stress for nucleation is dependent upon the local microstructural and defect environment around the particle. For example, dislocation or vacancy accumulation at the matrix-particle interface could weaken it, reducing the critical stress. This concept turns the typical framework for continuum void nucleation on its head: accumulation of plastic strain (e.g., defect accumulation) is usually treated as a driving force for nucleation rather than as a modifier of the material's resistance to nucleation. This evidence suggests that the influence of microstructure and microstructural evolution on a material's resistance to void nucleation needs further consideration.

Another point to make is the fact that at the microscale, a critical plastic strain for nucleation does not make much sense. Plastic strain in and of itself cannot provide a driving force for void nucleation. Rather, it is the indirect consequences of plastic strain that may drive nucleation. Principally these are the accumulation of dislocations (and other deformation-associated defects) in the material and the incompatibility stresses that develop if the matrix deforms plastically but the particle does not. For these reasons, we argue that it will always be difficult to connect micromechanical and microstructural insight with continuum models which invoke the notion of a critical plastic strain.

Indeed, it is observed at the continuum scale that the mean nucleation

strain ϵ_N is not a basic quantity. For instance, it varies strongly with stress triaxiality, as for the example inferred from Fig. 27a or Fig. 31a. Yet in practice, strain-controlled nucleation is most often used. While a mean nucleation stress σ_N may have more fundamental value, stress-controlled nucleation has fallen into disuse. One possible reason is that a format such as Eq. (38) leads to deviations from normality to the overall yield criterion, as discussed by Needleman and co-workers [254, 300]. A consequence is that stress-controlled nucleation can be particularly destabilizing in that it triggers formation of shear bands and subsequent failure. Clearly, more work is needed to resolve these issues on more fundamental grounds.

As was discussed on several occasions above, void nucleation is really a *process*, rather than an *event* (as is assumed by most continuum models). In the case of void nucleation by particle delamination, MD [25, 211] and finite element [226] simulations both show a two stage process: crack nucleation followed by crack extension along the matrix-particle interface. These two processes have different kinetics and respond to different driving forces, so they cannot be lumped together into a single event. Furthermore, defects are expected to influence the two processes in different ways. For example, MD simulations show (at high stresses and loading rates in a defect-free crystal) that crack nucleation is not associated with dislocation activity, but during crack growth dislocations play an important role [25, 211]. Finally, it is not always entirely clear when to declare that a void has "nucleated." We argue here that many reported observations of "nucleation", including some in our own prior work, are not actually incipient voids, but some intermediate stage of void growth, limited by the resolution of the microscope. Accordingly,

the mechanisms that appear responsible for "nucleation" may be distinct at different length scales. Disambiguation in reports of damage evolution processes will depend on careful word choices.

One challenging aspect of void nucleation is that crack nucleation is poorly understood in general. For example, fracture mechanics says little or nothing about how cracks appear, only how they grow after they have already formed. Several studies considering model brittle solids have shown that thermal activation theory can be used to describe the rate of crack nucleation [320–322], but extensions to ductile solids containing defects (e.g., engineering materials) are lacking. Without a solid fundamental foundation for the micromechanics of crack nucleation, mechanistic theories of void nucleation will be difficult to develop.

Another area of particular practical importance is the post-nucleation behavior of micro-cracks. When nucleation occurs by particle cracking, the nascent voids may be modeled as penny-shaped cracks the evolution of which is then handled using continuum scale extensions of the Gurson model (to be discussed below). A recurrent discrepancy noted in recent work is that the rate of opening of the microcracks, as predicted by continuum theories, is much faster than typically observed using high resolution tomography [323]. Analyses of this problem at the atomic scale would be quite challenging but would be worthwhile for a host of engineering applications.

As we have tried to emphasize above, defects play critical roles in the nucleation of voids. Below we briefly summarize the opportunities and challenges related to theory and modeling of each defect type:

- *Vacancies*—Vacancies are likely to influence void nucleation by forming

incipient void nuclei via vacancy agglomeration and by weakening or modifying interfaces/boundaries in the material (e.g., grain boundaries, particle interfaces). Several challenges exist in the modeling of vacancy-mediated void nucleation. Firstly, the rate of vacancy generation during plastic deformation is poorly understood. Most models are based on relatively simple concepts of dislocation intersections, but little work has gone into validating their underlying assumptions or revealing the essential mechanisms. Secondly, vacancy migration through the lattice of a deformed solid is influenced by the stress fields of defects and the possibility of accelerated diffusion kinetics at those defects (e.g., dislocation pipe diffusion). And thirdly, existing experimental evidence indicates dislocation interactions strongly influence when a vacancy cluster transitions from a "vacancy cluster" to a growing void [117]. Hence, void nucleation by vacancy condensation is a complex, multi-step process that is coupled to many features of the defect microstructure. Assembling a comprehensive model for vacancy-mediated void nucleation is a daunting task.

- *Dislocations*—Existing literature indicates that dislocation activity is strongly coupled with crack initiation and growth at particle interfaces. Furthermore, dislocations play an important role in void growth [126, 324]. No detailed theory exists that connects dislocation structure to these various void nucleation processes. Existing theories either assume simplified dislocation microstructures (e.g., pile ups) or smear-out the microstructure entirely (e.g, use of the Taylor relation in Goods and Brown's model, Eq. (29)). Based on current understanding, detailed

features of dislocation substructure (e.g, local density, slip systems, mobility) are likely to influence void nucleation. In particular, the accumulation of dislocation content at interfaces, coupled with the possibility for slip transmission across interfaces, is likely an important feature of void nucleation. The local stress fields produced by dislocation lines and their local perturbations of the crystal structure will alter the local driving force for nucleation and a material's resistance to crack initiation. Furthermore, the kinetics of incipient (nanoscale) crack/void growth is likely governed by dislocation processes (e.g., dislocation adsorption [126].). Additional research is necessary to elucidate the processes by which individual dislocations and dislocation substructure affect void nucleation.

- *Twins*—Compared to vacancies and dislocations the theoretical understanding of twin-mediated void nucleation is relatively more mature. Experimental, modeling, and theoretical literature all point to slip induced by thickening/extension of twins against boundaries (grain boundaries or other twin boundaries) as the primary driving force. Even still, a quantitative, predictive theory is lacking; Eqs. (8) and (9) provide a semi-quantitative scaling analysis for the propensity for nucleation, but additional work is necessary to establish a sound theory that connects with material properties. An additional challenge is predicting the density of twins as a function of deformation conditions, which is necessary to then predict the nucleation of voids.

- *Grain boundaries*—Most theories for void nucleation at GBs invoke the

same assumptions/mechanisms as with twin-mediated void nucleation (e.g., deformation bands impinging on GBs localize stress). However the problem is rendered more complex by the high dimensional nature of GBs because there are infinitely many possible GB structures. Moreover, the GB structure is not static but evolves with stress, temperature, and the incursion of matrix defects. Depending on the structure, dislocations may interact with the boundary in different ways, for example transmitting across and leaving a residual dislocation behind or absorbing into the boundary as a grain boundary dislocation. Generally, random high angle grain boundaries have greater capacity to accommodate the distortion of incurring defects through long-range reconfigurations whereas the limited free volume of low angle boundary or "special" low-index coincident site lattice boundaries require more localized, prescriptive reactions. Furthermore, point defects are also known to trap at GBs, which may alter the local propensity for void nucleation. As with all studies pertaining to GBs, their high dimensional nature is a tremendous challenge for the problem of void nucleation. Mesoscale models that assign the same properties to all grain boundaries or reduce them into simple scalar descriptors may serve as a first order approximation, but likely loses much of the detail that govern actual grain boundary dynamics.

- *Particles*—While the vast majority of macroscale theoretical work has been focused on the problem of void nucleation at particles (as shown by Section 3), a detailed understanding of the role played by local defects at the particle-matrix interface is lacking. On the other hand, compared

to other void nucleation cases, continuum models for predicting damage due to particle-mediated void nucleation are most mature. Perhaps the best known example of which is the Gurson-Tvergaard-Needleman model (discussed below), which explicitly invokes a void nucleation term in its formalism. This provides an opportunity for connections to be established between microscale processes which influence void nucleation and macroscale model predictions relevant to engineering systems.

What modeling techniques can help to reveal the fundamental micromechanics of void nucleation? A first point to reiterate is the intrinsically multiscale nature of void nucleation, illustrated in Figure 4. Crack nucleation is likely initiated by the rupturing of a few atomic bonds, or the agglomeration of a few local defects (e.g., vacancies). But the macroscopic driving force may derive from polycrystalline incompatibility stresses and/or plastic strain gradients spanning 100s of microns. Clearly, a range of modeling techniques is required. Molecular dynamics has already demonstrated its value in this area. Furthermore, crack nucleation is almost certainly initiated by bond breaking over atomistic length scales, making MD an essential tool. However, the severe length and time scale limitations are prohibitive. Defects associated with void nucleation (e.g., particles, twins, grains) are usually microns in size and many orders of magnitude too large for MD. Furthermore, high stresses/loading rates must be applied to accelerate void nucleation to atomistic timescales if MD is to be employed. Extrapolating findings from MD studies to experimentally relevant length and time scale is a major challenge.

One micromechanical tool of potential value which has seen little use in the study of void nucleation is discrete dislocation dynamics (DDD) [325, 326]. In DDD, the motion and interactions of discrete dislocation networks are explicitly accounted for as the networks are evolved spatiotemporally. Conceivably, DDD could be combined with an atomistically informed fracture model to construct a defect-informed model capable of simulating void nucleation at micron length scales. Alternatively, concurrent multiscale modeling techniques could be utilized, such as the coupled atomistic-discrete dislocation (CADD) [327, 328], concurrent atomistic-continuum (CAC) [329], or quasicontinuum methods [330]. Finally, we believe that crystal plasticity (CP) modeling will be an important modeling technique in the study of void nucleation. CP is a continuum modeling technique which applies macroscopic plasticity principles (e.g., the flow rule) to a polycrystalline microstructure while accounting for slip anisotropy due to the slip systems within each grain [331]. As such, CP is able to resolve incompatibility stresses among many grains and multi-phases up to millimeter scales. Some CP plasticity models evoke dislocation densities (and possibly other defect densities) in their underlying formalisms, making it possible to account for the influence of defects on void nucleation. For example, several research groups have studied void growth using CP [332–334] and used CP to identify stress and strain "hot spots" where void nucleation is most likely [335, 336].

As a final note, we comment on the potential impact of machine learning (ML) on the study of void nucleation. First, we note that MD simulations are only as accurate as the interatomic potentials upon which they are built. The availability and accuracy of interatomic potentials greatly limits MD

studies of void nucleation, especially in the case of multi-component and multi-phase materials whose microstructure and thermodynamics are complex. ML-generated interatomic potentials could revolutionize these simulations by providing a high fidelity toolset for the study of complex, engineering materials [337]. Another aspect of void nucleation which could benefit from ML is its high dimensional nature at the microstructural scale. We have identified many mechanisms by which different defect classes could influence the propensity for void nucleation. Disentangling the many ways these defects influence void nucleation is a major challenge. ML approaches for feature selection and engineering [338] could prove valuable in identifying what features of the microstructure are most important for void nucleation. Finally, machine learning can enable acceleration of molecular dynamics simulations, for example as a reduced order surrogate model e.g. [339]. Analogous to the roles that ML can play to enhance atomistic simulations, such advances are also being applied to relevant mesoscale models such as discrete dislocation dynamic [340]. Finally, there are seedling efforts to employ ML to bridge length- and time-scales in multiscale modeling [341].

4.3. The role of experiments

As far back as investigations of ductile failure go, experiments have provided far more input than could possibly be absorbed by available damage models. On the other hand, constitutive formulations have evolved in ways that warrant specific input from experiments and specific assessment against experiments, yet experimental protocols have not always provided the requisite calibration/validation data. This discrepancy between experiments and theory is not peculiar to ductile failure and is in part due to the constraints

under which theory and experiment develop in a given field. In the context of void nucleation in metals, generic issues of interest include: 1) which debated facts, if any, can be ascertained by means of discriminating experiments, 2) what input is needed from experiments to identify (in a robust way) failure models or to validate these models, 3) what new experiments would uncover new behavior?

Of the first kind, studies on the contributions of these various void nucleation mechanisms to mechanical properties, e.g. fracture toughness, are largely missing. A critical challenge within this is that it is extremely challenging to alter the dominant void nucleation mechanism without simultaneously altering mechanical properties of the matrix. In AZ31, suppressing void nucleation at grain boundary/deformation twin intersections by decreasing the grain size resulted in an increase in strength and ductility, yet it is unclear if this effect is due to the suppression of void nucleation, a Hall-Petch strengthening effect, or both. In dual-phase steels, a transition from void nucleation by particle debonding to particle fracture is associated with a decrease in ductility and an increase in strength. It is unclear if this difference can be credited to a different void nucleation mechanism or, more probably, to the higher martensite volume percentage producing a stronger material. By carefully controlling the percent of second-phase particles in two-phase copper-base alloys fabricated by powder metallurgy, Edelson et al. [342] determined that both strength and ductility increased with decreasing particle volume fraction. It was implied from this that the nucleation of voids at particles lead to premature failure. The recent study of Noell et al. [117] observed voids at dislocation boundaries in a Cu material, not at

oxide inclusions. Thus, how transitions from one dominant void nucleation mechanism to another affect material properties, e.g. fracture toughness, deserve considerably more study.

Additionally, experiments are needed to explore the transition between particle-mediated nucleation and failure of a particle-free microstructure, i.e. in the limit of very clean metals. The discovery that vacancy condensation produces voids at dislocation boundaries in a material containing submicron particles suggests that, as particle size decreases, other microstructural features become increasingly important to void nucleation and the early stages of void growth. This has practical value, as it is unclear if the results of [342] for Cu that a particle-free microstructure is more tough and ductile than one with particles is generally applicable. A hierarchy of scales for void nucleation sites is observed both for dynamic fracture [33, 34] and in Mg [148], where void spacing in both cases is of critical interest for ductile failure models. This implies that multiple void nucleation mechanisms may be operating simultaneously in these materials.

As void nucleation or the early stages of void growth in particle-free metals occurs at deformation-induced defects, it is plausible that particular configurations of these defects are preferable sites. Limited data suggests that void nucleation is stochastic and depends upon when nanoscale void nuclei formed by vacancy condensation are intersected by dislocation boundaries. Yet are there factors that allow some vacancy clusters to grow faster than others? Does viscinal dislocation activity serve to aggregate vacancies? Does the intersection between some deformation-induced features create stress concentrations, leading to void nucleation preferentially at these sites? Alterna-

tively, void nucleation may be probabilistic, with the likelihood increasing as the number of intersections between deformation-induced features increases. This might explain why the propensity for void nucleation increases with increasing strain-hardening capacity.

Another question that new experiments may be able to answer is if an increase in toughness imparted through metallurgical manipulations always accompany an increase in ductility. There are no systematic experiments addressing this issue. The limited data that is available suggest some puzzling trends; cf. data from Garrison's experiments discussed above. The contribution of void nucleation in settling the difference between toughness and ductility trends needs to be ascertained.

New experiments will be critical to developing models for grain-boundary cleavage. No current models truly identify a critical condition for nucleation, they simply provide a scaling analysis. For example, the debate harkening back to Zener-Stroh over the relative importance of energetic versus strength considerations remains unresolved by modern theories. Boundary cleavage is an important void nucleation mechanism in some materials that deform by twinning, even when particles are also present. It also occurs in materials where dislocation-mediated plasticity dominates, e.g. Mo. Additional work is necessary to determine the conditions that promote void nucleation at grain boundaries in both cases, particularly brittle BCC metals such as Mo and W. Surprisingly few studies have examined grain-boundary cleavage during quasistatic loading in materials that deform by slip. The role of slip bands in void nucleation in particle-free materials thus remains unclear. Hence, even though grain-boundary cleavage was one of the first void-nucleation

mechanisms proposed, additional research is still necessary to elucidate this mechanism.

Along the same lines, do deformation-induced defects play a role in particle cracking and/or debonding? Particle size and morphology influences how dislocations accumulate at boundaries, with limited data indicating that the rate at which dislocation boundaries form increases with increasing particle size [343, 344]. It has long been assumed that the accumulation of dislocations at the particle/matrix interface creates a stress concentration leading to void formation, but this hypothesis has proved challenging to assess experimentally. Alternatively, the accumulation of vacancies or the formation of vacancy clusters at the particle/matrix interface could, by lowering the energy needed to form a void, enable void nucleation at smaller strains.

An issue that lies between facts and input to modeling is that of the blunting of microcracks. Fundamentally, why a brittle microcrack that breaks open a particle would not (always) proceed in a brittle manner in the matrix is not fully understood from first principles of fracture mechanics. When continuum plasticity is used to represent the blunting of the microcracks, it predicts rates of blunting that are typically twice what is measured experimentally [305]. But available measurements are scarce and imprecise. Resolving this issue would have implications for a class of quasi-brittle, but technologically important materials, some of which are not structural but functional alloys, such as Fe-Co-2V and some shape memory alloys.

Some advanced ductile failure models require input about the spatial distribution of nucleation sites [281, 345], but experimental studies do not typically report that information, even in two dimensions. The role of automation

in material characterization and mechanical testing cannot be overstated. On the one hand, automation facilitates providing data that is tedious to obtain, yet needed to critically discriminate among models. On the other hand, automation can provide enough information about statistics for use either in setting proper initial conditions or together with emergent data-driven approaches. Machine learning will likely play a role in automating materials characterization. For example, Tsopanidis et al. recently developed a convolutional neural network for analyzing fracture surfaces which automatically identifies transgranular and intergranular fracture features [346]. Wittwer et al. demonstrated that high-throughput crystal orientation mapping could be extracted from optical images using a machine learning algorithm [347].

Regarding new critical experiments, modern SEM and TEM-based techniques will allow some of the questions raised in the previous paragraphs to be studied. As demonstrated in a recent study by the authors, TEM and FIB allow the role of nanoscale vacancy clusters during ductile fracture to be characterized [117]. These techniques will allow the role of these defects to be studied in pure metals with less ductility than Cu, e.g. Ni and Ta, or in engineering alloys. As demonstrated by Kacher and coworkers, EBSD allows the relationship between dislocation boundaries and particle cracking or debonding to be characterized [348]. High-resolution EBSD now allows the elastic strain state to be measured with a spatial resolution of ≈ 100 nm and a strain resolution of 10^{-4} across large areas of a sample. This technique may provide insights into the evolving stress state around dislocation boundaries, particularly at the intersections between these and other defects.

Many unanswered questions in the field of void nucleation center around

the difficulties of directly characterizing the evolving microstructure around incipient damage in-situ. X-ray tomography, which has historically been the primary tool for evaluating void nucleation in-situ, cannot provide insights into questions such as the role of local dislocation density or the stress concentration created by dislocation accumulation at a particle/matrix interface. In the past decade, several promising X-ray imaging techniques have been developed that will be useful to characterize the evolving dislocation structure and stress state during ductile failure. These include near and far field high-energy diffraction microscopy (HEDM), Bragg coherent diffractive imaging (BCDI), and dark-field X-ray microscopy. These are now discussed in more detail.

HEDM uses high-energy monochromatic synchrotron radiation to non-destructively characterize the grain structure and micromechanical state of a material [349, 350]. Far-field HEDM gives information on grain centroid locations, average grain orientation, and the average lattice strain tensor for each grain, with a strain resolution of $\approx 10^{-4}$. Near-field HEDM provides high-resolution characterization of the grain structure, including grain morphology, orientation, and boundaries with an angular resolution of $\approx 0.1°$. The spatial resolution of this technique, ≈ 2 μm, has been shown to be insufficient to accurately capture the development of dislocation structures during deformation [351]. Despite this shortcoming, these techniques, combined with X-ray absorption data, were successfully used to characterize fatigue crack nucleation [352] and the evolution of grain orientation during plastic deformation [351]. Such an approach is promising for assessing how orientation gradients around 2nd-phase particles evolve before void nucleation.

BCDI measures the full 3D displacement field of the lattice at the nanoscale using a coherent X-ray nanobeam [353]. Because these measurements are directly related to strain, individual defects including dislocations can be characterized during in-situ deformation [354]. Currently, this resolution is limited to nanoscale samples, which limits its applicability to the study of void nucleation in bulk parts [355].

Dark-field X-ray microscopy is a full-field imaging technique that maps the 3D crystallographic structure and strain of embedded elements in bulk samples [356]. It is typically combined with conventional X-ray tomography and diffraction contrast tomography (DCT) techniques, which allows specific elements to be identified and subsequently characterized using dark-field X-ray microscopy at resolutions as high as 30 nm. To date, applications of this technique include studying the evolution of grain orientations during recovery [357] and magnetic domain changes during deformation in barium titanate [358]. The high spatial resolution of this technique approach has clear advantages over HEDM-based techniques and could allow the evolving microstructure and micromechanical state around particles to be characterized in-situ.

4.4. Void nucleation in advanced materials

The present review focused on void nucleation in conventional polycrystalline bulk metals. In some cases, the knowledge gained in these materials can be applied to ductile fracture processes in the advanced metallic systems developed in the past decades, e.g. advanced high-strength steels. However, in some cases the unusual deformation processes in emerging advanced materials give rise to changes in the ductile rupture process, particularly

the void nucleation process, providing new opportunities for study and challenges for prediction. As the final section of this discussion, a few of the most important metallic systems, bulk metallic glasses, high entropy alloys, and nanostructured alloys, are reviewed briefly in the context of their distorted void nucleation processes, opening the door for expanded studies of void nucleation in the future.

Bulk metallic glasses (BMGs) represent the first such area of interest. BMGs deform predominantly via shear transformation zones [359]. While their fracture toughness can exceed 100 MPa $\sqrt{m}$ [360], they generally have quite poor tensile ductility [361]. In the case of unnotched BMGs, the quasi-brittle fracture contains an array of striated vein patterns through meniscus instability in the shear band [362]. The meniscus instability phenomena had been modeled as early as 1976 for glassy materials [363]. When the shear banding process is suppressed through the use of notched geometries, BMGs exhibit increases in ductility and strength [364]. Under these conditions of elevated triaxial stress, an alternative cavitation process, perhaps aided by vacancy coalescence, is proposed [365]. With shear banding suppressed, the fracture morphology appears to transition to a ductile dimple nucleation-growth-and-coalescence process bearing similarity to typical structural alloys [364]. While the morphology bears similarity to traditional metals, the mechanism for the void nucleation process is not clear, as traditional dislocation-based processes or particle-based processes are thought to be absent.

High entropy alloys (HEAs) otherwise known as Compositionally Complex Alloys or Multi-principal-Element-Alloys [366], represent a second area of intense recent interest. The single-phase equiatomic 5-component Cantor

alloy, Co-Cr-Fe-Mn-Ni, is the flag bearer for this class of alloys. Owing to the disordered solid solution of the FCC lattice these are described as "frustrated" in their energy well landscape, with 3-component medium entropy alloys being additionally magnetically frustrated [367, 368]. Yet generally, their deformation still proceeds via dislocation and twinning mechanisms [369]. When inclusions are present, void nucleation has been ascribed to interfacial decohesion, and thus consistent with traditional structural metals. In the absence of nucleation at particles, deformation twins are strongly correlated to sites of void nucleation [370]. Perhaps the most curious aspect of rupture in these HEAs is the remarkable suppression of rupture processes at cryogenic temperatures and corresponding astonishing fracture toughness values in excess of 300 MPa $\sqrt{m}$ [371]. Deformation at cryogenic temperatures proceeds by extensive nanoscale twinning [371], analogous to TWIP steels, and also by a FCC-HCP phase transformation [372]. Recent studies have also suggested the importance of local (short-range) chemical ordering contributing to a low fraction of thin HCP laths that enhance strain hardening [373]. Yet the details behind the process of void nucleation remain unclear. In that regard, there have been several recent atomistic simulations of the role of pre-existing nanoscale voids on the rupture process in HEAs [374–376], which is relevant to the earliest stages of void growth.

Nanostructured alloys are a third class of emerging metallic systems that have garnered extensive interest over the past two decades. The original motivation for nanocrystalline metals was the extensive Hall-Petch strengthening arising from the high density of grain boundaries. However, these metals typically suffer from limited work-hardening and a corresponding propensity

for shear localization [377] that causes premature void nucleation along grain boundaries [378]. While the strains-to-failure are quite low, the fracture surfaces that form in the shear-localized zones still contain ductile dimples [379], suggestive of a nucleation-growth-and-coalescence process. These metals can also exhibit mechanically-induced grain growth [380, 381], a deformation process that can accommodate plasticity and enhance ductility [382]. Alloying has been explored as a way to control the boundary stability [383, 384], and suppress shear localization [385], although some segregating solute additions can serve to embrittle grain boundaries [386, 387] and promote intergranular cracking. Nanotwinned metals represent a special subclass of nanostructured metals, with enhanced ductility compared to nanocrystalline metals [388]. The increased resistance to void nucleation in nanotwinned metals compared to their nanocrystalline counterparts has been attributed to dislocation-twin boundary interactions that offer plastic relaxation and reduce the large incompatibility stresses that can develop at nanocrystalline grain boundaries [389, 390]. A more in-depth summary on the fracture and fatigue processes in nanostructured metals is presented elsewhere [391].

5. Conclusions

Our review of microstructural aspects of void nucleation has demonstrated a number of significant insights gained from recent work. The key role played by dislocation boundaries in particle-free and particle-mediated void nucleation have been made clear thanks to recent experimental and modeling efforts. The potential for void nucleation by vacancy condensation in both particle free and particle-containing materials was also recently demonstrated. Several experimental and modeling works have demonstrated

mechanisms for twin-mediated void nucleation, along with semi-quantitative insights on governing physical principles. Despite this progress, our theoretical understanding of microstructure's role in void nucleation is rather weak across the board; often theories based on largely debunked ideas from the 1950s (e.g., dislocation pile-ups, cavity dislocations) are heralded as fact.

From the continuum perspective, our understanding is relatively more mature. Several landmark experimental programs (c.f. Psioda's work) and modeling efforts (c.f. Lee and Mear's work) have revealed quantitative trends for key variables such as yield strength, stress state, and particle shape. And yet, often these results are either narrow in scope (e.g., data only for martensitic steels) or rely on strong assumptions (e.g., uniform fields in particles, indirect incorporation of dislocation effects). One challenge is designing experiments which isolate individual phenomena while still employing engineering-relevant materials.

In terms of paths forward, a critical knowledge gap is identifying the overall importance of void nucleation for mechanical properties. We have emphasized that while it is commonly assumed that void nucleation adversely affects ductility and toughness, the evidence supporting this claim is often weak. Another critical area of research is in the coupling between microscale and continuum descriptions of void nucleation, which is often weak or nonexistent. The Gurson-Tvergaard-Needleman continuum damage model may present an opportunity for this coupling as it at least has the appropriate formalism in place for incorporating microscale insights. And yet significant challenges still remain, for example how to move away from strain-driven nucleation laws which appear inconsistent with the micromechanical picture

of void nucleation. Finally, up-and-coming x-ray and microscopy techniques along with machine learning and large-scale computations stand to advance understanding in many different areas.

Acknowledgements

AAB is grateful to Alan Needleman for fruitful discussions and to support from NSF (grants CMMI-1932975 and CMMI-1950027) and Sandia National Laboratories (Contract No. 2209309). RBS acknowledges support from the National Science Foundation under Grant CMMI-2034074. BLB acknowledges support from the Center for Integrated Nanotechnologies. Sandia National Laboratories is a multi-mission laboratory managed and operated by National Technology and Engineering Solutions of Sandia, LLC., a wholly owned subsidiary of Honeywell International, Inc., for the U.S. Department of Energy's National Nuclear Security Administration under contract DE-NA-0003525. This paper describes objective technical results and analysis. Any subjective views or opinions that might be expressed in the paper do not necessarily represent the views of the U.S. Department of Energy or the United States Government.

References

[1] J Dyneley Prince. The code of hammurabi, 1904.

[2] Sean Potter. Retrospect: January 15, 1919: Boston molasses flood. *Weatherwise*, 64(1):10–11, 2011.

[3] Yao Xu, Limin Zhang, and Jinsheng Jia. *Lessons from catastrophic*

dam failures in August 1975 in Zhumadian, China, pages 162–169. American Society of Civil Engineers, 2008.

[4] George FW Hauck. Hyatt-regency walkway collapse: Design alternates. *Journal of Structural Engineering*, 109(5):1226–1234, 1983.

[5] María Victoria Biezma and Frank Schanack. Collapse of steel bridges. *Journal of Performance of Constructed Facilities*, 21(5):398–405, 2007.

[6] National Transportation Safety Board. Aircraft Accident Report, Aloha Airlines Flight 243, Boeing 737-100, N73711, Near Maui, Hawaii, April 28, 1988. Report NTSB/AAR-89/03, National Transportation Safety Board, 1989.

[7] D. B. Gero. *Military Aviation Disasters: Significant Losses Since 1908*. Haynes Publishing, 2010.

[8] Wei Zhang. Technical problem identification for the failures of the liberty ships. *Challenges*, 7(2):20, 2016.

[9] Tim Foecke. What really sank the titanic? *Materials Today*, 11(10):48, 2008.

[10] Richard Palmer Reed, JH Smith, and BW Christ. The economic effects of fracture in the united states. *National Bureau of Standards Special Publication*, pages 1–24, 1983.

[11] Stephen D Antolovich, Ashok Saxena, and William W Gerberich. Fracture mechanics–an interpretive technical history. *Mechanics Research Communications*, 91:46–86, 2018.

[12] Alten F Grandt Jr. *Fundamentals of structural integrity: damage tolerant design and nondestructive evaluation*. John Wiley & Sons, 2003.

[13] Geoffrey Ingram Taylor and CF Elam. The plastic extension and fracture of aluminium crystals. *Proceedings of the Royal Society of London. Series A, Containing Papers of a Mathematical and Physical Character*, 108(745):28–51, 1925.

[14] Egon Orowan. Fracture and strength of solids. *Reports on progress in physics*, 12(1):185, 1949.

[15] Philip J Noell, Jay D Carroll, and Brad L Boyce. The mechanisms of ductile rupture. *Acta Materialia*, 161:83–98, 2018.

[16] A. Pineau, A. A. Benzerga, and T. Pardoen. Failure of metals I: Brittle and ductile fracture. *Acta Materialia*, 107:424–483, 2016.

[17] P Ludwik. Bestimmung der reißfestigkeit aus der gleichmäßigen dehnung. *Ztsch. Metallkunde*, 9:269–272, 1926.

[18] V. Tvergaard and A. Needleman. Analysis of the cup–cone fracture in a round tensile bar. *Acta Metallurgica*, 32:157–169, 1984.

[19] S Hao and W Brocks. The gurson-tvergaard-needleman-model for rate and temperature-dependent materials with isotropic and kinematic hardening. *Computational Mechanics*, 20(1):34–40, 1997.

[20] Yi Guo, Timothy L Burnett, Samuel A McDonald, Michael Daly, Andrew H Sherry, and Philip J Withers. 4d imaging of void nucleation,

growth, and coalescence from large and small inclusions in steel under tensile deformation. *Journal of Materials Science & Technology*, 123:168–176, 2022.

[21] Cihan Tekoglu, J-B Leblond, and Thomas Pardoen. A criterion for the onset of void coalescence under combined tension and shear. *Journal of the Mechanics and Physics of Solids*, 60(7):1363–1381, 2012.

[22] B. L. Boyce, S. L. B. Kramer, T. R. Bosiljevac, E. Corona, J. A. Moore, K. Elkhodary, C. H. M. Simha, B. W. Williams, A. R. Cerrone, A. Nonn, et al. The second sandia fracture challenge: predictions of ductile failure under quasi-static and moderate-rate dynamic loading. *International Journal of Fracture*, 198(1-2):5–100, 2016.

[23] Brad L. Boyce, Sharlotte L. B. Kramer, H. Eliot Fang, Theresa E. Cordova, Michael K. Neilsen, K. Dion, Amy K. Kaczmarowski, Erin Karasz, Liang Xue, Andrew J. Gross, et al. The sandia fracture challenge: blind round robin predictions of ductile tearing. *International Journal of Fracture*, 186(1-2):5–68, 2014.

[24] Coleman N Alleman, James W Foulk, Alejandro Mota, Hojun Lim, and David J Littlewood. Concurrent multiscale modeling of microstructural effects on localization behavior in finite deformation solid mechanics. *Computational Mechanics*, 61(1):207–218, 2018.

[25] Qian Qian Zhao, Brad L Boyce, and Ryan B Sills. Micromechanics of void nucleation and early growth at incoherent precipitates:

Lattice-trapped and dislocation-mediated delamination modes. *Crystals*, 11(1):45, 2021.

[26] E. Maire and P.J. Withers. Quantitative X-ray tomography. *Inter. Mater. Rev.*, 59:1–43, 2014.

[27] L. Babout, E. Maire, and R. Fougères. Damage initiation in model metallic materials: X-ray tomography and modelling. *Acta Materialia*, 52:2475–2487, 2004.

[28] S. C. O'Keeffe, S. Tang, A. M. Kopacz, J. Smith, D. J. Rowenhorst, G. Spanos, W. K. Liu, and G. B. Olson. Multiscale ductile fracture integrating tomographic characterization and 3-d simulation. *Acta Materialia*, 82:503–510, 2015.

[29] A. Buljac, F. Hild, L. Helfen, and T. F. Morgeneyer. On deformation and damage micromechanisms in strong work hardening 2198 T3 aluminium alloy. *Acta Materialia*, 149:29–45, 2018.

[30] Tom Petit, Jacques Besson, Claire Ritter, Kimberly Colas, Lukas Helfen, and Thilo F. Morgeneyer. Effect of hardening on toughness captured by stress-based damage nucleation in 6061 aluminum alloy. *Acta Materialia*, 180:349–365, 2019.

[31] Brendan P Croom, Helena Jin, Philip J Noell, Brad L Boyce, and Xiaodong Li. Collaborative ductile rupture mechanisms of high-purity copper identified by in situ x-ray computed tomography. *Acta Materialia*, 181:377–384, 2019.

[32] GI Kanel. Spall fracture: methodological aspects, mechanisms and governing factors. *International journal of fracture*, 163(1-2):173–191, 2010.

[33] Curt Allan Bronkhorst, George Thompson Gray III, Francis L Addessio, Veronica Livescu, NK Bourne, SA McDonald, and PJ Withers. Response and representation of ductile damage under varying shock loading conditions in tantalum. *Journal of Applied Physics*, 119(8):085103, 2016.

[34] M Cheng, C Li, MX Tang, L Lu, Z Li, and SN Luo. Intragranular void formation in shock-spalled tantalum: Mechanisms and governing factors. *Acta Materialia*, 148:38–48, 2018.

[35] DR Curran, L Seaman, and DA Shockey. Dynamic failure of solids. *Physics reports*, 147(5-6):253–388, 1987.

[36] Evan J Lieberman, Ricardo A Lebensohn, David B Menasche, Curt A Bronkhorst, and Anthony D Rollett. Microstructural effects on damage evolution in shocked copper polycrystals. *Acta Materialia*, 116:270–280, 2016.

[37] Marc André Meyers and Catherine Taylor Aimone. Dynamic fracture (spalling) of metals. *Progress in Materials Science*, 28(1):1–96, 1983.

[38] Eric Nicholas Hahn, Saryu Jindal Fensin, and Timothy Clark Germann. The role of grain boundary orientation on void nucleation in tantalum. Report, Los Alamos National Lab.(LANL), Los Alamos, NM (United States), 2017.

[39] P. Kumar, M. E. Kassner, and T. G. Langdon. Fifty years of harper-dorn creep: a viable creep mechanism or a californian artifact? *Journal of Materials Science*, 42:409–420, 2007.

[40] M. E. Kassner and M. T. Perez-Prado. Five-power-law creep in single phase metals and alloys. *Progress in Materials Science*, 45:1–102, 2000.

[41] M. E. Kassner and T. A. Hayes. Creep cavitation in metals. *International Journal of Plasticity*, 19(10):1715–1748, 2003.

[42] Michael E. Kassner. *Fundamentals of creep in metals and alloys*. Butterworth-Heinemann, 2015.

[43] Hermann Riedel. *Fracture at high Temperatures*. Springer Verlag, 1987.

[44] Shi-Hao Li, Jing-Ting Li, and Wei-Zhong Han. Radiation-induced helium bubbles in metals. *Materials*, 12(7):1036, 2019.

[45] Jie Gao, Hefei Huang, Jizhao Liu, Jianrong Zeng, Ruobing Xie, and Yan Li. Coalescence mechanism of helium bubble during tensile deformation revealed by in situ small-angle x-ray scattering. *Scripta Materialia*, 158:121–125, 2019.

[46] JH Evans. An interbubble fracture mechanism of blister formation on helium-irradiated metals. *Journal of Nuclear Materials*, 68(2):129–140, 1977.

[47] Ming-Shuai Ding, Jun-Ping Du, Liang Wan, Shigenobu Ogata, Lin Tian, Evan Ma, Wei-Zhong Han, Ju Li, and Zhi-Wei Shan. Radiation-

induced helium nanobubbles enhance ductility in submicron-sized single-crystalline copper. *Nano letters*, 16(7):4118–4124, 2016.

[48] H Wiedersich. On the theory of void formation during irradiation. *Radiation Effects*, 12(1-2):111–125, 1972.

[49] A. V. Barashev and S. I. Golubov. Steady-state size distribution of voids in metals under cascade irradiation. *Journal of Nuclear Materials*, 389:407–409, 2009.

[50] R. H. Van Stone, T. B. Cox, J. R. Low, and J. A. Psioda. Microstructural aspects of fracture by dimpled rupture. *International Metals Reviews*, 30:157–179, 1985.

[51] W. M. Garrison and N. R. Moody. The Influence of Inclusion Spacing and Microstructure on the Fracture Toughness of the Secondary Hardening Steel AF1410. *Metallurgical Transactions*, 18A:1257–1263, 1987.

[52] V. Tvergaard. Material failure by void growth to coalescence. *Advances in Applied Mechanics*, 27:83–151, 1990.

[53] A. A. Benzerga and J.-B. Leblond. Ductile fracture by void growth to coalescence. *Advances in Applied Mechanics*, 44:169–305, 2010.

[54] J. Besson. Continuum Models of Ductile Fracture: A Review. *International Journal of Damage Mechanics*, 19:3–52, 2010.

[55] A. A. Benzerga, J.-B. Leblond, A. Needleman, and V. Tvergaard. Duc-

tile Failure Modeling. *International Journal of Fracture*, 201:29–80, 2016.

[56] S. H. Goods and L. M. Brown. The nucleation of cavities by plastic deformation. *Acta Metallurgica*, 27:1–15, 1979.

[57] Wei Cai and William D. Nix. *Imperfections in crystalline solids*. Cambridge University Press, 2016.

[58] S.R. Kalidindi, M. Buzzy, B.L. Boyce, and R. Dingreville. Digintal twins for materials. *Frontiers in Materials*, 2022.

[59] K. Linga Murty, K. Detemple, O. Kanert, and J. Th M. Dehosson. In-situ nuclear magnetic resonance investigation of strain, temperature, and strain-rate variations of deformation-induced vacancy concentration in aluminum. *Metallurgical and Materials Transactions A*, 29(1):153–159, 1998.

[60] Tamas Ungar, Erhard Schafler, Peter Hanak, Sigrid Bernstorff, and Michael Zehetbauer. Vacancy production during plastic deformation in copper determined by in situ x-ray diffraction. *Materials Science and Engineering: A*, 462(1):398–401, 2007.

[61] Michael J. Zehetbauer. Effects of non-equilibrium vacancies on strengthening. In *Key Engineering Materials*, volume 97, pages 287–306, 1994.

[62] G. Saada. Interaction of dislocations and creation of point defects in work hardening. In *Acta Crystallographica*, volume 13, pages 1115–1115, 1960.

[63] G. Saada. Production de defauts ponctuels par ecrouissage dans un metal cubique a faces centrees. *Physica*, 27(7):657–660, 1961.

[64] G. Saada. Sur la nature des defauts ponctuels crees par le croisement des dislocations. *Acta Metallurgica*, 9(10):965–966, 1961.

[65] M. J. Zehetbauer, J. Kohout, E. Schafler, F. Sachslehner, and A. Dubravina. Plastic deformation of nickel under high hydrostatic pressure. *Journal of alloys and compounds*, 378(1):329–334, 2004.

[66] A. M. Cuitiño and M. Ortiz. Ductile fracture by vacancy condensation in fcc single crystals. *Acta materialia*, 44(2):427–436, 1996.

[67] Markus J Buehler, Alexander Hartmaier, Huajian Gao, Mark A Duchaineau, and Farid F Abraham. The dynamical complexity of work-hardening: a large-scale molecular dynamics simulation. *Acta Mechanica Sinica*, 21(2):103–111, 2005.

[68] SJ Zhou, DL Preston, and F Louchet. Investigation of vacancy formation by a jogged dissociated dislocation with large-scale molecular dynamics and dislocation energetics. *Acta materialia*, 47(9):2695–2703, 1999.

[69] H. I. Dawson. Experimental verification of saada's relation on the production of point defects in fcc metals by plastic straining at -195 c. *Physica*, 31(3):342–348, 1965.

[70] P. B. Hirsch, J. Silcox, R. E. Smallman, and K. H. Westmacott. Dislocation loops in quenched aluminium. *Philosophical Magazine*, 3(32):897–908, 1958.

[71] Michio Kiritani. Formation of voids and dislocation loops in quenched aluminum. *Journal of the Physical Society of Japan*, 19(5):618–631, 1964.

[72] Yoshiharu Shimomura and Sho Yoshida. Heterogeneous nucleation of voids in quenched aluminum. *Journal of the Physical Society of Japan*, 22(1):319–331, 1967.

[73] J. E. Epperson, K. W. Gerstenberg, D. Berner, G. Kostorz, and C. Ortiz. Voids formed in quenched and annealed nial. *Philosophical Magazine A*, 38(5):529–541, 1978.

[74] O. Seydel, G. Frohberg, and H. Wever. Quenching-in of vacancies in pure α-iron. *physica status solidi (a)*, 144(1):69–79, 1994.

[75] Andy Horsewell and Bachu N. Singh. Influence of grain and subgrain boundaries on void formation and growth in aluminum irradiated with fast neutrons. In *Radiation-Induced Changes in Microstructure: 13th International Symposium (Part I)*, 1987.

[76] D. I. R. Norris. Voids in irradiated metals (part i). *Radiation Effects*, 14(1-2):1–37, 1972.

[77] K. Petersen, B. Nielsen, and N. Thrane. Void formation by annealing of neutron-irradiated plastically deformed molybdenum. *Philosophical Magazine*, 34(5):693–699, 1976.

[78] JP Hirth and WD Nix. Analysis of cavity nucleation in solids subjected to external and internal stresses. *Acta metallurgica*, 33(3):359–368, 1985.

[79] KC Russell. The theory of void nucleation in metals. *Acta Metallurgica*, 26(10):1615–1630, 1978.

[80] C. S. Sundar, A. Bharathi, and K. P. Gopinathan. Positron annihilation studies of electron-irradiated, cold-worked and hydrogen-charged nickel. *Philosophical magazine. A. Physics of condensed matter. Defects and mechanical properties*, 50(5):635–651, 1984.

[81] Steven J. Zinkle and Bachu N. Singh. Microstructure of neutron-irradiated iron before and after tensile deformation. *Journal of nuclear materials*, 351(1):269–284, 2006.

[82] Philip J Noell, Ryan B Sills, and Brad L. Boyce. Suppression of ductile rupture in aluminum via dynamic recrystallization. *Metallurgical and Materials Transactions A*, 2019.

[83] Patrick D Zarnas, Brad L Boyce, Jianmin Qu, and Rémi Dingreville. Stress-induced transition from vacancy annihilation to void nucleation near microcracks. *International Journal of Solids and Structures*, 213:103–110, 2021.

[84] Derek Hull and David J Bacon. *Introduction to dislocations*. Butterworth-Heinemann, 2001.

[85] A Wronski and A Fourdeux. Slip-induced cleavage in polycrystalline tungsten. *Journal of the Less Common Metals*, 6(6):413–429, 1964.

[86] B. Bay, N. Hansen, D. A. Hughes, and D. Kuhlmann-Wilsdorf. Overview no. 96 evolution of fcc deformation structures in polyslip. *Acta metallurgica et materialia*, 40(2):205–219, 1992.

[87] Niels Hansen and Robert F. Mehl. New discoveries in deformed metals. *Metallurgical and materials transactions A*, 32(12):2917–2935, 2001.

[88] D. Kuhlmann-Wilsdorf. Theory of plastic deformation:-properties of low energy dislocation structures. *Materials Science and Engineering: A*, 113:1–41, 1989.

[89] Doris Kuhlmann-Wilsdorf. Dislocation cells, redundant dislocations and the leds hypothesis. *Scripta materialia*, 34(4):641–650, 1996.

[90] D. Kuhlmann-Wilsdorf. Overview no. 131 regular deformation bands (dbs) and the leds hypothesis. *Acta materialia*, 47(6):1697–1712, 1999.

[91] Frederick John Humphreys and Max Hatherly. *Recrystallization and related annealing phenomena*. Elsevier, 2012.

[92] Doris Kuhlmann-Wilsdorf. The impact of frn nabarro on the leds theory of workhardening. *Progress in Materials Science*, 54(6):707–739, 2009.

[93] D. Kuhlmann-Wilsdorf and Niels Hansen. Geometrically necessary, incidental and subgrain boundaries. *Scripta metallurgica et materialia*, 25(7):1557–1562, 1991.

[94] Niels Hansen and Dorte Juul Jensen. Development of microstructure in fcc metals during cold work. *Philosophical Transactions of the Royal Society of London A: Mathematical, Physical and Engineering Sciences*, 357(1756):1447–1469, 1999.

[95] ToH Blewitt, RR Coltman, and JK Redman. Low-temperature defor-

mation of copper single crystals. *Journal of Applied Physics*, 28(6):651–660, 1957.

[96] JC Huang and GT Gray III. Microband formation in shock-loaded and quasi-statically deformed metals. *Acta Metallurgica*, 37(12):3335–3347, 1989.

[97] Fang Cao, Irene J Beyerlein, Francis L Addessio, Bulent H Sencer, Carl P Trujillo, Ellen K Cerreta, and George T Gray III. Orientation dependence of shock-induced twinning and substructures in a copper bicrystal. *Acta Materialia*, 58(2):549–559, 2010.

[98] LE Murr, MA Meyers, C-S Niou, YJ Chen, S Pappu, and C Kennedy. Shock-induced deformation twinning in tantalum. *Acta materialia*, 45(1):157–175, 1997.

[99] Thomas E Buchheit, Corbett C Battaile, Christopher R Weinberger, and Elizabeth A Holm. Multi-scale modeling of low-temperature deformation in bcc metals. *JOM*, 63(11):33–36, 2011.

[100] John Wyrill Christian and Subhash Mahajan. Deformation twinning. *Progress in materials science*, 39(1-2):1–157, 1995.

[101] Irene J Beyerlein, Xinghang Zhang, and Amit Misra. Growth twins and deformation twins in metals. *Annual Review of Materials Research*, 44:329–363, 2014.

[102] Hamidreza Abdolvand and Angus J Wilkinson. Assessment of residual stress fields at deformation twin tips and the surrounding environments. *Acta Materialia*, 105:219–231, 2016.

[103] JS Chen, Y Liu, RJ McCabe, J Wang, and CN Tomé. Quantifying elastic strain near coherent twin interface in magnesium with nanometric resolution. *Materials Characterization*, 160:110082, 2020.

[104] B Clausen, CN Tomé, DW Brown, and SR Agnew. Reorientation and stress relaxation due to twinning: modeling and experimental characterization for mg. *Acta Materialia*, 56(11):2456–2468, 2008.

[105] ZP Pi, QH Fang, B Liu, H Feng, Y Liu, YW Liu, and PH Wen. A phase field study focuses on the transverse propagation of deformation twinning for hexagonal-closed packed crystals. *International Journal of Plasticity*, 76:130–146, 2016.

[106] Mingyu Gong, John P Hirth, Yue Liu, Yao Shen, and Jian Wang. Interface structures and twinning mechanisms of twins in hexagonal metals. *Materials Research Letters*, 5(7):449–464, 2017.

[107] Philip Noell, Jay Carroll, Khalid Hattar, Blythe Clark, and Brad Boyce. Do voids nucleate at grain boundaries during ductile rupture? *Acta Materialia*, 137:103–114, 2017.

[108] I. Cottrell. Ah (1959) theoretical aspects of fracture. *BL Averbach, OK Felbeck, GT Hahn, and OA Thomas (OOs.), Fracture. MIT press, Cambridge. Massachusetts, USA*, pages 20–45, 1959.

[109] Vasily Bulatov and Wei Cai. *Computer simulations of dislocations*, volume 3. Oxford University Press on Demand, 2006.

[110] D Rodney, L Ventelon, E Clouet, L Pizzagalli, and F Willaime. Ab

initio modeling of dislocation core properties in metals and semiconductors. *Acta Materialia*, 124:633–659, 2017.

[111] Luis A Zepeda-Ruiz, Alexander Stukowski, Tomas Oppelstrup, and Vasily V Bulatov. Probing the limits of metal plasticity with molecular dynamics simulations. *Nature*, 550(7677):492, 2017.

[112] Wei-Wei Pang, Ping Zhang, Guang-Cai Zhang, Ai-Guo Xu, and Xian-Geng Zhao. Dislocation creation and void nucleation in FCC ductile metals under tensile loading: A general microscopic picture. *Scientific Reports*, 4(1):6981, May 2015.

[113] Peter Müllner. On the ductile to brittle transition in austenitic steel. *Materials Science and Engineering: A*, 234:94–97, 1997.

[114] P Müllner, C Solenthaler, P Uggowitzer, and MO Speidel. *On the effect of nitrogen on the dislocation structure of austenitic stainless steel*, pages 164–169. Elsevier, 1993.

[115] P Müllner, C Solenthaler, PJ Uggowitzer, and MO Speidel. Brittle fracture in austenitic steel. *Acta metallurgica et materialia*, 42(7):2211–2217, 1994.

[116] R. H. Van Stone, J. R. Low, and J. L. Shannon. Investigation of the fracture mechanism of ti-5ai-2.5 sn at cryogenic temperatures. *Metallurgical Transactions A*, 9(4):539–552, 1978.

[117] Philip J Noell, Julian EC Sabisch, Douglas L Medlin, and Brad L Boyce. Nanoscale conditions for ductile void nucleation in copper: Va-

cancy condensation and the growth-limited microstructural state. *Acta Materialia*, 184:211–224, 2020.

[118] Heinz G. F. Wilsdorf. The role of glide and twinning in the final separation of ruptured gold crystals. *Acta Metallurgica*, 30(6):1247–1258, 1982.

[119] B. F. Dyson and M. J. Rodgers. Prestrain, cavitation, and creep ductility. *Metal Science*, 8(1):261–266, 1974.

[120] B. F. Dyson, M. S. Loveday, and M. J. Rodgers. Grain boundary cavitation under various states of applied stress. *Proc. R. Soc. Lond. A*, 349(1657):245–259, 1976.

[121] C. Reina, J. Marian, and M. Ortiz. Nanovoid nucleation by vacancy aggregation and vacancy-cluster coarsening in high-purity metallic single crystals. *Physical Review B*, 84(10):104117, 2011.

[122] Jaime Marian, Jaroslaw Knap, and Michael Ortiz. Nanovoid cavitation by dislocation emission in aluminum. *Physical review letters*, 93(16):165503, 2004.

[123] Sirirat Traiviratana, Eduardo M Bringa, David J Benson, and Marc A Meyers. Void growth in metals: atomistic calculations. *Acta Materialia*, 56(15):3874–3886, 2008.

[124] Marc A Meyers, Sirirat Traiviratana, VA Lubarda, David J Benson, and Eduardo M Bringa. The role of dislocations in the growth of nanosized voids in ductile failure of metals. *Jom*, 61(2):35, 2009.

[125] LD Nguyen and DH Warner. Improbability of void growth in aluminum via dislocation nucleation under typical laboratory conditions. *Physical review letters*, 108(3):035501, 2012.

[126] R. B. Sills and B. L. Boyce. Void growth by dislocation adsorption. *Materials Research Letters*, 8(3):103–109, March 2020.

[127] H. G. F. Wilsdorf. The ductile fracture of metals: a microstructural viewpoint. *Materials Science and Engineering*, 59(1):1–39, 1983.

[128] R. N. Gardner, T. C. Pollock, and H. G. F. Wilsdorf. Crack initiation at dislocation cell boundaries in the ductile fracture of metals. *Materials Science and Engineering*, 29(2):169–174, 1977.

[129] T. C. Pollock and H. G. F. Wilsdorf. Beryllium fracture observed by in situ high voltage electron microscopy. *Materials Science and Engineering*, 61(1):7–15, 1983.

[130] R. N. Gardner and H. G. F. Wilsdorf. Ductile fracture initiation in pure α-fe: Part i. macroscopic observations of the deformation history and failure of crystals. *Metallurgical Transactions A*, 11(4):653–658, 1980.

[131] R. N. Gardner and H. G. F. Wilsdorf. Ductile fracture initiation in pure α-fe: Part ii. microscopic observations of an initiation mechanism. *Metallurgical Transactions A*, 11(4):659–669, 1980.

[132] Osamu Furukimi, Chatcharit Kiattisaksri, Yuji Takeda, Masatoshi Aramaki, Satoshi Oue, Shinji Munetoh, and Masaki Tanaka. Void nucleation behavior of single-crystal high-purity iron specimens subjected to

tensile deformation. *Materials Science and Engineering: A*, 701:221–225, 2017.

[133] Hojun Lim, Philip J Noell, and Jay D Carroll. Crystallographic orientation dependent fracture behavior in tantalum single crystals. *Scripta Materialia*, 191:76–80, 2021.

[134] TR Bieler, P Eisenlohr, Chun Zhang, HJ Phukan, and MA Crimp. Grain boundaries and interfaces in slip transfer. *Current Opinion in Solid State and Materials Science*, 18(4):212–226, 2014.

[135] T. R. Bieler, M. A. Crimp, Y. Yang, L. Wang, P. Eisenlohr, D. E. Mason, W. Liu, and G. E. Ice. Strain heterogeneity and damage nucleation at grain boundaries during monotonic deformation in commercial purity titanium. *Jom*, 61(12):45–52, 2009.

[136] D Kumar, TR Bieler, P Eisenlohr, DE Mason, MA Crimp, F Roters, and D Raabe. On predicting nucleation of microcracks due to slip-twin interactions at grain boundaries in duplex near γ-tial. *Journal of Engineering Materials and Technology*, 130(2):021012, 2008.

[137] B. C. Ng, B. A. Simkin, M. A. Crimp, and T. R. Bieler. The role of mechanical twinning on microcrack nucleation and crack propagation in a near-γ tial alloy. *Intermetallics*, 12(12):1317–1323, 2004.

[138] Ao N. Stroh. A theory of the fracture of metals. *Advances in Physics*, 6(24):418–465, 1957.

[139] Clarence Zener. The micro-mechanism of fracture. *ASM, Cleveland*, 3, 1948.

[140] JA Querin, JA Schneider, and MF Horstemeyer. Analysis of micro void formation at grain boundary triple points in monotonically strained aa6022-t43 sheet metal. *Materials Science and Engineering: A*, 463(1-2):101–106, 2007.

[141] J Weertman. Zener–stroh crack, zener–hollomon parameter, and other topics. *Journal of applied physics*, 60(6):1877–1887, 1986.

[142] Brady G Butler, James D Paramore, Jonathan P Ligda, Chai Ren, Z Zak Fang, Scott C Middlemas, and Kevin J Hemker. Mechanisms of deformation and ductility in tungsten–a review. *International Journal of Refractory Metals and Hard Materials*, 2018.

[143] Tadao Watanabe. Grain boundary design for the control of intergranular fracture. In *Materials Science Forum*, volume 46, pages 25–48. Trans Tech Publ, 1989.

[144] CD Calhoun and NS Stoloff. The effects of particles on fracture processes in magnesium alloys. *Metallurgical Transactions*, 1(4):997–1006, 1970.

[145] P Lhuissier, M Scheel, L Salvo, M Di Michiel, and JJ Blandin. Continuous characterization by x-ray microtomography of damage during high-temperature deformation of magnesium alloy. *Scripta Materialia*, 69(1):85–88, 2013.

[146] Michael J Nemcko and David S Wilkinson. On the damage and fracture of commercially pure magnesium using x-ray microtomography. *Materials Science and Engineering: A*, 676:146–155, 2016.

[147] SH Mohamadi Azghandi, M Weiss, BD Arhatari, and MR Barnett. Grain size and void formation in mg alloy az31. *Journal of Alloys and Compounds*, 816:152618, 2020.

[148] SH Mohamadi Azghandi, Matthias Weiss, BD Arhatari, J Adrien, E Maire, and MR Barnett. A rationale for the influence of grain size on failure of magnesium alloy az31: An in situ x-ray microtomography study. *Acta Materialia*, 200:619–631, 2020.

[149] AS Argon and SR Maloof. Plastic deformation of tungsten single crystals at low temperatures. *Acta metallurgica*, 14(11):1449–1462, 1966.

[150] RG Garlick and HB Probst. Investigation of room-temperature slip in zone-melted tungsten single crystals. *Transactions of the Metallurgical Society of AIME*, 1964.

[151] Robert M Rose. Yielding and plastic flow in single crystals of tungsten. *Trans. Met. Soc. AIME*, 224:981–989, 1962.

[152] Rollin E Hook and Attwell M Adair. On recrystallization embrittlement of chromium. *Transactions of the Metallurgical Society of AIME*, 227(1):151, 1963.

[153] Y Cheng, M Mrovec, and P Gumbsch. Crack nucleation at the $\sigma 9(2\bar{2}1)$ symmetrical tilt grain boundary in tungsten. *Materials Science and Engineering: A*, 483:329–332, 2008.

[154] S. J. Fensin, E. K. Cerreta, G. T. Gray III, and S. M. Valone. Why are some Interfaces in Materials Stronger than others? *Scientific Reports*, 4(1):5461, May 2015.

[155] Garvit Agarwal and Avinash M. Dongare. Defect and damage evolution during spallation of single crystal Al: Comparison between molecular dynamics and quasi-coarse-grained dynamics simulations. *Computational Materials Science*, 145:68–79, April 2018.

[156] Philip J. Noell, Nipal Deka, Ryan B. Sills, and Brad L. Boyce. Identifying the microstructural features associated with void nucleation during elevated temperature deformation of copper. *Submitted*, 2021.

[157] A. N. Stroh. The formation of cracks as a result of plastic flow. *Proc. R. Soc. Lond. A*, 223(1154):404–414, 1954.

[158] JD Eshelby, FC Frank, and FRN Nabarro. Xli. the equilibrium of linear arrays of dislocations. *The London, Edinburgh, and Dublin Philosophical Magazine and Journal of Science*, 42(327):351–364, 1951.

[159] John R. Low Jr. The fracture of metals. *Progress in materials science*, 12:3–96, 1963.

[160] JS Koehler. The production of large tensile stresses by dislocations. *Physical Review*, 85(3):480, 1952.

[161] Jacques Friedel. *Dislocations: International Series of Monographs on Solid State Physics*, volume 3. Elsevier, 2013.

[162] Yongfeng Zhang, Paul C Millett, Michael Tonks, and Bulent Biner. Deformation-twin-induced grain boundary failure. *Scripta Materialia*, 66(2):117–120, 2012.

[163] Thomas Pardoen, D Dumont, A Deschamps, and Y Brechet. Grain boundary versus transgranular ductile failure. *Journal of the Mechanics and Physics of Solids*, 51(4):637–665, 2003.

[164] D Dumont, A Deschamps, and Y Brechet. A model for predicting fracture mode and toughness in 7000 series aluminium alloys. *Acta Materialia*, 52(9):2529–2540, 2004.

[165] Thomas Pardoen and Y Brechet. Influence of microstructure-driven strain localization on the ductile fracture of metallic alloys. *Philosophical Magazine*, 84(3-5):269–297, 2004.

[166] AK Vasudevan and RD Doherty. Grain boundary ductile fracture in precipitation hardened aluminum alloys. *Acta metallurgica*, 35(6):1193–1219, 1987.

[167] PNT Unwin, GW Lorimer, and RB Nicholson. The origin of the grain boundary precipitate free zone. *Acta Metallurgica*, 17(11):1363–1377, 1969.

[168] Deschamps Dumont, Alexis Deschamps, and Y Brechet. On the relationship between microstructure, strength and toughness in aa7050 aluminum alloy. *Materials Science and Engineering: A*, 356(1-2):326–336, 2003.

[169] TF Morgeneyer, MJ Starink, SC Wang, and I Sinclair. Quench sensitivity of toughness in an al alloy: Direct observation and analysis of failure initiation at the precipitate-free zone. *Acta Materialia*, 56(12):2872–2884, 2008.

[170] RH Van Stone, TB Cox, JR Low, and JA Psioda. Microstructural aspects of fracture by dimpled rupture. *International Metals Reviews*, 30(1):157–180, 1985.

[171] TB Cox and John R Low. An investigation of the plastic fracture of aisi 4340 and 18 nickel-200 grade maraging steels. *Metallurgical Transactions*, 5(6):1457–1470, 1974.

[172] JW Bray, JL Maloney, KS Raghavan, and WM Garrison. A comparison of the fracture behavior of two commercially produced heats of hy180 steel differing in sulfide type. *Metallurgical Transactions A*, 22(10):2277–2285, 1991.

[173] Pranay Choudhary and Warren M Garrison Jr. The effect of inclusion type on the toughness of 4340 steel. *Materials and Manufacturing Processes*, 25(1-3):180–184, 2010.

[174] Yoshiyuki Tomita. Fracture toughness of calcium-modified ultrahigh-strength 4340 steel. *Metallurgical Transactions A*, 21(10):2739–2746, 1990.

[175] Dierk Raabe, Dirk Ponge, Peter Uggowitzer, Moritz Roscher, Mario Paolantonio, Chuanlai Liu, Helmut Antrekowitsch, Ernst Kozeschnik, David Seidmann, Bat Gault, et al. Making sustainable aluminum by recycling scrap: The science of "dirty" alloys. *Progress in Materials Science*, page 100947, 2022.

[176] JJ Williams, Z Flom, AA Amell, Nikhilesh Chawla, X Xiao, and F De Carlo. Damage evolution in sic particle reinforced al alloy ma-

trix composites by x-ray synchrotron tomography. *Acta Materialia*, 58(18):6194–6205, 2010.

[177] Laurent Babout, Eric Maire, and Roger Fougeres. Damage initiation in model metallic materials: X-ray tomography and modelling. *Acta Materialia*, 52(8):2475–2487, 2004.

[178] L Babout, Wolfgang Ludwig, E Maire, and JY Buffiere. Damage assessment in metallic structural materials using high resolution synchrotron x-ray tomography. *Nuclear Instruments and Methods in Physics Research Section B: Beam Interactions with Materials and Atoms*, 200:303–307, 2003.

[179] Laurent Babout, Yves Brechet, Eric Maire, and Roger Fougeres. On the competition between particle fracture and particle decohesion in metal matrix composites. *Acta materialia*, 52(15):4517–4525, 2004.

[180] Arnaud Weck, DS Wilkinson, and Eric Maire. Observation of void nucleation, growth and coalescence in a model metal matrix composite using x-ray tomography. *Materials Science and Engineering: A*, 488(1-2):435–445, 2008.

[181] Y Charles, R Estevez, Y Bréchet, and E Maire. Modelling the competition between interface debonding and particle fracture using a plastic strain dependent cohesive zone. *Engineering fracture mechanics*, 77(4):705–718, 2010.

[182] Akihide Hosokawa, David S Wilkinson, Jidong Kang, and Eric Maire.

Onset of void coalescence in uniaxial tension studied by continuous x-ray tomography. *Acta materialia*, 61(4):1021–1036, 2013.

[183] Florent Hannard, Thomas Pardoen, Éric Maire, Christophe Le Bourlot, Rajmund Mokso, and Aude Simar. Characterization and micromechanical modelling of microstructural heterogeneity effects on ductile fracture of 6xxx aluminium alloys. *Acta Materialia*, 103:558–572, 2016.

[184] Christian C Roth, Thilo F Morgeneyer, Yin Cheng, Lukas Helfen, and Dirk Mohr. Ductile damage mechanism under shear-dominated loading: In-situ tomography experiments on dual phase steel and localization analysis. *International Journal of Plasticity*, 109:169–192, 2018.

[185] Ning Dang, Lingyu Liu, Jérôme Adrien, Sophie Cazottes, Wenlong Xiao, Chaoli Ma, Lian Zhou, and Eric Maire. Crack nucleation and growth in α/β titanium alloy with lamellar microstructure under uniaxial tension: 3d x-ray tomography analysis. *Materials Science and Engineering: A*, 747:154–160, 2019.

[186] Md Shahnewaz Bhuiyan, Hiroyuki Toda, Kentaro Uesugi, Akihisa Takeuchi, and Yoshio Watanabe. Damage micromechanisms in high mn and zn content 7xxx aluminum alloys. *Materials Science and Engineering: A*, 793:139423, 2020.

[187] N Pathak, J Adrien, C Butcher, E Maire, and M Worswick. Experimental stress state-dependent void nucleation behavior for advanced high strength steels. *International Journal of Mechanical Sciences*, 179:105661, 2020.

[188] Andre Pineau and Thomas Pardoen. Failure mechanisms of metals. *Comprehensive structural integrity encyclopedia*, 2, 2007.

[189] TC Lindley, G Oates, and CE Richards. A critical appraisal of carbide cracking mechanisms in ferride/carbide aggregates. *Acta metallurgica*, 18(11):1127–1136, 1970.

[190] M Gell and PJ Worthington. The plastic deformation and fracture of iron-3% silicon in the temperature range 295 k–473 k. *Acta Metallurgica*, 14(10):1265–1271, 1966.

[191] MR Warren and OJ Beevers. The interrelationship between deformation and crack nucleation and propagation in zirconium containing hydride precipitates. *Journal of Nuclear Materials*, 26(3):273–284, 1968.

[192] MF Ashby. Work hardening of dispersion-hardened crystals. *Philosophical Magazine*, 14(132):1157–1178, 1966.

[193] JT Barnby. The initiation of ductile failure by fractured carbides in an austenitic stainless steel. *Acta Metallurgica*, 15(5):903–909, 1967.

[194] AJ Gross and K Ravi-Chandar. On the deformation and failure of al 6061-t6 in plane strain tension evaluated through in situ microscopy. *International Journal of Fracture*, 208(1):27–52, 2017.

[195] Yung Suk Jeremy Yoo, Hojun Lim, John Emery, and Josh Kacher. Relating microstructure to defect behavior in aa6061 using a combined computational and multiscale electron microscopy approach. *Available at SSRN 3358892*, 2019.

[196] C Shashank Kaira, Tyler J Stannard, Vincent De Andrade, Francesco De Carlo, and Nikhilesh Chawla. Exploring novel deformation mechanisms in aluminum–copper alloys using in situ 4d nanomechanical testing. *Acta Materialia*, 176:242–249, 2019.

[197] H Ghadbeigi, Christophe Pinna, and Steven Celotto. Failure mechanisms in dp600 steel: Initiation, evolution and fracture. *Materials Science and Engineering: A*, 588:420–431, 2013.

[198] Qingquan Lai, Olivier Bouaziz, Mohamed Gouné, Laurence Brassart, Marc Verdier, Guillaume Parry, Astrid Perlade, Yves Bréchet, and Thomas Pardoen. Damage and fracture of dual-phase steels: Influence of martensite volume fraction. *Materials Science and Engineering: A*, 646:322–331, 2015.

[199] J Kadkhodapour, A Butz, and S Ziaei Rad. Mechanisms of void formation during tensile testing in a commercial, dual-phase steel. *Acta Materialia*, 59(7):2575–2588, 2011.

[200] Cemal Cem Tasan, Johan PM Hoefnagels, Martin Diehl, Dingshun Yan, Franz Roters, and Dierk Raabe. Strain localization and damage in dual phase steels investigated by coupled in-situ deformation experiments and crystal plasticity simulations. *International Journal of Plasticity*, 63:198–210, 2014.

[201] Lei Liu, Francesco Maresca, Johan PM Hoefnagels, Tijmen Vermeij, Marc GD Geers, and Varvara G Kouznetsova. Revisiting the marten-

site/ferrite interface damage initiation mechanism: The key role of substructure boundary sliding. *Acta Materialia*, 205:116533, 2021.

[202] Orlando León-García, Roumen Petrov, and Leo AI Kestens. Void initiation at tin precipitates in if steels during tensile deformation. *Materials Science and Engineering: A*, 527(16-17):4202–4209, 2010.

[203] H. C. Rogers. Tensile Fracture of Ductile Metals. *Transactions of AIME*, 218:498–506, 1960.

[204] W. M. Garrison and N. R. Moody. Ductile fracture. *Journal of Physics and Chemistry of Solids*, 48(11):1035–1074, 1987.

[205] Frédéric Bron, Jacques Besson, and André Pineau. Ductile rupture in thin sheets of two grades of 2024 aluminum alloy. *Materials Science and Engineering: A*, 380(1-2):356–364, 2004.

[206] JB Jordon, MF Horstemeyer, K Solanki, JD Bernard, JT Berry, and TN Williams. Damage characterization and modeling of a 7075-t651 aluminum plate. *Materials Science and Engineering: A*, 527(1-2):169–178, 2009.

[207] JP Bandstra and DA Koss. Modeling the ductile fracture process of void coalescence by void-sheet formation. *Materials Science and Engineering: A*, 319:490–495, 2001.

[208] Viktor V. Pogorelko and Alexander E. Mayer. Influence of copper inclusions on the strength of aluminum matrix at high-rate tension. *Materials Science and Engineering: A*, 642:351–359, August 2015.

[209] Victor V. Pogorelko and Alexander E. Mayer. Influence of titanium and magnesium nanoinclusions on the strength of aluminum at high-rate tension: Molecular dynamics simulations. *Materials Science and Engineering: A*, 662:227–240, April 2016.

[210] V V Pogorelko and A E Mayer. Tensile strength of Al matrix with nanoscale Cu, Ti and Mg inclusions. *Journal of Physics: Conference Series*, 774:012034, November 2016.

[211] Yi Cui and Zengtao Chen. Void initiation from interfacial debonding of spherical silicon particles inside a silicon-copper nanocomposite: A molecular dynamics study. *Modelling and Simulation in Materials Science and Engineering*, 25(2):025007, February 2017.

[212] V V Pogorelko and A E Mayer. Tensile strength of Fe–Ni and Mg–Al nanocomposites: Molecular dynamic simulations. *Journal of Physics: Conference Series*, 946:012043, January 2018.

[213] JI Beltrán and MC Muñoz. Ab initio study of decohesion properties in oxide/metal systems. *Physical Review B*, 78(24):245417, 2008.

[214] Kaoru Nakamura, Toshiharu Ohnuma, and Takashi Ogata. First-principles study of structure, vacancy formation, and strength of bcc fe/v4c3 interface. *Journal of materials science*, 46(12):4206–4215, 2011.

[215] John Gurland and J Plateau. The mechanism of ductile rupture of metals containing inclusions. Report, Brown Univ., Providence; Institut de Recherches de la Siderugie, St.-Germain ..., 1963.

[216] M. F. Ashby. Work hardening of dispersion–hardened crystals. *The Philosophical Magazine*, 14:1157–1178, 1966.

[217] K Tanaka, T Mori, and T Nakamura. Cavity formation at the interface of a spherical inclusion in a plastically deformed matrix. *Philosophical Magazine*, 21(170):267–279, 1970.

[218] A. S. Argon and J. Im. Separation of Second Phase Particles in Spheroidized 1045 Steel, Cu-0.6pct Cr Alloy, and Maraging Steel in Plastic Straining. *Met. Trans.*, 6A:839–851, 1975.

[219] L. M. Brown and W. M. Stobbs. The work hardening of copper–silica, v. equilibrium plastic relaxation by secondary dislocation. *The Philosophical Magazine*, 34:351–372, 1976.

[220] J. Gurland and J. Plateau. The mechanism of ductile rupture of metals containing inclusions. *Trans ASM*, 56:442–454, 1963.

[221] A. S. Argon. Formation of Cavities from Nondeformable Second–Phase Particles in Low Temperature Ductile Fracture. *Journal of Engineering Materials and Technology*, 18:60–68, 1976.

[222] F. M. Beremin, A. Pineau, F. Mudry, J.C. Devaux, Y. D'Escatha, and P. Ledermann. Cavity formation from inclusions in ductile fracture of A508 steel. *Metallurgical Transactions A.*, 12A:723–731, 1981.

[223] P. Gilormini and F. Montheillet. Deformation of an inclusion in a viscous matrix and induced stress concentrations. *J. Mech. Phys. Solids*, 34(2):97–123, 1986.

[224] F. Montheillet and P. Gilormini. Amorçage de l'endommagement. In F. Montheillet and F. Moussy, editors, *Physique et mécanique de l'endommagement*, pages 122–181. Les éditions de physique, Les Ulis, 1986.

[225] R. D. Thomson and J. W. Hancock. Ductile failure by void nucleation, growth and coalescence. *International Journal of Fracture*, 26:99–112, 1984.

[226] A. Needleman. A continuum model for void nucleation by inclusion debonding. *Journal of Applied Mechanics*, 54:525–531, 1987.

[227] O. P. Sovik. *Numerical Modelling of Ductile Fracture — A Damage Mechanics Approach*. PhD thesis, Norges teknisk–naturvitenskapelige universitet Trondheim, Norway, 1996.

[228] B. Wilner. Stress analysis of particles in metals. *Journal of the Mechanics and Physics of Solids*, 36(2):141–165, 1988.

[229] B. J. Lee and M. E. Mear. Stress concentration induced by an elastic spheroidal particle in a plastically deforming solid. *Journal of the Mechanics and Physics of Solids*, 47:1301–1336, 1999.

[230] J. N. Goodier. Concentration of stress around spherical and cylindrical inclusions and flaws. *ASME Appl. Mech. Mag.*, 55:39, 1933.

[231] J. D. Eshelby. The determination of the elastic field of an ellipsoidal inclusion, and related problems. *Proceedings of the Royal Society of London A*, 241:376–396, 1957.

[232] Bengt Sundström. An energy condition for initiation of interfacial microcracks at inclusions. *Engineering Fracture Mechanics*, 6(3):483–492, 1974.

[233] J. R. Fisher and J. Gurland. Void nucleation in spheroidized carbon steels. Part II. Theory. *J. Metal. Sci.*, 15:193, 1981.

[234] M. Berveiller and A. Zaoui. An extension of the self-consistent scheme to plastically-flowing polycrystals. *Journal of the Mechanics and Physics of Solids*, 26:325–344, 1978.

[235] Y. Huang, J. W. Hutchinson, and V. Tvergaard. Cavitation instabilities in elastic–plastic solids. *Journal of the Mechanics and Physics of Solids*, 39:223–241, 1991.

[236] H.-S. Hou and R. Abeyaratne. Cavitation in elastic and elastic-plastic solids. *Journal of the Mechanics and Physics of Solids*, 40:571–592, 1992.

[237] Marc André Meyers and Catherine Taylor Aimone. Dynamic fracture (spalling) of metals. *Progress in Materials Science*, 28:1–96, 1983.

[238] T. J. Baker, K. B. Gove, and J. A. Charles. Inclusion deformation and toughness anisotropy in hot–rolled steels. *Met Tech*, 3:183–193, 1976.

[239] HC Chao, L Thomassen, and LH Van Vlack. Deformation and fracture of mns crystals. *ASM Trans. Quart.*, 57(2):386–98, 1964.

[240] A Srivastava and A Needleman. Effect of crystal orientation on porosity

evolution in a creeping single crystal. *Mechanics of Materials*, 2015. In Press.

[241] T. Malkiewicz and S. Rudnik. Deformation of non-metallic inclusions during rolling of steel. *J. Iron Steel Inst.*, 201:33–38, 1963.

[242] R. Kiessling. The influence of non-metallic inclusions on the properties of steel. *J. Met.*, 21:47–54, 1969.

[243] A. Costa e Silva. The effects of non-metallic inclusions on properties relevant to the performance of steel in structural and mechanical applications. *Journal of Materials Research and Technology*, 8:2408–2422, 2019.

[244] M. L. Turpin and J. F. Elliot. Nucleation of oxide inclusions in iron melts. *J. Iron and Steel Inst.*, 204:217, 1966.

[245] C. J. Middleton. Reheat cavity nucleation and nucleation control in bainitic creep-resisting low-alloy steels - roles of manganese sulfide, residual, and sulfur-stabilizing elements. *J. Metal. Sci.*, 15:154–167, 1981.

[246] B. J. Cane and C. J. Middleton. Intergranular creep-cavity formation in low-alloy bainitic steels. *J. Metal. Sci.*, 15:295–301, 1981.

[247] C. L. Smith and J. R. Low. Effect of prior austenitic grain-boundary composition on temper brittleness in ni-cr-sb steel. *Met. Trans.*, 5:279, 1974.

[248] L. E. Iorio and W. M. Garrison Jr. Effects of gettering sulfur as CrS or MnS on void generation behavior in ultra-high strength steel. *Scripta Materialia*, 46:863–868, 2002.

[249] D. Lassance, D. Fabrègue, F. Delannay, and T. Pardoen. Micromechanics of room and high temperature fracture in 6xxx Al alloys. *Progress in Materials Science*, 52:62–129, 2007.

[250] J. A. Psioda. *The effect of microstructure and strength on the fracture toughness of an 18 Ni, 300 grade maraging steel*. PhD thesis, Carnegie Mellon University, Pittsburgh, USA, 1977.

[251] G. T. Hahn and A. R. Rosenfield. Metallurgical Factors Affecting Fracture Toughness of Aluminum Alloys. *Metallurgical Transactions A.*, 6A:653–668, 1975.

[252] L. Babout, Y. Bréchet, E. Maire, and R. Fougères. On the competition between particle fracture and particle decohesion in metal matrix composites. *Acta Materialia*, 52:4517–4525, 2004.

[253] T. B. Cox and J. R. Low. An Investigation of the Plastic Fracture of AISI 4340 and 18 Nickel–200 Grade Maraging Steels. *Met. Trans.*, 5:1457–1470, 1974.

[254] C. Chu and A. Needleman. Void nucleation effects in biaxially stretched sheets. *Journal of Engineering Materials and Technology*, 102:249–256, 1980.

[255] P. Ponte Castaneda. The effective mechanical properties of nonlinear

composites. *Journal of the Mechanics and Physics of Solids*, 39:45–71, 1991.

[256] C. Tekoglu and T. Pardoen. A micromechanics based damage model for composite materials. *International Journal of Plasticity*, 26:549–69, 2010.

[257] A. A. Benzerga. An analysis of exhaustion hardening in micron-scale plasticity. *International Journal of Plasticity*, 24:1128–1157, 2008.

[258] A. Pineau and T. Pardoen. Failure of Metals. *Comprehensive Structural Integrity*, 2:684–797, 2007. Chapter 2.06.

[259] R. Hill. New horizons in the mechanics of solids. *Journal of the Mechanics and Physics of Solids*, 5:66, 1956.

[260] B. Budiansky, J. W. Hutchinson, and S. Slutsky. Void growth and collapse in viscous solids. In H. G. Hopkins and M. J. Sowell, editors, *Mechanics of Solids, The Rodney Hill 60th Anniversary Volume*, pages 13–45. Pergamon press, 1982.

[261] L. M. Brown and D. R. Clarke. Work hardening due to internal stresses in composite materials. *Acta Metallurgica*, 23:821–830, 1975.

[262] W. M. Garrison Jr. Ultrahigh-Strength Steels for Aerospace Applications. *JOM*, 42:20–24, 1990.

[263] LE Iorio and WM Garrison. The effects of titanium additions on af1410 ultra-high-strength steel. *Metallurgical and Materials Transactions A*, 37(4):1165–1173, 2006.

[264] E. Maire, O. Bouaziz, M. Di Michiel, and C. Verdu. Initiation and growth of damage in a dual-phase steel observed by X-ray microtomography. *Acta Materialia*, 56:4954–4964, 2008.

[265] C. Landron, O. Bouaziz, E. Maire, and J. Adrien. Characterization and modeling of void nucleation by interface decohesion in dual phase steels. *Scripta Materialia*, 63:973–976, 2010.

[266] M. N. Shabrov, E. Sylven, S. Kim, D. H. Sherman, L. Chuzhoy, C. L. Briant, and A. Needleman. Void nucleation by inclusion cracking. *Metallurgical and Materials Transactions A.*, 35A:1745–1755, 2004.

[267] A. S. Argon, J. Im, and R. Safoglu. Cavity Formation from Inclusions in Ductile Fracture. *Metallurgical Transactions A.*, 6A:825–837, 1975.

[268] A. S. Argon, J. Im, and A. Needleman. Distribution of Plastic Strain and Negative Pressure in Necked Steel and Copper Bars. *Met. Trans.*, 6A:815–824, 1975.

[269] A. A. Benzerga and J.-B. Leblond. Effective Yield Criterion Accounting for Microvoid Coalescence. *Journal of Applied Mechanics*, 81(3):031009, 2014.

[270] M. Achouri, G. Germain, P. Dal Santo, and D. Saidane. Experimental characterization and numerical modeling of micromechanical damage under different stress states. *Materials & Design*, 50:207–222, 2013.

[271] K. Siruguet and J.-B. Leblond. Effect of void locking by inclusions upon the plastic behavior of porous ductile solids–part II: Theoreti-

cal modeling and numerical study of void coalescence. *International Journal of Plasticity*, 20:255–268, 2004.

[272] K. Siruguet and J.-B. Leblond. Effect of void locking by inclusions upon the plastic behavior of porous ductile solids—I: theoretical modeling and numerical study of void growth. *International Journal of Plasticity*, 20:225–254, 2004.

[273] M. F. Horstemeyer and A. M. Gokhale. A void-crack nucleation model for ductile metals. *International Journal of Solids and Structures*, 36:5029–5055, 1999.

[274] Matthieu Marteleur, Julien Leclerc, Marie-Stéphane Colla, Van-Dung Nguyen, Ludovic Noels, and Thomas Pardoen. Ductile fracture of high strength steels with morphological anisotropy, part i: Characterization, testing, and void nucleation law. *Engineering Fracture Mechanics*, 244:107569, 2021.

[275] A. A. Benzerga. *Rupture ductile des tôles anisotropes*. PhD thesis, Ecole Nationale Supérieure des Mines de Paris, 2000.

[276] F. A. McClintock. A criterion for ductile fracture by the growth of holes. *Journal of Applied Mechanics*, 35:363–371, 1968.

[277] Bengt Sundstrom. Plastic deformation of an infinite plate with elliptic inclusion. *Journal of Composite Materials*, 5(2):277–278, 1971.

[278] RH Zeisloft and WF Hosford. Deformation of artificial inclusions in compressive plane strain. *ASM TRANS QUART*, 62(1):297–300, 1969.

[279] Mamoru Shibata and Kanji Ono. Stress concentration due to an oblate spheroidal inclusion. *Materials Science and Engineering*, 34(2):131–137, 1978.

[280] A. A. Benzerga, J. Besson, and A. Pineau. Anisotropic ductile fracture. Part I: experiments. *Acta Materialia*, 52:4623–4638, 2004.

[281] A. A. Benzerga, J. Besson, and A. Pineau. Anisotropic ductile fracture. Part II: theory. *Acta Materialia*, 52:4639–4650, 2004.

[282] Anthony G Evans and John W Hutchinson. A critical assessment of theories of strain gradient plasticity. *Acta Materialia*, 57(5):1675–1688, 2009.

[283] J. D. Eshelby. The elastic field outside an ellipsoidal inclusion. *Proceedings of the Royal Society of London A*, 252:561–569, 1959.

[284] H. Gao, Y. Huang, W. D. Nix, and J. W. Hutchinson. Mechanism-based strain gradient plasticity - I. Theory. *Journal of the Mechanics and Physics of Solids*, 47:1239–1263, 1999.

[285] D. Teirlinck, F. Zok, J.D. Embury, and M.F. Ashby. Fracture mechanism maps in stress space. *Acta Metallurgica*, 36:1213–1228, 1988.

[286] N. A. Fleck, J. W. Hutchinson, and V. Tvergaard. Softening by void nucleation and growth in tension and shear. *Journal of the Mechanics and Physics of Solids*, 37:515–540, 1989.

[287] K. Kuna and D. Z. Sun. Three-dimensional cell model analyses of

void growth in ductile materials. *International Journal of Fracture*, 81:235–258, 1996.

[288] Bo Gao, Ying Li, Tian Fu Guo, Xu Guo, and Shan Tang. Void nucleation in alloys with lamella particles under biaxial loadings. *Extreme Mechanics Letters*, 22:42–50, 2018.

[289] M. N. Shabrov and A. Needleman. An analysis of inclusion morphology effects on void nucleation. *Modelling and Simulation in Materials Science and Engineering*, 10:163–183, 2002.

[290] W David Kingery, Harvey Kent Bowen, and Donald R Uhlmann. *Introduction to ceramics*, volume 17. John wiley & sons, 1976.

[291] C Barry Carter, M Grant Norton, et al. *Ceramic materials: science and engineering*, volume 716. Springer, 2007.

[292] A Gangulee and J Gurland. On the fracture of silicon particles in aluminum- silicon alloys. *AIME Met Soc Trans*, 239(2):269–272, 1967.

[293] JJ Williams, Z Flom, AA Amell, Nikhilesh Chawla, X Xiao, and F De Carlo. Damage evolution in sic particle reinforced al alloy matrix composites by x-ray synchrotron tomography. *Acta Materialia*, 58(18):6194–6205, 2010.

[294] Aude Hauert, Andreas Rossoll, and Andreas Mortensen. Particle fracture in high-volume-fraction ceramic-reinforced metals: Governing parameters and implications for composite failure. *Journal of the Mechanics and Physics of Solids*, 57(11):1781–1800, 2009.

[295] FM Beremin. Cavity formation from inclusions in ductile fracture of a508 steel. *Metallurgical Transactions A*, 12(5):723–731, 1981.

[296] Mark F Horstemeyer and Arun M Gokhale. A void–crack nucleation model for ductile metals. *International Journal of Solids and Structures*, 36(33):5029–5055, 1999.

[297] BS Majumdar and AB Pandey. Deformation and fracture of a particle-reinforced aluminum alloy composite: Part ii. modeling. *Metallurgical and Materials Transactions A*, 31(13):937–950, 2000.

[298] CA Lewis and PJ Withers. Weibull modelling of particle cracking in metal matrix composites. *Acta metallurgica et materialia*, 43(10):3685–3699, 1995.

[299] A. L. Gurson. *Plastic flow and fracture behavior of ductile materials incorporating void nucleation, growth and interaction*. PhD thesis, Brown University, Providence, 1975.

[300] A. Needleman and J. R. Rice. Limits to ductility set by plastic flow localization. In D. P. Koistinen and N.-M. Wang, editors, *Mechanics of sheet metal forming*, pages 237–267. Plenum Press, 1978.

[301] A. L. Gurson. Continuum Theory of Ductile Rupture by Void Nucleation and Growth: Part I– Yield Criteria and Flow Rules for Porous Ductile Media. *Journal of Engineering Materials and Technology*, 99:2–15, 1977.

[302] M. Gologanu, J.-B. Leblond, and J. Devaux. Approximate Models for

Ductile Metals Containing Non–spherical Voids — Case of Axisymmetric Oblate Ellipsoidal Cavities. *Journal of Engineering Materials and Technology*, 116:290–297, 1994.

[303] A. A. Benzerga, J. Besson, and A. Pineau. Coalescence–Controlled Anisotropic Ductile Fracture. *Journal of Engineering Materials and Technology*, 121:221–229, 1999.

[304] T. Pardoen, D. Dumont, A. Deschamps, and Y. Bréchet. Grain boundary versus transgranular ductile failure. *Journal of the Mechanics and Physics of Solids*, 51:637 – 665, 2003.

[305] B. Kondori and A. A. Benzerga. Modeling damage accumulation to fracture in a magnesium-rare earth alloy. *Acta Materialia*, 124:225–236, 2017.

[306] S. H. Goods and L. M. Brown. Overview no. 1: The nucleation of cavities by plastic deformation. *Acta Metallurgica*, 27(1):1–15, 1979.

[307] K. Gall, N. Yang, H. Sehitoglu, and Y. I. Chumlyakov. Fracture of precipitated NiTi shape memory alloys. *International Journal of Fracture*, 109:189–207, 2001.

[308] J. Makkar and T. Baxevanis. On the fracture response of shape memory alloys by void growth and coalescence. *Mechanics of Materials*, 153:103682, 2021.

[309] C. H. Shang, T. P. Weihs, R. C. Cammarata, Y. Ji, and C. L. Chien. Anisotropy in magnetic and mechanical properties in textured Hiperco FeCoV alloys. *Journal of Applied Physics*, 87:6508–6510, 2000.

[310] B. Kondori and A. A. Benzerga. Effect of Stress Triaxiality on the Flow and Fracture of Mg Alloy AZ31. *Metallurgical and Materials Transactions A.*, 45:3292–3307, 2014.

[311] J. G. Cowie, M. Azrin, and G. B. Olson. Microvoid formation during shear deformation of ultrahigh strength steels. *Metallurgical Transactions A.*, 20:143–153, 1989.

[312] G. Lacroix, T. Pardoen, and P.J. Jacques. The fracture toughness of trip-assisted multiphase steels. *Acta Materialia*, 56:3900–3913, 2008.

[313] M. R. Barnett. Twinning and the ductility of magnesium alloys Part I: "tension" twins. *Materials Science and Engineering: A*, 464:1–7, 2007.

[314] A. K. Rodriguez, G. Ayoub, B. Mansoor, and A. A. Benzerga. Effect of strain rate and temperature on fracture of AZ31B magnesium alloy. *Acta Materialia*, 112:194–208, 2016.

[315] W. M. Garrison Jr. and A. L. Wojcieszynski. A discussion of the effect of inclusion volume fraction on the toughness of steel. *Materials Science and Engineering: A*, 464:321–329, 2007.

[316] W. M. Garrison Jr. and A. L. Wojcieszynski. A discussion of the spacing of inclusions in the volume and of the spacing of inclusion nucleated voids on fracture surfaces of steels. *Materials Science and Engineering: A*, 505:52–61, 2009.

[317] J. R. Rice and M. A. Johnson. *Inelastic behavior of solids*, chapter The role of large crack tip geometry changes in plane strain fracture, pages 641–672. Mc Graw Hill, 1970.

[318] A. Srivastava, L. Ponson, S. Osovski, E. Bouchaud, V. Tvergaard, and A. Needleman. Effect of inclusion density on ductile fracture toughness and roughness. *Journal of the Mechanics and Physics of Solids*, 63:62–79, 2014.

[319] Y. Liu, X. Zheng, S. Osovski, and A. Srivastava. On the micromechanism of inclusion driven ductile fracture and its implications on fracture toughness. *Journal of the Mechanics and Physics of Solids*, 130:21–34, 2019.

[320] Leonardo Golubović and Anatoli Peredera. Mechanism of time-delayed fractures. *Physical Review E*, 51(4):2799–2804, April 1995.

[321] Victor Berdichevsky and Khanh Chau Le. On The Microcrack Nucleation In Brittle Solids. *International Journal of Fracture*, 133(4):L47–L54, June 2005.

[322] Cristiano L. Dias, Jens Kröger, Daniel Vernon, and Martin Grant. Nucleation of cracks in a brittle sheet. *Physical Review E*, 80(6):066109, December 2009.

[323] B. Kondori, T. Morgeneyer, L. Helfen, and A. A. Benzerga. Void growth and coalescence in a magnesium alloy studied by synchrotron radiation laminography. *Acta Materialia*, 155:80–94, 2018.

[324] VA Lubarda, MS Schneider, DH Kalantar, BA Remington, and MA Meyers. Void growth by dislocation emission. *Acta Materialia*, 52:1397–1408, 2004.

[325] Ladislas Kubin. *Dislocations, Mesoscale Simulations and Plastic Flow*. Oxford University Press, Oxford, 2013.

[326] Ryan B. Sills, William P. Kuykendall, Amin Aghaei, and Wei Cai. Fundamentals of Dislocation Dynamics Simulations. In Christopher R. Weinberger and Garritt J. Tucker, editors, *Multiscale Materials Modeling for Nanomechanics*, volume 245, pages 53–87. Springer International Publishing, Cham, 2016.

[327] L. E. Shilkrot, R. E. Miller, and W. A. Curtin. Coupled Atomistic and Discrete Dislocation Plasticity. *Physical Review Letters*, 89(2):025501, June 2002.

[328] G. Anciaux, T. Junge, M. Hodapp, J. Cho, J.-F. Molinari, and W.A. Curtin. The Coupled Atomistic/Discrete-Dislocation method in 3d part I: Concept and algorithms. *Journal of the Mechanics and Physics of Solids*, 118:152–171, September 2018.

[329] Youping Chen, Sergei Shabanov, and David L McDowell. Concurrent atomistic-continuum modeling of crystalline materials. *Applied Physics*, page 20, 2019.

[330] Dennis M. Kochmann and Jeffrey S. Amelang. The Quasicontinuum Method: Theory and Applications. In Christopher R. Weinberger and Garritt J. Tucker, editors, *Multiscale Materials Modeling for Nanomechanics*, volume 245, pages 159–193. Springer International Publishing, Cham, 2016.

[331] F. Roters, P. Eisenlohr, L. Hantcherli, D.D. Tjahjanto, T.R. Bieler, and D. Raabe. Overview of constitutive laws, kinematics, homogenization and multiscale methods in crystal plasticity finite-element modeling: Theory, experiments, applications. *Acta Materialia*, 58(4):1152–1211, February 2010.

[332] W.H. Liu, X.M. Zhang, J.G. Tang, and Y.X. Du. Simulation of void growth and coalescence behavior with 3D crystal plasticity theory. *Computational Materials Science*, 40(1):130–139, July 2007.

[333] Ulrik Borg, Christian F. Niordson, and Jeffrey W. Kysar. Size effects on void growth in single crystals with distributed voids. *International Journal of Plasticity*, 24(4):688–701, April 2008.

[334] Qingcheng Yang and Somnath Ghosh. A crystal plasticity model for porous hcp crystals in titanium alloys under multiaxial loading conditions. *International Journal of Solids and Structures*, 238:111400, 2022.

[335] Tiantian Zhang, Jun Jiang, Ben Britton, Barbara Shollock, and Fionn Dunne. Crack nucleation using combined crystal plasticity modelling, high-resolution digital image correlation and high-resolution electron backscatter diffraction in a superalloy containing non-metallic inclusions under fatigue. *Proceedings of the Royal Society A: Mathematical, Physical and Engineering Sciences*, 472(2189):20150792, May 2016.

[336] Tuncay Yalçinkaya, Serhat Onur Çakmak, and Cihan Tekoğlu. A crystal plasticity based finite element framework for RVE calculations of

two-phase materials: Void nucleation in dual-phase steels. *Finite Elements in Analysis and Design*, 187:103510, May 2021.

[337] Y. Mishin. Machine-learning interatomic potentials for materials science. *Acta Materialia*, 214:116980, August 2021.

[338] Jie Cai, Jiawei Luo, Shulin Wang, and Sheng Yang. Feature selection in machine learning: A new perspective. *Neurocomputing*, 300:70–79, July 2018.

[339] JCS Kadupitiya, Fanbo Sun, Geoffrey Fox, and Vikram Jadhao. Machine learning surrogates for molecular dynamics simulations of soft materials. *Journal of Computational Science*, 42:101107, 2020.

[340] Mohammad H Rafiei, Yejun Gu, and Jaafar A El-Awady. Machine learning of dislocation-induced stress fields and interaction forces. *JOM*, 72(12):4380–4392, 2020.

[341] Grace CY Peng, Mark Alber, Adrian Buganza Tepole, William R Cannon, Suvranu De, Savador Dura-Bernal, Krishna Garikipati, George Karniadakis, William W Lytton, Paris Perdikaris, et al. Multiscale modeling meets machine learning: What can we learn? *Archives of Computational Methods in Engineering*, 28(3):1017–1037, 2021.

[342] Burton Irving Edelson and WM Baldwin Jr. The effect of second phases on the mechanical properties of alloys. Report, CASE INST OF TECH CLEVELAND OH, 1959.

[343] W Xu, M Ferry, JM Cairney, and FJ Humphreys. Three-dimensional

investigation of particle-stimulated nucleation in a nickel alloy. *Acta Materialia*, 55(15):5157–5167, 2007.

[344] CY Barlow and N Hansen. Deformation structures and flow stress in aluminium containing short whiskers. *Acta metallurgica et materialia*, 39(8):1971–1979, 1991.

[345] M. E. Torki and A. A. Benzerga. A mechanism of failure in shear bands. *Extreme Mechanics Letters*, 23:67–71, 2018.

[346] Stylianos Tsopanidis, Raúl Herrero Moreno, and Shmuel Osovski. Toward quantitative fractography using convolutional neural networks. *Engineering Fracture Mechanics*, 231:106992, May 2020.

[347] Mallory Wittwer and Matteo Seita. A machine learning approach to map crystal orientation by optical microscopy. *npj Computational Materials*, 8(1):1–9, 2022.

[348] Yung Suk Jeremy Yoo, Hojun Lim, John Emery, and Josh Kacher. Relating microstructure to defect behavior in aa6061 using a combined computational and multiscale electron microscopy approach. *Acta Materialia*, 174:81–91, 2019.

[349] SF Li, J Lind, CM Hefferan, R Pokharel, U Lienert, AD Rollett, and RM Suter. Three-dimensional plastic response in polycrystalline copper via near-field high-energy x-ray diffraction microscopy. *Journal of Applied Crystallography*, 45(6):1098–1108, 2012.

[350] AD Rollett, GS Rohrer, and RM Suter. Understanding materials microstructure and behavior at the mesoscale. *MRS Bulletin*, 40(11):951–960, 2015.

[351] Reeju Pokharel, Jonathan Lind, Shiu Fai Li, Peter Kenesei, Ricardo A Lebensohn, Robert M Suter, and Anthony D Rollett. In-situ observation of bulk 3d grain evolution during plastic deformation in polycrystalline cu. *International Journal of Plasticity*, 67:217–234, 2015.

[352] Clayton A Stein, Albert Cerrone, Tugce Ozturk, Sukbin Lee, Peter Kenesei, Harris Tucker, Reeju Pokharel, Jonathan Lind, Christopher Hefferan, Robert M Suter, et al. Fatigue crack initiation, slip localization and twin boundaries in a nickel-based superalloy. *Current Opinion in Solid State and Materials Science*, 18(4):244–252, 2014.

[353] Maxime Dupraz, Guillaume Beutier, Thomas W Cornelius, Guillaume Parry, Zhe Ren, Stéphane Labat, M-I Richard, Gilbert A Chahine, Oleg Kovalenko, Marc De Boissieu, et al. 3d imaging of a dislocation loop at the onset of plasticity in an indented nanocrystal. *Nano letters*, 17(11):6696–6701, 2017.

[354] Tobias U Schülli and Steven J Leake. X-ray nanobeam diffraction imaging of materials. *Current Opinion in Solid State and Materials Science*, 22(5):188–201, 2018.

[355] Anton Davydok, Thomas W Cornelius, Zhe Ren, Cedric Leclere, Gilbert Chahine, Tobias Schülli, Florian Lauraux, Gunther Richter, and Olivier Thomas. In situ coherent x-ray diffraction during three-

point bending of a au nanowire: visualization and quantification. *Quantum Beam Science*, 2(4):24, 2018.

[356] M Kutsal, P Bernard, G Berruyer, PK Cook, R Hino, AC Jakobsen, W Ludwig, Jeppe Ormstrup, T Roth, Hugh Simons, et al. The esrf dark-field x-ray microscope at id06. In *IOP Conference Series: Materials Science and Engineering*, volume 580, page 012007. IOP Publishing, 2019.

[357] Hugh Simons, A King, Wolfgang Ludwig, C Detlefs, Wolfgang Pantleon, Søren Schmidt, F Stöhr, I Snigireva, A Snigirev, and Henning Friis Poulsen. Dark-field x-ray microscopy for multiscale structural characterization. *Nature communications*, 6(1):1–6, 2015.

[358] Jeppe Ormstrup, Emil V Østergaard, Carsten Detlefs, Ragnvald H Mathiesen, Can Yildirim, Mustafacan Kutsal, Philip K Cook, Yves Watier, Carlos Cosculluela, and Hugh Simons. Imaging microstructural dynamics and strain fields in electro-active materials in situ with dark field x-ray microscopy. *Review of Scientific Instruments*, 91(6):065103, 2020.

[359] AL Greer, YQ Cheng, and E Ma. Shear bands in metallic glasses. *Materials Science and Engineering: R: Reports*, 74(4):71–132, 2013.

[360] Marios D Demetriou, Maximilien E Launey, Glenn Garrett, Joseph P Schramm, Douglas C Hofmann, William L Johnson, and Robert O Ritchie. A damage-tolerant glass. *Nature materials*, 10(2):123–128, 2011.

[361] Christopher A Schuh, Todd C Hufnagel, and Upadrasta Ramamurty. Mechanical behavior of amorphous alloys. *Acta Materialia*, 55(12):4067–4109, 2007.

[362] ZF Zhang, G He, J Eckert, and L Schultz. Fracture mechanisms in bulk metallic glassy materials. *Physical review letters*, 91(4):045505, 2003.

[363] AS Argon and M Salama. The mechanism of fracture in glassy materials capable of some inelastic deformation. *Materials Science and Engineering*, 23(2-3):219–230, 1976.

[364] J Pan, YX Wang, and Y Li. Ductile fracture in notched bulk metallic glasses. *Acta Materialia*, 136:126–133, 2017.

[365] X Huang, Z Ling, and LH Dai. Cavitation instabilities in bulk metallic glasses. *International Journal of Solids and Structures*, 50(9):1364–1372, 2013.

[366] Easo P George, Dierk Raabe, and Robert O Ritchie. High-entropy alloys. *Nature reviews materials*, 4(8):515–534, 2019.

[367] Changning Niu, Carlyn R LaRosa, Jiashi Miao, Michael J Mills, and Maryam Ghazisaeidi. Magnetically-driven phase transformation strengthening in high entropy alloys. *Nature communications*, 9(1):1–9, 2018.

[368] Wenqiang Feng, Yang Qi, and Shaoqing Wang. Effects of mn and al addition on structural and magnetic properties of feconi-based high entropy alloys. *Materials Research Express*, 5(10):106511, 2018.

[369] Easo P George, WA Curtin, and Cemal Cem Tasan. High entropy alloys: A focused review of mechanical properties and deformation mechanisms. *Acta Materialia*, 188:435–474, 2020.

[370] Bo Gao, Gang Zhang, Tianfu Guo, Chao Jiang, Xu Guo, and Shan Tang. Voiding and fracture in high-entropy alloy under multi-axis stress states. *Materials Letters*, 237:220–223, 2019.

[371] Bernd Gludovatz, Anton Hohenwarter, Dhiraj Catoor, Edwin H Chang, Easo P George, and Robert O Ritchie. A fracture-resistant high-entropy alloy for cryogenic applications. *Science*, 345(6201):1153–1158, 2014.

[372] Qingyun Lin, Junpeng Liu, Xianghai An, Hao Wang, Yong Zhang, and Xiaozhou Liao. Cryogenic-deformation-induced phase transformation in an fecocrni high-entropy alloy. *Materials Research Letters*, 6(4):236–243, 2018.

[373] Dong Liu, Qin Yu, Saurabh Kabra, Ming Jiang, Paul Forna-Kreutzer, Ruopeng Zhang, Madelyn Payne, Flynn Walsh, Bernd Gludovatz, Mark Asta, et al. Exceptional fracture toughness of crconi-based medium-and high-entropy alloys at 20 kelvin. *Science*, 378(6623):978–983, 2022.

[374] Yi Cui, Zengtao Chen, and Yang Ju. Fracture of void-embedded high-entropy-alloy films: A comprehensive atomistic study. *Materialia*, 12:100790, 2020.

[375] Yi Cui, Zengtao Chen, Shaojie Gu, Wenzhi Yang, and Yang Ju. Investigating size dependence in nanovoid-embedded high-entropy-alloy films under biaxial tension. *Archive of Applied Mechanics*, pages 1–19, 2022.

[376] Dinh-Quan Doan, Te-Hua Fang, Tao-Hsing Chen, and Thi-Xuyen Bui. Effects of void and inclusion sizes on mechanical response and failure mechanism of alcrcufeni2 high-entropy alloy. *Engineering Fracture Mechanics*, 252:107848, 2021.

[377] Marc A Meyers, A Mishra, and David J Benson. Mechanical properties of nanocrystalline materials. *Progress in materials science*, 51(4):427–556, 2006.

[378] Y Yang, B Imasogie, GJ Fan, Peter K Liaw, and WO Soboyejo. Fatigue and fracture of a bulk nanocrystalline nife alloy. *Metallurgical and Materials Transactions A*, 39(5):1145–1156, 2008.

[379] John A Sharon, Henry A Padilla, and Brad L Boyce. Interpreting the ductility of nanocrystalline metals1. *Journal of Materials Research*, 28(12):1539–1552, 2013.

[380] JA Sharon, PC Su, FB Prinz, and KJ Hemker. Stress-driven grain growth in nanocrystalline pt thin films. *Scripta Materialia*, 64(1):25–28, 2011.

[381] DS Gianola, S Van Petegem, M Legros, S Brandstetter, H Van Swygenhoven, and KJ Hemker. Stress-assisted discontinuous grain growth and

its effect on the deformation behavior of nanocrystalline aluminum thin films. *Acta Materialia*, 54(8):2253–2263, 2006.

[382] F Tang, DS Gianola, MP Moody, KJ Hemker, and JM Cairney. Observations of grain boundary impurities in nanocrystalline al and their influence on microstructural stability and mechanical behaviour. *Acta Materialia*, 60(3):1038–1047, 2012.

[383] Jason R Trelewicz and Christopher A Schuh. Grain boundary segregation and thermodynamically stable binary nanocrystalline alloys. *Physical Review B*, 79(9):094112, 2009.

[384] Yang Zhang, Garritt J Tucker, and Jason R Trelewicz. Stress-assisted grain growth in nanocrystalline metals: Grain boundary mediated mechanisms and stabilization through alloying. *Acta Materialia*, 131:39–47, 2017.

[385] Glenn H Balbus, Fulin Wang, and Daniel S Gianola. Suppression of shear localization in nanocrystalline al–ni–ce via segregation engineering. *Acta Materialia*, 188:63–78, 2020.

[386] Nathan M Heckman, Stephen M Foiles, Christopher J O'Brien, Michael Chandross, Christopher M Barr, Nicolas Argibay, Khalid Hattar, Ping Lu, David P Adams, and Brad L Boyce. New nanoscale toughening mechanisms mitigate embrittlement in binary nanocrystalline alloys. *Nanoscale*, 10(45):21231–21243, 2018.

[387] Michael A Gibson and Christopher A Schuh. Segregation-induced

changes in grain boundary cohesion and embrittlement in binary alloys. *Acta Materialia*, 95:145–155, 2015.

[388] K Lu. Stabilizing nanostructures in metals using grain and twin boundary architectures. *Nature Reviews Materials*, 1(5):1–13, 2016.

[389] Zesheng You and Lei Lu. Deformation and fracture mechanisms of nanotwinned metals. *National Science Review*, 4(4):519–521, 2017.

[390] ZX Wu, YW Zhang, and DJ Srolovitz. Dislocation–twin interaction mechanisms for ultrahigh strength and ductility in nanotwinned metals. *Acta Materialia*, 57(15):4508–4518, 2009.

[391] Lei Lu, Qingsong Pan, Khalid Hattar, and Brad L Boyce. Fatigue and fracture of nanostructured metals and alloys. *MRS Bulletin*, 46(3):258–264, 2021.